1-1-2010

Assessment And Energy Benchmarking For Two Archetype Sustainable Houses Through Comprehensive Long Term Monitoring

Rupayan Barua
Ryerson University

ASSESSMENT AND ENERGY BENCHMARKING FOR TWO ARCHETYPE SUSTAINABLE HOUSES THROUGH COMPREHENSIVE LONG TERM MONITORING

By

Rupayan Barua
B.Sc. (Mechanical Engineering)
Chittagong University of Engineering and Technology (CUET), Bangladesh, 1992

A thesis

presented to Ryerson University

In partial fulfillment of the

requirements for the degree of

MASTER OF APPLIED SCIENCE

In the program of

Mechanical Engineering

Toronto, Ontario, Canada, 2010

Author's Declaration

I hereby declare that I am the sole author of this thesis.

I authorize Ryerson University to lend this thesis to other institutions or purpose of scholarly research.

Rupayan Barua

I further authorize Ryerson University to reproduce this thesis by photocopying or by other means, in total or in part, at the request of other institutions or individuals for the purpose of scholarly research

Dated: ----------------------------

Rupayan Barua

ASSESSMENT AND ENERGY BENCHMARKING FOR TWO ARCHETYPE SUSTAINABLE HOUSES THROUGH COMPREHENSIVE LONG TERM MONITORING

Rupayan Barua

Master of Applied Science

Program of Mechanical Engineering

Ryerson University, Toronto, Ontario, Canada, 2010

Abstract

A long term monitoring system has been developed and implemented in the Sustainable Archetype House built at Kortright Conservation Centre of Toronto and Region Conservation Authority (TRCA) in Vaughan, Ontario, Canada. To comprehensively monitor the energy performance and to investigate the effectiveness and efficiency of the mechanical systems over 300 sensors of various types were installed. These are sufficient for energy monitoring details in the twin houses. An expandable distributed data acquisition (DAQ) system has been adopted for monitoring and control purpose. Data analysis of House-B has been performed. Results of monitoring data of energy recovery ventilator (ERV), radiant in-floor heating system, total electrical energy consumption, photovoltaic (PV) system, micro combined heat and power (CHP) unit and evacuated tube solar collector are described in Chapter 5. The sensible and latent heat recovery of the ERV increased with the increase of indoor-outdoor temperature difference and specific humidity difference, respectively. Higher radiant in-floor heating demand is observed on the 3rd floor. One year of data of the 4.08 kWp photovoltaic (PV) system has been collected and annual electricity generation is 4160 kWh. The average thermal and electrical efficiency of Whispergen micro combined heat and power (CHP) unit achieved 80% and 7% respectively. The average overall efficiency achieved 87% (based on higher heating value of natural gas). The average instantaneous efficiency of evacuated tube solar collector achieved 74%.

Acknowledgements

This thesis would not have been come to the light without extended cooperation of author's supervisor Dr. Alan S. Fung. His guidance helped to finish this stupendous task. The author conveys from the bottom of his heart, his total indebtedness to his supervisor. The author is ever grateful to Dahai Zhang, a Ph.D. candidate for his generous help. He also expresses gratitude to his colleagues for their continuous support. He is very grateful to the Regional Municipality of Peel, Regional Municipality of York, City of Toronto, Building Industry and Land Development (BILD) Association, Toronto Region and Conservation Authority (TRCA), MITACS Accelerate, Reliance Home Comfort and Union Gas Ltd for their financial support to implement the monitoring project. The author would also express special thanks to Mr. David Nixon, Warren Yates, Derrik Ashby for their concerted effort on implementing the instrumentation of monitoring system and Professor Leo Salemi of George Brown College for system networking support.

This work is dedicated to my respected parents, my kith and kin, my wife and my beloved son. All of whom tried me in various ways to guide me and help forward the cause espoused by me.

Table of Contents

List of Figures

List of Tables

Abbreviations

A/C	Air Conditioning
ACH	Air Change Per Hour
AFUE	Annual Fuel Utilization Efficiency
AHU	Air Handling Unit
ARI	Air Conditioning and Refrigeration Institute
ASME	American Society of Mechanical Engineers
ASHP	Air Source Heat Pump
ASHRAE	American Society of Heating, Refrigerating and Air-Conditioning Engineers
BILD	Building Industry and Land Development Association
BIPV/T	Building-Integrated Photovoltaic Thermal system
BTU	British Thermal Unit
CCHT	Canadian Centre for Housing Technology
CEC	California Energy Commission, USA
CFM	Cubic Feet Per Minute
CFP	Compact Field Point
CHP	Combined Heat and Power
CMHC	Canada Mortgage and Housing Corporation
COP	Coefficient of Performance
CPUC	The California Public Utilities Commission
CSA	Canadian Standard Association
CT	Current Transformer
DAQ	Data Acquisition System

DB	Dry Bulb
DOE	US Department of Energy
DWHR	Drain Water Heat Recovery
DHWT	Domestic Hot Water Tank
DHW	Domestic Hot Water
ECM	Electrically Commutated Motor
EER	Energy Efficiency Rating
EMIS	Energy Management Information System
EnoB	Energy-Optimized Buildings
ERV	Energy Recovery Ventilation
EU	European Union
EVO	Efficiency Valuation Organization
GAL	Gallon (3.78 LITERS)
GHG	Greenhouse Gas
GPM	Gallon Per Minute
GSHP	Ground Source Heat Pump
GWHR	Grey Water Heat Recovery
HDD	Heating Degree Day (^{o}C)
HfH	Habitat for Humanity
HHV	Higher Heating Value (for natural gas 37.8 MJ/m^3)
HRV	Heat Recovery Ventilation
HP	Heat Pump
HVAC	Heating, Ventilating and Air Conditioning
IC	Internal Combustion

kBTU	Kilo BTU
kWh	Kilowatt Hour
LCD	Liquid Crystal Display
LEED	Leadership in Energy and Environmental Design
MB	Megabyte
MBH	Mega BTU per Hour
MCHP	Micro Combined Heat and Power
MCS	Model Conservation Standards
MT	Metric Ton
NIST	National Institute of Standards and Technology
NI	National Instrument
NRCan	Natural Resources Canada
NRDC	US-based Natural Resources Defence Council
NSERC	Natural Sciences and Engineering Research Council of Canada
OBC	Ontario Building Code
ORNL	Oak Ridge National Laboratory
PAC	Programmable Automation Controller
Pt	Platinum
PG	Propylene Glycol
PV	Photovoltaic
Pa	Pascal (Pressure Unit N/m^2)
RSDP	Residential Standards Demonstration Program
RTD	Resistance Temperature Detector
RSI	Relative Strength Index

SEER	Seasonal Energy Efficiency Ratio
SQL	Structured Query Language
SRCC	Solar Rating and Certification Corporation
SSMS	SQL Server Management Studio
STC	Standard Test Condition
TOU	Time-of-use
TRCA	Toronto and Region Conservation Authority
USG	US Gallon
USP	United States Pharmacopeia
UoW	University of Waterloo
UoT	University of Toronto
VAT	Value Added Tax
VAV	Variable Air Volume
WB	Wet Bulb

Nomenclature

A	gross area of the solar collector, (m^2)
AF	air flow rate, (CFM)
A_{duct}	area of duct, (m^2)
AF_{min}	minimum air flow rate, (CFM)
A_{floor}	floor area of house, (ft^2)
AT	dry-bulb temperature of air, ($^{\circ}C$)
AT_{in}	entering dry-bulb temperature of air, ($^{\circ}C$)
AT_{out}	leaving dry-bulb temperature of air, ($^{\circ}C$)
AV	air velocity, (m/sec)
C	capacity rate for the water = $q \rho c_{water}$ (kJ/K.sec)
C_{min}	minimum capacity rate, (kJ/K.sec)
c_{air}	specific heat of air = 1.006 (kJ/kg.K)
c_{PG}	specific heat of PG, (kJ/kg.K)
c_{water}	specific heat of water = 4.1813 (kJ/kg.K)
FL_{min}	minimum liquid flow rate, (GPM)
h	enthalpy of air, (kJ/kg)
h_{in}	enthalpy of air entering heat exchanger, (kJ/kg)
h_{out}	enthalpy of air leaving heat exchanger, (kJ/kg)
N	number of bedrooms
Q	thermal power, (kW)
$Q_{Electrical}$	electrical power, (kW)
$Q_{sensible}$	sensible heat of air, (kW)
Q_V	heat flow from solar wall, (kW)

q	flow rate, (m^3/sec)
T	temperature, ($^{\circ}$C)
T_{cold}	cold water temperature, ($^{\circ}$C)
T_{hot}	hot water temperature, ($^{\circ}$C)
T_m	mean air temperature in the solar wall gap, ($^{\circ}$C)
T_{room}	room air temperature, ($^{\circ}$C)

Greek symbols

ρ_{air}	density of air, (kg/m^3)
ρ_{PG}	density of PG, (kg/m^3)
ρ_{water}	density of water, (kg/m^3)
ω	humidity ratio of air, ($kg_{vapour}/kg_{dry\ air}$)
I_T	solar irradiance, (W/m^2)
ε	total effectiveness
η	efficiency, (%)

Chapter 1

Introduction and Objectives

1.1 Background

In the cold climate regions, the building sector is responsible for the major portion of energy consumption and GHG emission. The growing awareness of the transformation of fossil fuel sources of energy to renewable energy and the government efforts to control climate change are helping the building industry towards sustainable development and setting the national target for low energy buildings worldwide. Table 1.1 shows the planned energy targets of some European Union (EU) countries.

Table 1.1 The planned energy targets of some EU countries (Thomsen et al., 2008)

Country	Year	Planned Energy Target
Austria	By 2015	Social housing subsidies will be available for passive buildings.
Denmark	By 2020	All new buildings should use 75% less energy than current building regulations (base year: 2006).
France	By 2020	All new buildings should produce more energy than they consume.
Germany	In 2020	All new buildings should be operated without using any fossil fuel.
Hungary	From 2020	All new buildings should be zero emission buildings.
Ireland	After July 1, 2008	All new buildings are of a low-energy standard.
Italy	In 2010	All new buildings should have an approximately 10% reduction from the 2008 standard U-value.
Netherland	In 2020	All new buildings should be energy neutral.
Norway	In 2017	Passive house standard will be required as minimum standard.
Switzerland	By 2010	Reduction of CO_2 emission by 10% from 1990 level, limiting the growth of electricity consumption to a maximum of 5% over the 2000 level and doubling the new renewable forms of energy used in electricity and heat production.
U.K.	In 2010 In 2013 In 2016	25% better than current regulations. 44% better i.e. similar to PassiveHaus. Zero carbon for all energy including appliances.

The U.S. Department of Energy (DOE) Building Technology Program (BTP) set the target of net-zero energy residential houses by 2025 (US Department of Energy, 2009). The Council of Energy Ministers in Canada also set a target: by 2030, all new homes will be built to net zero energy standards (Marrone, 2007). In Canada, buildings consume 33% of total energy production, use 50% of Canada's natural resources and emit 35% of GHGs into the atmosphere. The residential building sector is also responsible for approximately 80 megatons of CO_2 emissions annually (Miller et al., 2008). In this regard, various advanced technologies have been adopted for efficient energy uses, less energy wastage, higher home comfort and low GHG emission. The government also attaches a great importance to energy conservation by providing encouraging initiatives, rules and regulations. The leaders in the residential construction sector are also starting to look at alternative mechanical systems and renewable energy sources as means to maintain their market position. In this regard Natural Resources Canada (NRCan) and the National Research Council (NRC) of Canada have been playing a pioneering role in energy efficient housing. The latter organization sponsored the building of the first super insulation demonstration house in Regina, Saskatchewan in 1977. The Saskatchewan house was cube shaped, equipped with an air to air heat exchanger for ventilation and had no furnace (Parker, 2009). The former organization launched the Advanced House program in 1991. Ten R-2000 standard advanced houses were constructed across Canada at the end of 1992. During 1993, all houses were open to the public for a one-year demonstration, then sold and finally monitored for a one-year period under normal occupancy (Stover, 1994). In 2007, the Canada Mortgage and Housing Corporation (CMHC) took the initiative for 15 net zero energy home projects as the "CMHC Equilibrium™ Sustainable Housing Demonstration Initiative". Once the projects are finished, the homes will be open to the public for at least six months for demonstrations, then they will be sold and performance monitoring will be started for one year with full occupancy (CMHC, 1996).

In Ontario, the Toronto and Region Conservation Authority (TRCA) plays an important role in green education and the promotion of green buildings. Along with the Building Industry and Land Development (BILD) Association, they have implemented the "Sustainable Archetype House" project at The Living City Campus at Kortright Centre in Vaughan, Ontario, Canada. This Archetype Sustainable House is designed to demonstrate viable, sustainable housing technologies in the near and medium terms through research, demonstration, education, training, market transformation and partnership programs (TRCA and BILD, 2009).

1.2 Objectives

In order to evaluate the benefits from various structural and mechanical advancements, it is necessary to carry out a comprehensive monitoring on every aspect of thermal performance in the TRCA twin houses.

The specific objectives of the monitoring are listed below:

- From energy point of view, comparison of current practice and technologies in House-A and sustainable technologies of future practice in House-B
- Comparison of different HVAC technologies that are used in both houses, e.g., two stage air source heat pump in House-A and ground source heat pump in House-B, boiler in House-A and micro CHP unit in House-B, HRV in House-A and ERV in House-B and so on.
- Performance evaluation of each piece of mechanical equipment and compare with the manufacturer manual
- Calibrate the simulation result against gathered data from experiment according to the International Performance Measurement and Verification Protocol (Efficiency Valuation Organization (EVO), 2007)
- From the experimental result build a model benchmarking, which will be used to design of new sustainable houses

1.3 Literature review

There is growing awareness worldwide about energy conservation and transformation to clean energy generation for meeting residential house energy demands. In this regard, several monitoring projects have been conducted in the past few decades to assess the actual energy consumption of newly built sustainable houses. The Northwest Power Planning Council, Oregon, USA developed the Model Conservation Standards (MCS) in 1983 to save large amounts of space heating energy in the houses of the Northwest Pacific region of the U.S (Parker, 1989). Under the Residential Standards Demonstration Program (RSDP) in 1984, 410 energy-efficient single-family homes in the states of Washington, Oregon, Montana and Idaho were constructed. The design features of these houses were high levels of insulation for the attic, walls and floors, triple-glazed windows and airtight construction with a mechanical ventilation system by means of a heat recovery unit. These MCS houses have been compared with another group of 410 newly built conventional technology houses in the same region. Each house was monitored for at least one year. Monitored space heating energy savings of the MCS over newly built conventional houses averaged 27.5 kWh/(m^2-yr) (8.72 kBtu/ft^2-yr). It was found that space heating consumption is a function of overall heat loss coefficient of the building and the cumulative temperature difference between inside and outside temperatures. Forced air heating systems performed poorly relative to others. Heat pumps showed lower space heating electricity consumption. Homes heated primarily with wood stoves showed much lower space heating electricity consumption. The average temperature in the main living room of the energy-efficient MCS houses was 0.8°C (1.44°F) warmer than newly built conventional houses.

Similar studies have been conducted in Kirov, Russia. Matrosov et al., (1994) mentioned that, as Russia moved toward a market economy, it was increasingly important to understand the energy characteristics of residential houses because of fuel supply conditions and continuous price fluctuations. Their growing concern is that single family houses in the middle zone of Russia consume about 600-800 kWh/(m^2-yr) (190 – 253.5 kBtu/ft^2-yr) of primary energy. Whereas in Germany, average single family houses consume 250 kWh/(m^2-yr) (79 kBtu/ft^2-yr), in Sweden, the figure is 135 kWh/(m^2-yr) (43 kBtu/ft^2-yr). Highly efficient single family houses in Germany consume only 90 to 120 kWh/(m^2-yr) (28.5 to 38 kBtu/ft^2-yr). The Research Institute for Buildings Physics (NIISF) of Gosstroy, Russia and the US-based Natural Resources Defence Council (NRDC) established a joint collaboration on energy efficiency studies of buildings in 1988. They constructed a standard two-storey, unoccupied single-family house with three rooms on the first floor and two rooms on the second floor. The floor area of this house was 112.8 m^2 (1,214 ft^2). This fabricated house was assembled in Kirov, where the average winter temperature is -5.8°C (21.56°F), and the duration of the heating season is 231 days. The design features of this model house included a 160 mm thick wall structure, and it was composed of three-tier panels and a wooden-frame work. Windows were double-glazed with a coupled-type double sash. The floor structure was composed of decking on joists. Gaps between joists were filled with mineral wool. The roof used the same insulating materials as the floors. This house was equipped with nine electric radiators of 1 kW (3.41 MBH) capacity each for space heating. After monitoring it was found that there was a linear correlation of energy consumption with the indoor and outdoor temperature difference. Another outcome of their study was that reduced infiltration and increased shell insulation provided low energy consumption. They suggested that, a good level of air tightness would be possible if frost-resistant weather stripping between the sash and frame of the window, and sealant between sash and glass were used. Air tightness can also be improved by caulking around the windows, joints between wall panels, between the panels and ceiling, and between panels and the first floor. This combination should reduce annual specific heating energy consumption by 37% from 448 to 253 kWh/(m^2-yr) (142 to 80 kBtu/ft^2-yr) when electric heating is used.

Another study has been conducted in Germany. Doreen et al., (2009) conducted comprehensive research on among others, 10 low-energy non-residential buildings with net floor area range of 1700-21,500 m^2 (18,292 – 231,340 ft^2), one office building with area of 950 m^2 (10,222 ft^2) and one residential building with total area of 300 m^2 (3,228 ft^2). This project was spearheaded by the German Federal Ministry of Economics and Technology (BMWi) under an intensive research program “Energy-Optimized Buildings” or EnoB. The objective of their study was to analyze the end and primary energy as well as auxiliary energy use of these buildings with regard to heating, cooling, ventilation and lighting. The residential house was a two-person household. It had a total heated net floor area of 294 m^2 (3163 ft^2) and the surface area to volume ratio was 0.63 m^{-1}. The design features of the envelope systems were for exterior walls 0.12 W/(m^2.K), with window ratio of 38% of façade area. In the mechanical system, this house employed environment friendly energy sources and energy sinks – such as the ground, rainwater and the ambient air. The rain water was collected in two cisterns. A ground source heat pump was used for space heating. In the mechanical ventilation system, supply air was conditioned by an earth-to-air heat exchanger which pre-heated the incoming fresh outdoor air in winter and pre-cooled it in summer. Cistern water was used as a heat sink in summer. After monitoring in 2007, the total annual primary energy consumption of this newly constructed residential house was 55 kWh/(m^2-yr) (17.43 kBtu/ft^2-yr) without lighting energy consumption. In addition, about 30% of the annual auxiliary energy was used for primary pump operation, energy distribution and delivery systems. The other findings of this study on the minimization of auxiliary energy requirements are: i) Pumps that can be controlled according to heating and cooling demand, ii) employed high efficiency pumps, iii) select accurately sized pumps with respect to pressure drop, iv) adjustment of the volume flow rate according to the heating and cooling demand, v) hydraulic adjustment (small pressure losses) within the primary cycle, vi) pump operation only when required and vii) sufficient control algorithms.

Different net zero and near zero energy projects in the U.S. have been described by Parker (2009). He mentioned that in the late 1980s, the cost of solar electricity production by photovoltaic systems declined which made the opportunity to use them in the residential housing sector. In the early 1990s, the Florida Energy Center undertook a simulation exercise in this regard and determined that photovoltaic systems could help make annual net zero energy homes possible. He also added that following the concepts of solar resources, some net zero energy houses were built across the U.S. A few examples are i) Lakeland, Florida in 1998, ii) Solar Patriot, Washington DC in 2001, iii) Livermore, California in 2002, iv) Lenoir City, Tennessee in 2002-05, v) Armory Park del Sol in Tucson, Arizona in 2003, vi) Wheat Ridge, Colorado in 2005, vi) Community level project in Sacramento, California in 2005.

A near zero energy house research project was built in Lenoir City, Tennessee, near Knoxville. The Habitat for Humanity (HfH) house ZEH 3 in this project was designed to surpass the energy consumption efficiency set forth by the US Department of Energy (DOE) Building America benchmark house model by 50% (Christian et al., 2006). This research project consisted of five houses. The design process for this series of five near zero-energy houses started at the Oak Ridge National Laboratory (ORNL). The floor area of the houses varies from 100 m^2 (1056 ft^2) to 111.5 m^2 (1200 ft^2). The nomenclatures of the five houses were: Base House, ZEH 1, ZEH 2, ZEH 3, and ZEH 4. The discussion here focuses on the ZEH 3 house, which has a total floor area of 100 m^2 (1060 ft^2). This house features structural insulated panels (SIP), geothermal space heating and cooling and a 2 kW grid tied roof-top photovoltaic system, which had a construction cost of less than \$100/ft^2. A total of 49 sensors were used to capture the continuous thermal and energy performance of this house. This house was monitored for more than two years of occupancy from December 2003 to 2005. After two years of monitoring, it was found that the PV system produced 24% of the total required energy. The house was heated and ventilated according to the ASHRAE standard 62.2 (ASHRAE, 2004) in the winter of 2003-2004 for less than \$40. The total energy use of the house was 11,000 kWh/yr (37,510 kBtu/yr) while a traditional home of similar area consumed around 26,970 kWh/yr (91,968 kBtu/yr). In 2005 it had a net daily cost for off-site energy of only \$0.79 (based on the local electric rate of

$0.068/kWh). Parker (2009) summarised from this project a variety of efficient building methods and technologies such as:

- Heat pump water heater linked to the refrigerator for heat recovery.
- Unvented crawl space controlled by the thermostat for supplemental space cooling and dehumidification in the summer and as radon mitigation in the heating mode.
- Ground source heat pump using foundation heat recovery.
- Structural insulated panels throughout.
- Interior duct system within the insulated envelope.
- High performance windows, efficient appliances.
- Grey water heat recovery system.

Similar, but a different study has been conducted in Canada. Located in Ottawa, the Canadian Centre for Housing Technology (CCHT) house is one of these. This project consists of two side-by-side identical houses built in 1998. One is the reference house and the other one is the test house. Both houses have two storeys and each one has a total floor area of 210 m^2 (2260 ft^2). To evaluate the performance of these two R-2000 certified houses, a comprehensive monitoring system was employed and more than 300 sensors were implemented. Simulated occupancy of four family members was used in the houses. The long term monitoring results have been used in the model benchmarking, used to predict residential energy performance for different locations across Canada (Swinton et al., 2001).

Another similar study is the Mattamy homes project in Milton, Ontario. This project consists of two houses built in 2005: one house is known as “The Wellington” and the other is known as “The Standbury”. Both houses are equipped with solar thermal collectors and grey water heat exchangers to recover drain water heat. The Wellington house has a solar thermal collector integrated ground source heat pump for space heating and cooling and a photovoltaic (PV) system for power generation. The Standbury house uses a two-stage high efficiency natural gas furnace with ECM motor and SEER 14 central A/C for space heating and cooling. Hot water is produced by the solar thermal collectors with a natural gas mini boiler as backup (Cohen, 2010).

A short study has been conducted in the Factor-9 home in Regina, Canada. This is a one-storey R-2000 certified single family house. This house has a floor area of 301 m^2 (3239 ft^2) where four occupants are living. Passive solar systems are employed for space heating, and ground source energy is used for space cooling. The energy performance of this house was monitored for only one year from June 1, 2007 to May 31, 2008. The measured annual energy consumption of the house was 33.1 kWh/(m^2-yr) (10.5 kBtu/ft^2-yr). This amount was 10 times less than homes in Regina built from 1970-73 (Dumont, 2008).

A research project on near net-zero energy demonstration homes named ÉcoTerra has been conducted in Quebec. This is one of the fifteen CMHC Equilibrium Demonstration projects. This is a 240 m^2 (2600 ft^2) prefabricated home assembled in 2007 in Eastman, Quebec. The envelope of this house is well insulated and air tight. The combined resistance of the walls is RSI 6.6 (R-37.5) and the ceiling is RSI 9.5 (R-54.2). Blower door test result showed 0.8 ACH at 50 Pa. This is a south facing house utilizing passive solar heating, where 40% of the south facing facade is covered with triple glazed windows. The house is equipped with a building-integrated photovoltaic-thermal system (BIPV/T) on the roof which generates 2.8 kW of electricity and 10 kW of thermal energy. The house has a concrete slab in the basement, which contains air channels that allow the slab to absorb heat from the hot air heated by BIPV/T collector. This slab acts as a thermal mass, i.e., during the day the slab stores solar heat gain and releases it gradually at night. This house has a ground source heat pump for heating and cooling, waste water and ventilation air heat recovery systems. All appliances are energy efficient. This house is being monitored by a research team from Concordia University (Solar Buildings Research Network, 2007).

Chapter 2

House Description

The Archetype House is a semi-detached twin-house. Two different sets of HVAC systems were installed in each of these twin houses: current practice and technologies in House-A, and sustainable technologies for future practice in House-B. Each house is attached to a garage. An in-law suite is built above the garage of House-B. Figure 2.1 shows the south side view of the Archetype Sustainable House with House A on the left-hand side and the in-law suite on the extreme right. Both houses are R-2000 and LEED Platinum certified (Dembo et al., 2010).

Figure 2.1 South-west views of the Archetype Sustainable twin houses

Although both houses are built based on the R-2000 standard, there are a few differences in the insulation, windows and mechanical systems. A comparison of the HVAC system among different housing standards is given in Table 2.1. Blower door tests have been conducted in both houses by Dembo et al. (2010). The air tightness in House-A is 1.317 ACH@50 Pa and in House-B is 1.214 ACH@50 Pa.

Table 2.1 Comparison of HVAC and energy feedback systems among housing standards (Zhang at al., 2010)

Equipment	Traditional house	R-2000 standard	TRCA sustainable House
Solar collector for hot water generation	No	No	Yes
Cogeneration systems for power and hot water generation	No	No	Yes
Solar wall for supply of hot air to the zone	No	No	Yes
PV cells for power generation	No	No	Yes
Wind turbine for power generation	No	No	Yes
GSHP for space heating/cooling	No	Yes	Yes
Desuperheater of GSHP for hot water generation	No	No	Yes
HRV/ERV for recovery of heat from exhaust air	No	Yes	Yes
DWHR from drain water	No	No	Yes
Radiant floor heating	No	Yes	Yes

Table 2.2 Details of basic design features of House-A, House-B and inlaw suite.

Table 2.2 Basic design features of the twin houses (Zhang et al., 2010)

Features	House-A	House-B	In-law suite (House-B)
Orientation	South facing	South facing	South facing
Stories	3	3	2 (Garage in ground floor)
Floor	232 m^2/25′×40′ (2500 ft^2)	232 m^2/25′×40′ (2500 ft^2)	32 m^2/28′×12.5′ (350 ft^2)
Natural Infiltration	0.06 ACH	0.06 ACH	0.06 ACH
Winter design conditions	Outdoor temp.: -22°C /-7.6°F Indoor temp.: 22°C/71.6°F	Outdoor temp.: -22°C /-7.6°F Indoor temp.: 22°C /71.6°F	Outdoor temp.: -22°C /-7.6°F Indoor temp.: 22°C/71.6°F
Summer design conditions	Outdoor DB: 31°C /87.8°F Outdoor WB: 24°C/75.2°F Indoor temp.: 24°C/75.2°F	Outdoor DB: 31°C/87.8°F Outdoor WB: 24°C/75.2°F Indoor temp.: 26°C/78.8°F	Outdoor DB: 31°C/87.8°F Outdoor WB: 24°C/75.2°F Indoor temp.: 24°C/75.2°F
Heating load	7.91 kW/27 MBH	7.94 kW/27.1 MBH	1.64 kW/5.6 MBH
Cooling load	4.92 kW/16.8MBH	6.18 kW/21.1 MBH	1.61 kW/5.5 MBH
Ventilation	85.42 Litres/sec (181 CFM)	70.79 Litres/sec (150 CFM)	9.44 Litres/sec (20 CFM)

Detail structural features of House-A, House-B and in-law suite are described in Table 2.3. In both houses, similar structural features were used except wall insulation and windows.

Table 2.3 Structural features of the twin houses (Zhang et al., 2010)

Features	House-A	House-B	In-law suite (House-B)
Basement walls	RSI 3.54 (R20) with Durisol blocks	RSI 3.54 (R20) with Durisol blocks	RSI 5.31 (R30)
Walls	RSI 5.31 (R30)	RSI 5.31 (R30)	RSI 5.31 (R30)
Wall insulation	Roxul Batt Fibre (R21) + 3″ Styrofoam	Heat-Lock Soya Polyurethane Foam and Lcynene spray foam	Heat-Lock Soya Polyurethane Foam and Lcynene spray foam
Windows	2.19 $W/m^2.K$ (0.39 $Btu/ft^2 \cdot {}^{\circ}F$) and double paned, low "E", fiberglass framed	1.59 $W/m^2 \cdot K$ (0.28 $Btu/ft^2 \cdot {}^{\circ}F$) and all triple glazed, low "E" , with argon filled	1.59 $W/m^2 \cdot K$ (0.28 $Btu/ft^2 \cdot {}^{\circ}F$) and all triple glazed, low "E" , with argon filled
Roof	RSI 7 (R40) Structurally Insulated Panels (SIPs), which are insulated Styrofoam panels	RSI 7 (R40) Structurally Insulated Panels (SIPs), which are insulated Styrofoam panels	RSI 7 (R40) Structurally Insulated Panels (SIPs), which are insulated Styrofoam panels

The mechanical features of House-A, House-B and the in-law suite are described in Table 2.4. Only a solar collector is used in House-A as a renewable energy sources. Photovoltaic system, Wind Turbine, Solar Thermal Collector, GSHP in House-B and a Solar Wall in in-law suite are used as renewable energy sources.

Table 2.4 Mechanical features of the twin houses (Zhang et al., 2010)

Features	House-A	House-B	In-law suite (House-B)
Solar collector	Flat plate collectors	Evacuated tube collectors	No
PV system	No	Yes	No
Wind turbine	No	Yes	No
Heating and cooling	Two-stage air source heat pump packaged with AHU	Ground source heat pump with horizontal loops	From House B
	Wall mounted mini gas boiler	Stirling engine micro-cogeneration unit	From House B
Ventilation system	HRV	ERV	HRV
Auxiliary water heating	Mini gas boiler	Desuperheater & Electric (TOU)	No
Infloor heating	Basement only	All three floors & basement	No
Heat recovery from drain water	Yes	Yes	No

Table 2.4 continued

Appliances	ENERGY STAR®	ENERGY STAR®	ENERGY STAR®
Lighting	compact florescence bulbs	compact florescence bulbs	compact florescence bulbs
Solar wall	No	No	Yes

2.1 HVAC system of House-A

Figure 2.2 shows the ventilation and hydronic system of House-A. This house features with a one-tank hot water system. This tank has two coils: one is connected to a flat plate solar collector and the other is connected to the wall mounted mini boiler for backup supply. A two-stage air-to-air source heat pump is used to supply warm/cold air for space heating/cooling. The air source heat pump is connected to the air handling unit (AHU), which has a variable speed blower and supplies forced air to the zones above the basement. If the heat pump cannot supply sufficient heat to the space during low outdoor temperature, the mini boiler will start to supply hot water to the heating coil of the AHU for supplementary heat to the zone. The return warm water will circulate in the radiant in-floor heating system for basement space heating. In the mechanical ventilation system a heat recovery ventilator (HRV) is used for heat recovery from the stale air. A grey water heat exchanger was installed to recover heat from drain water. Detail specifications of equipment/appliances, manufacturer/distributor and model number are shown in Tables 2.5, 2.6 and 2.7.

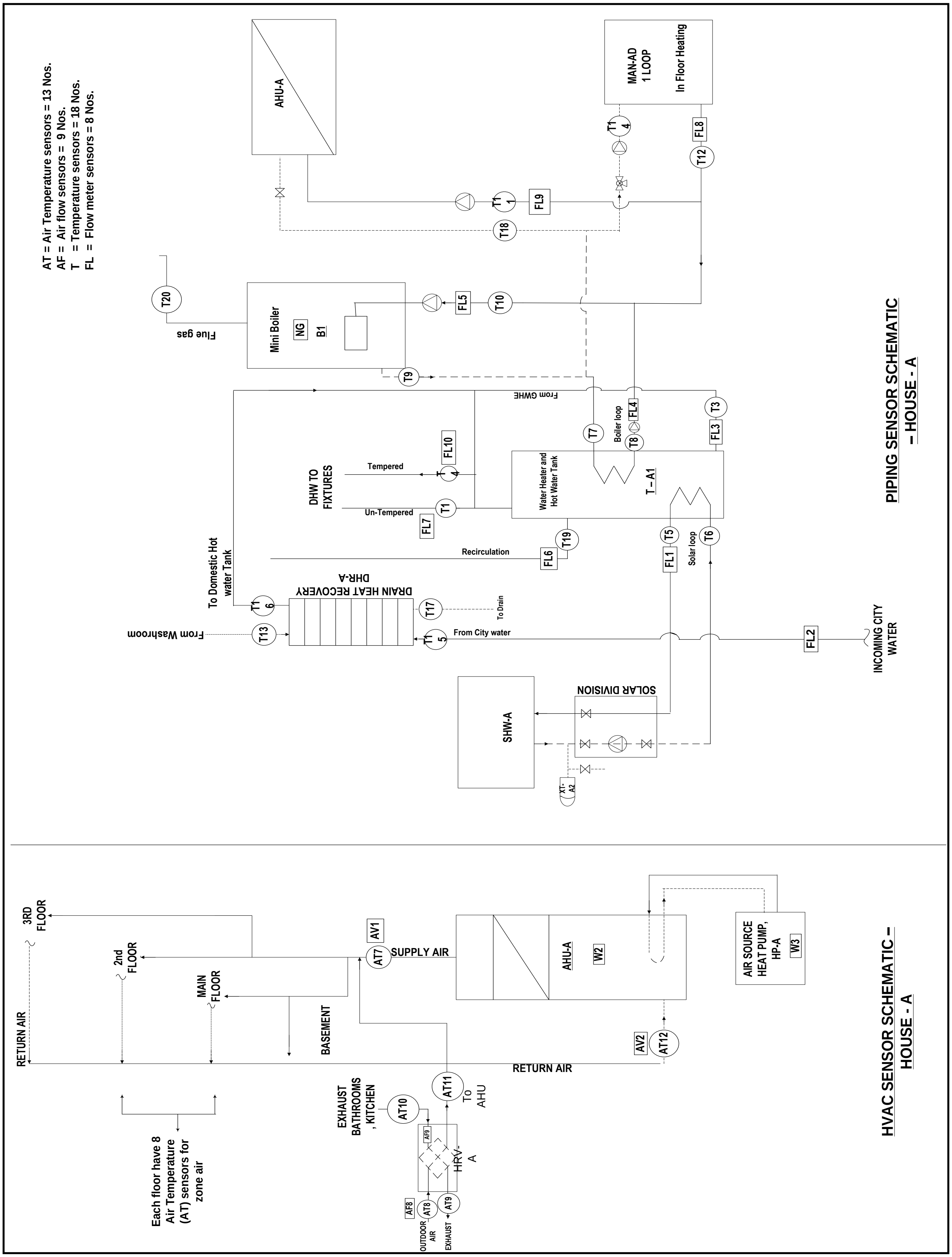

Figure 2.2 Layout of HVAC system and monitoring points in House-A

Table 2.5 Detail specifications of HVAC equipment in House-A (Zhang et al., 2010)

Equipment	Technical Information
Flat plate solar collector	Gross area: 2.51 m^2 (27 ft^2), Absorber area: 2.32 m^2 (25 ft^2)
Wall type mini boiler	Capacity: 18.46 kW (63 MBH)
Domestic hot water tank	Capacity: 300 litre (79 USG)
Heat pump matched with Air Handling unit (AHU)	HEAT PUMP HEATING CAPACITIES: COP: 3.45, Heating capacity: 11.06 kW (38 MBH) at 8.3°C (47°F), HSPF: 9.4 HEAT PUMP COOLING CAPACITIES: Cooling capacity: 10.48 kW (36 MBH), SEER: 16, EER: 17.6 AIR HANDLING UNIT (AHU): Cooling range: Max. 565.72 Litres/sec (1200 CFM) Heating range: Max. 565.72 Litres/sec (1200 CFM) Cooling capacity: 8.73 kW (30MBH) Water heating capacity: 16.73 kW (57.48 MBH) at 377.14 Litres/sec (800 CFM) and at 82.22°C (180°F) EWT
Heat recovery ventilator (HRV)	Surface area: 17.10 m^2 (184 ft^2), net air flow rate: 198 m^3/h (117 CFM), Sensible recovery efficiency: 74% at supply air temperature -25°C (-13°F)
Drain water heat exchanger	Length: 91.44 cm (36″), diameter: 7.62 cm (3″)

Table 2.6 Manufacturer/Distributor and Model number of HVAC equipment in House-A

Equipment	Manufacturer/Distributor	Model
Heat recovery ventilator (HRV)	Venmar Ventilation Inc.	VanEE 3000HE
a) Heat pump b) Air handler	a) Mitshubishi Electric b) Advanced Distributor Products	a) PLA-A36BA, PUZ-HA36NHA b) BVRMB6230S3P3
Drain water heat exchanger	RenewABILITY Energy Inc.	R3-36
Wall mounted mini boiler	VIESSMANN Manufacturing Company Inc.	WB1A 8-24
Domestic hot water tank	VIESSMANN Manufacturing Company Inc.	VITOCELL-B 100
Flat plate solar collector	VIESSMANN Manufacturing Company Inc.	Vitosol 100 SV1

Table 2.7 Detail specifications of appliances in House-A

Appliances	Energuide rating (kWh/yr)	Manufacturer and Model number
Dish washer	415	Kenmore Elite, 465.13333600
Clothes washer	176	Kenmore Elite, H7CA3C0A(3B)
Fridge	448	Kenmore Elite, 596.66133701
Electric range/oven	244	Kenmore Elite, 41823

2.2 HVAC system of House-B

Figure 2.3 shows the more advanced HVAC systems of House-B. A two-tank system was adopted for hot water production. One is a preheat tank and the other is a time-of-use (TOU) tank. The preheat tank is heated by an evacuated tube solar collector and the TOU tank has two electric coils for back up hot water generation. Desuperheater of GSHP also generates hot water. The radiant in-floor heating system is used for space heating in each floor. A ground source heat pump (GSHP) is connected to two horizontal loops in the yard. In the cooling season, the GSHP supplies chilled water to the multi-zone AHU. A Stirling engine based micro combined heat and power (CHP) unit substitutes for the GSHP during the winter months. This CHP unit can generate electricity and hot water at the same time. Because this unit is thermal load based, it is not operated in the cooling season. A buffer tank is used in between the GSHP/CHP and the infloor system/AHU to minimize short cycling. There is a roof-top PV system, and wind turbine for renewable energy production. An energy recovery ventilator (ERV) was installed in the mechanical ventilation system. A grey water heat exchanger was installed for grey water heat recovery. There is a 10 m^3 (2642 USG) underground cistern in the field that collects rain water for toilet flushing and gardening. Detail specifications of equipment/appliances, manufacturer/distributor and model number are shown in Tables 2.8, 2.9 and 2.10.

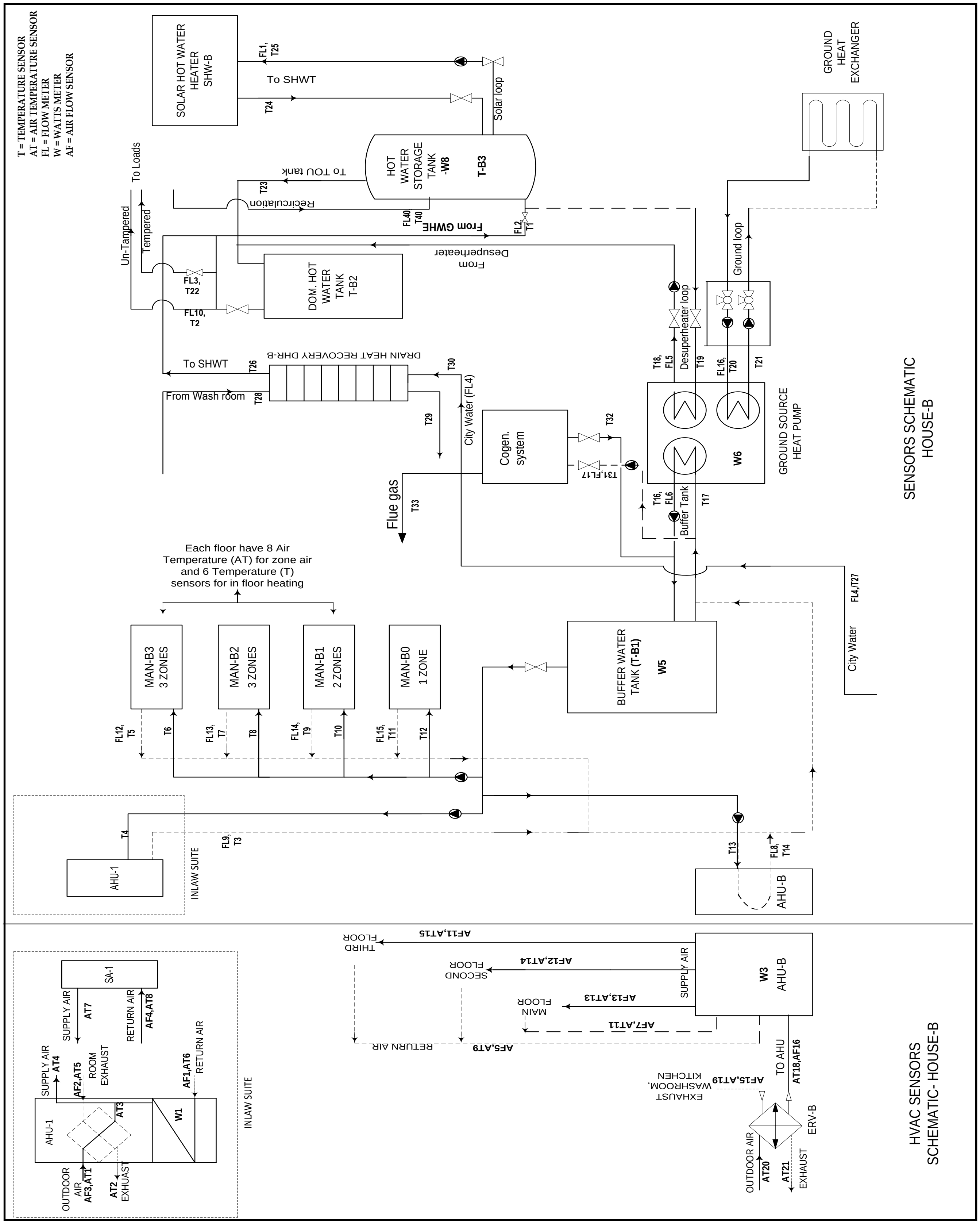

Figure 2.2 Layout of HVAC system and monitoring points in House-B and in-law suite

Table 2.8 Detail specifications of HVAC equipment in House-B (Zhang et al., 2010)

Equipment	Technical Information
Evacuated tube solar collector	Gross Area: 2.88 m^2 (31 ft^2), Absorber area: 2.05 m^2 (22 ft^2)
Solar hot water tank	Capacity: 300 Litres (79 USG)
Auxiliary hot water tank	Capacity: 175 Litres (50 USG), Maximum heating capacity: 6 kW (20 MBH)
Buffer tank	270 litres (71 USG)
Ground source heat pump (GSHP)	a) Heating capacity at 0°C (32°F) Entering Water Temperature (EWT) and 1.04 Litres/sec (16.5 GPM) water flow rate, COP: 3.0 (13.3 kW) b) Cooling capacity at 25°C (77°F) Entering Water Temperature (EWT) and 1.04 Litres/sec (16.5 GPM) water flow rate, COP: 2.86 (12.66 kW), EER: 12.86 c) Length of horizontal loop: 152.39m (500′), Number of loop: 2, Depth of ground level: 1.83m (6′)
Air handling unit (AHU)	a) Maximum heating capacity at 82°C (180°F) Entering Water Temperature (EWT): 28 kW (95 MBH) b) Cooling capacity: 5.27 to 12.3 kW (1.5 to 3.5 tons) c) Nominal air flow rate: 660 Litres/sec (1400 CFM)
Energy recovery ventilator (ERV)	a) Surface area: 14.51 m^2 (156 ft^2), b) Heating capacity at -15°C (5°F) supply air temperature Sensible recovery efficiency: 55% , Latent recovery moisture transfer: 0.26, Net air flow rate: 52 Litre/sec (110 CFM) c) Cooling capacity at 35°C (95°F) supply air temperature Total recovery efficiency: 41%, Net air flow rate: 50 Litres/sec (106 CFM)
Drain water heat exchanger	Length: 91.44 cm (36″), diameter: 7.62 cm (3″)
Photovoltaic (PV) system	Size: 0.125 × 0.125 m (0.41′×0.41′), Capacity: 85 W/cell (0.29 MBH /cell), Module: 48 nos. Total capacity: 4.08kW (13.93 MBH).
Wind turbine	Rated capacity: 2.4 kW (8.19 MBH), Rotor diameter: 3.72 m (12′)
Micro CHP system	Electrical power: 1 kW (3.4 MBH), Thermal energy: 12.0 kW (40.98 MBH)

Table 2.9 Manufacturer/Distributor and Model number of HVAC equipment in House-B

Equipment	Manufacturer/Distributor	Model
Energy recovery ventilator (ERV)	Venmar Ventilation Inc.	VanEE 45808
Air handler	Ecologix Heating Technologies Inc.	C3-06
Drain water heat exchanger	RenewABILITY Energy Inc.	R3-36
Solar hot water tank	VIESSMANN Manufacturing Company Inc.	VITOCELL-B 100

Table 2.9 continued

Evacuated tube solar collector	VIESSMANN Manufacturing Company Inc.	Vitosol 300, SP3, Type 2m^2
Auxiliary hot water tank	GSW Water Heating	6G50SDE1
Buffer tank	GSW Water Heating	CST-80
Ground source heat pump	WaterFurnace International, Inc.	EW 042 R12SSA
Micro combined heat and power (microCHP) system	Whispergen Limited	PPS24-ACLG-5
PV system	ARISE TECHNOLOGIES DEUTSCHLAND GmbH	MSK roof top 85 W modules.

Table 2.10 Detail specifications of appliances in House-B

Appliances	Energuide rating (kWh/yr)	Manufacturer and Model number
Dish washer	290	GEC Profile, GSD1-807K00SS
Clothes washer	191	GEC Profile, WPDH8800J
Fridge	458	GEC Profile, PPCS1PJXASS
Electric range/oven	329	GEC Profile, PCT920
Clothes dryer	930	GEC Profile, UPVH880EJMG

2.3 HVAC system of In-law suite

The in-law suite is a separate living room above the garage. It is interconnected with House-B via a wooden platform. The unique feature of the mechanical system of this suite is the solar wall. Return air from the room passes through the solar wall, receiving heat and re-circulating as warm air into the room.

In addition, there is an integrated HRV and AHU unit for the ventilation system. The function of this integrated unit is to draw fresh air from outdoors into the HRV core so that the energy from the outgoing stale air is transferred to the incoming fresh air. The conditioned fresh air is then blended with the circulating air of the heating/cooling system and distributed to the living areas of the home through the supply ductwork. Hot and cold water are supplied to the integrated unit from the buffer tank of House-B in the heating and cooling seasons. The detail specifications, manufacturer/distributor and model number of equipment are shown in Table 2.11.

Table 2.11 Specifications of HVAC equipment in in-law suite

Equipment	**Technical information**	**Manufacturer/Distributor and Model number**
Solar wall	a) Surface area: 2.4 m^2 (26 ft^2) b) Maximum heat generating capacity at 49°C (120°F) and 33.5 Litres/sec (71 CFM) air flow rate Energy rating: 1.76 kWh/day (6 kBTU/day)	Your Solar Home Inc., SH1500-G
Air handling unit (AHU)	Maximum air flow rate for both heating and cooling: 212 Litres/sec (450 CFM)	Nu-Air Ventilation Systems Inc., Enerboss 400C

Chapter 3

Monitoring system

Monitoring projects range from broad research studies to very specific savings verification. The TRCA Archetype House monitoring project is developed for broad research studies. Monitoring priority is given to performance evaluation of different mechanical equipment, whole house energy consumption and on-site renewable energy production rather than envelope retrofit performance. For development of this monitoring project ASHRAE Standards and Codes for energy monitoring in buildings have been followed (ASHRAE, 1999). In the monitoring project, the following activities are involved (ASHRAE, 1999):

- Project planning
- Installation of sensors and data acquisition equipment
- Calibration, ongoing data collection, and verification
- Data analysis and reporting.

3.1 Project Planning

For planning of this monitoring system, the following information was collected:

- Design characteristics of the house
- Envelope features
- Specifications of HVAC systems, i.e., duct sizes, fan capacity, maximum ventilation rate etc.
- Mechanical equipment installation layout
- Specifications of hydronic systems, i.e., flow rate, range of operative temperature, sizes of pipes, fittings, pump etc.
- Equipment specifications and their controlling systems

After collecting the above information, necessary equations for equipment performance were incorporated, and based on these equations relevant sensors and monitoring points were selected. The monitoring points for the mechanical system are demonstrated in Figures 2.2, 2.3 and 3.1.

3.2 Installation of Sensors

In both houses, over 300 sensors of various types covering sufficient energy monitoring details have been installed. Sensor installation strictly follows the manufacturer's instruction to avoid any electrical damage and inaccurate readings of the signal. For instance, air temperaure/relative huimidity sensors are located away from the bend of ducts or the inlet of fans to ensure uniform flow.

A summary of monitored components and their required inputs are provided in Table 3.1.

Table 3.1 Assessment of components and required sensors (Zhang et al., 2010)

Component	Input Parameters	Sensors
Solar collectors (vacuum tube or flat plate)	USP grade Propylene Glycol temperature (inlet and outlet) and flow rate, solar radiation	RTD probe, flow rate sensor and pyranometer
PV	Power generation, solar radiation at different tilt surfaces (horizontal, vertical and roof angle)	Wattnode sensor (bi-directional AC), pyranometer
Wind turbine	Power generation	Wattnode sensor (bi-directional)
HRV/ERV	Air temperature and relative humidity (inlet and outlet), air flow rate (inlet and outlet), power consumption	Air temperature (AT) & relative humidity (RH) sensors, pressure sensors with flow stations and wattnode sensor
Integrated AHU/Air HP	Air temperature and relative humidity (to/from each zone), air flow rate (to/from each zone), power consumption	Air temperature (AT) & relative humidity (RH) sensors, pressure sensors with flow stations and wattnode sensor
Mini-boiler	Mass of natural gas, exhaust gas temperature, supply and return water temperature and flow rate (on return), power consumption	RTD, air flow rate sensor, natural gas meter, matched delta T probe and wattnode sensor
DHW tank	Water temperature (supply and return), flow rate (on return) and power consumption	Matched delta T probe, flow rate sensor and wattnode sensor
GSHP	Water and anti-freeze temperature (supply and return), flow rate (on return), power consumption, soil temperature and moisture	Matched delta T probe, flow rate sensor, wattnode sensor, soil temperature and moisture sensor
Co-gen system	Mass of natural gas, exhaust gas temperature, water temperature (supply and return), flow rate (on return) and power consumption	Matched delta T probe, flow rate sensor, natural gas meter and wattnode sensor
Radiant floor heating	Water temperature (supply and return) and flow rate (on return)	Matched delta T probe and flow rate sensor

Table 3.1 continued

Solar wall	Air temperature and relative humidity (inlet and outlet), air flow rate (inlet and outlet), solar radiation, power consumption	Air temperature (AT) & relative humidity (RH) sensors, pressure sensors with flow stations, pyranometer, and wattnode sensor
Drain water heat recovery (DWHR)	Water temperature (supply and return) and flow rate (on supply) of both city and grey water	Matched delta T probe, surface mounted RTD and flow rate sensor
Ground soil	Soil temperature and moisture (various locations), pipe surface temperature	Soil sensors and RTD sensors
Appliances	Power consumption	Wattnode sensor
Pump/fans	Power consumption	Wattnode sensor
Lighting and receptacle	Power consumption	Wattnode sensor

Figure 3.1 shows that a total of 12 soil sensors at different depths in four locations and 12 surface mounted RTD sensors on the supply and return horizontal earth loop in four locations. All RTD sensors were installed at a depth of 1.83 m (6 ft) except RTD-5 and RTD-6. The depth of earth loop in the latter sensors location was only 1.52 m (5 ft).

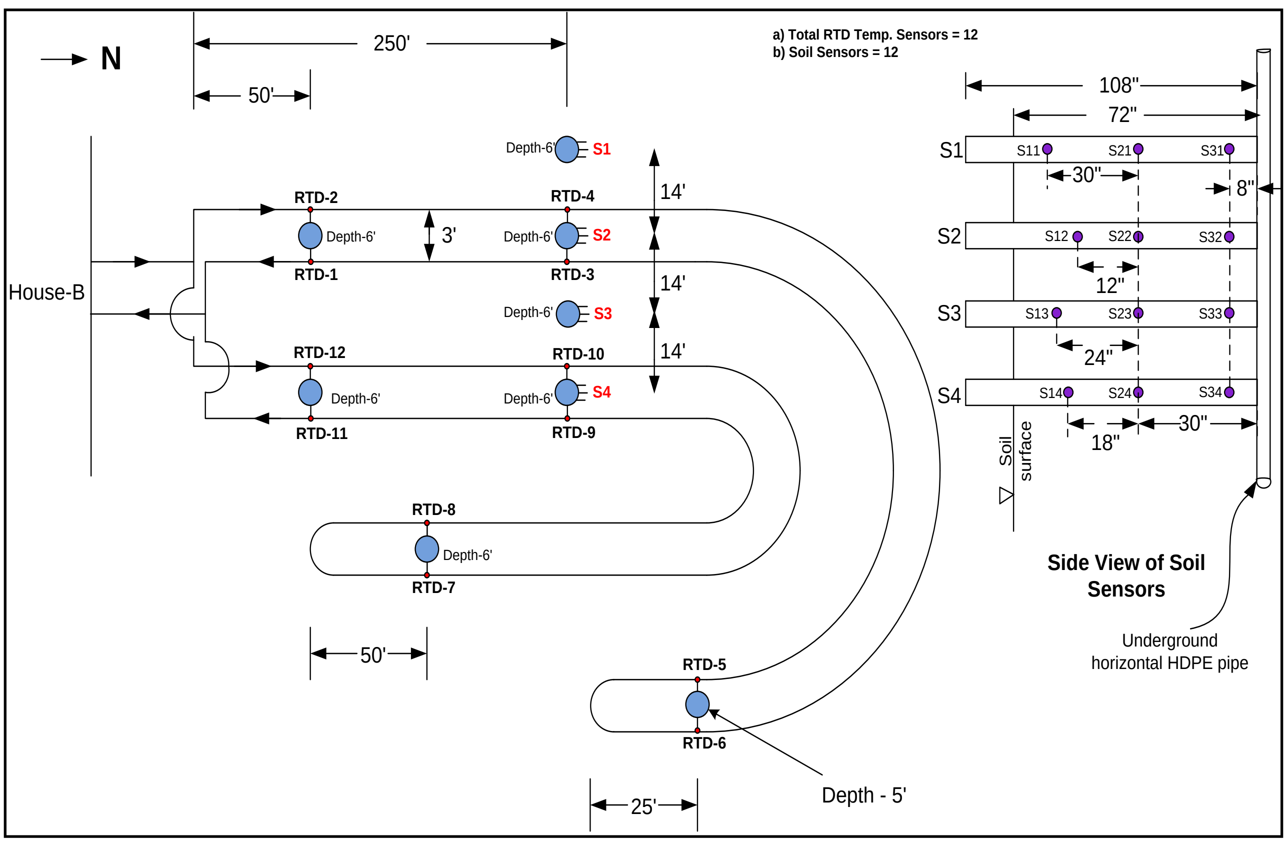

Figure 3.1 Layout of soil temperature and moisture sensors around the loop and RTD sensors on the loop

The connection between the sensors and the connector block of the DAQ system are installed according to the National Instruments (NI) supplied circuit diagram. These sensors are properly connected to the chassis of DAQ system. Two ends of each wire of the respective sensors are properly labelled and recorded (Appendix A).

3.3 Installation of Data Acquisition (DAQ) Systems

The DAQ system is very flexible in layout so as to have distributed sub-central DAQ. In this way, the wiring of sensors can be significantly reduced and the associated signal interference can be minimized.

The DAQ system consists of backplane, controller, module, connector block, power supplier, LabVIEW software platform and the computer. The selection of modules depends on the output signal of sensors. This output signal is converted into corresponding engineering units by the LabVIEW software (Table 3.2).

Table 3.2 Sensor name and its output signal

Sensors	**Nomenclature**	**Output signal**	**Conversion unit**
Flow rate sensor (liquid flow rate)	FL	Pulse (Hz) or V	GPM (USG)
Direct immersed RTD probe	T	ohm	^oC
Surface mounted RTD sensor	T	ohm	^oC
Air temperature and Relative humidity (RH) sensor	AT RH	mA	^oC %
Pressure transducer (air flow rate)	AF	mA	CFM
Air velocity transmitter	AV	mA	m/s
Gas meter	NG	mA or V	lpm
Wattnode	W	Pulse	W
Pyranometer (solar radiation)	I_T	mA	W/m^2
Soil sensor (moisture content and temperature)	SM T	V	wfv (water fraction by volume) ^oC

As the houses are extensively wired from different locations, a flexible and expandable distributed DAQ system is essential to obtain good quality data with minimal noise. The NI Compact FieldPoint system is an ideal system which provides an easy-to-use, highly expandable programmable automation controller (PAC) composed of rigid I/O modules and intelligent communication interfaces. The Compact FieldPoint I/O modules filter, calibrate, and scale raw sensor signals as well as performing self-diagnostics. Figure 3.2 shows the central DAQ system located in the mechanical room of the basement of each house, where the majority of the sensors are installed. In addition, each floor is equipped with a distributed chassis to collect room stratification air temperature and floor temperature data. The in-law suite of House B also has a dedicated chassis to process various signals, including a solar wall air heater, AHU, photovoltaic system and wind turbine. An external chassis is well insulated and located on the ground field to connect the soil sensors as well as the RTD sensors.

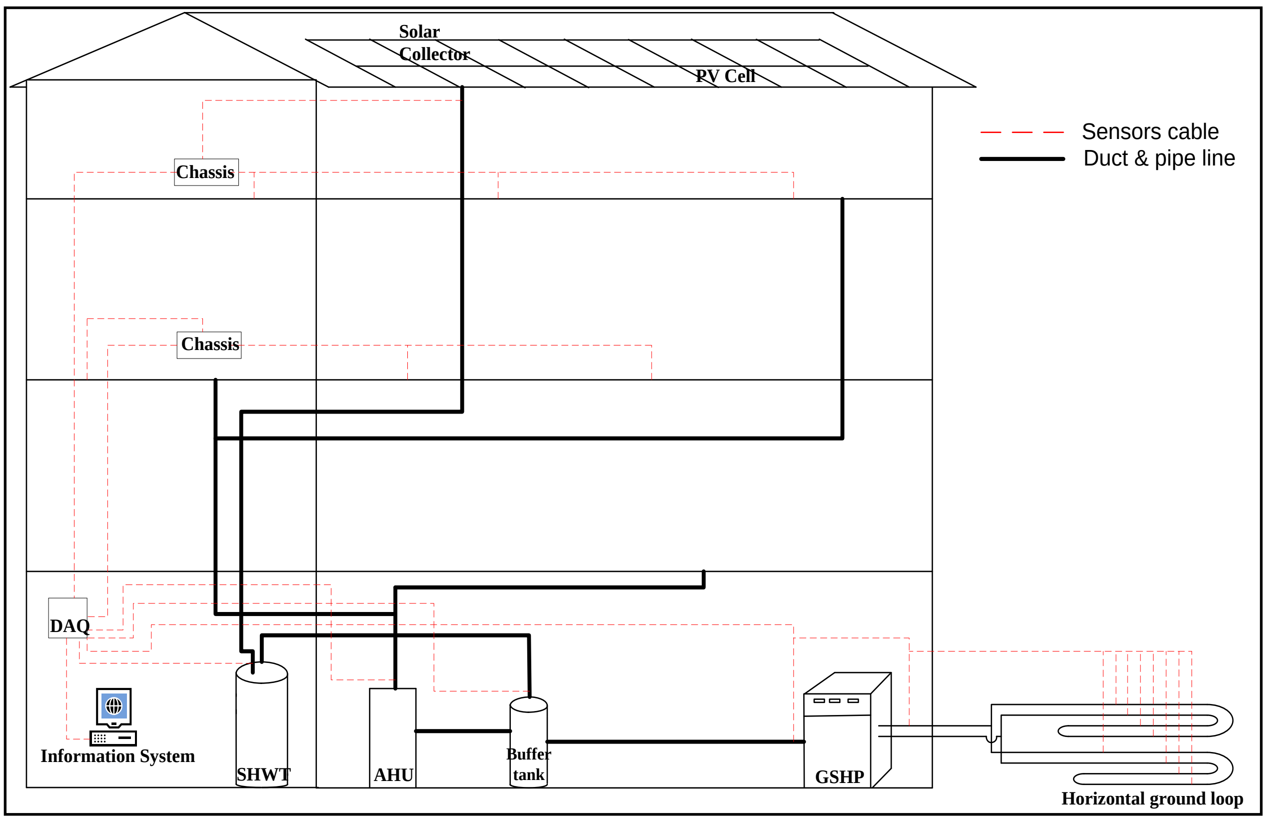

Figure 3.2 Diagram of monitoring system layout

All Compact Field Point (CFP) or chassis is connected to the central computer through a network hub. As such, sensor data is captured by the LabVIEW software platform and sensors are addressed in this software according to the nomenclature (Appendix A). The sensors output mentioned in Table 3.2 are converted into corresponding engineering units by software. For instance, the pressure transducer output is 4 to 20 mA corresponding to 0 to 1″ of water column (WC) of pressure. With this value, an equation is implemented into the LabVIEW program, which converts the mA signal to air flow rate in CFM (cubic feet per minute). With the

LabVIEW program, all equipment performance can be evaluated as well. Collected data sampling frequency will be adjusted in this program according to the actual requirement of data acquisition.

3.4 Calibration of Sensors

Calibration is the process of mapping raw sensor readings into corrected values by identifying and correcting systematic bias. Sensor calibration is an inevitable requirement due to the natural process of decadence and imperfection. Calibration is a technically challenging task mainly due to the existance of random noise and the absence of suitable error models (Feng et al., 2003).

In the calibration process of this monitoring system, the off-line calibration technique is applied for temperature sensors. In the context of off-line calibration, the collected data has two components: raw sensor readings and data captured by high quality and high-cost light wieght calibrators measuring the same set of readings. The second set of data serves as the standards of what the sensors should measure. The goal of the off-line calibration is to determine a compact function that provides the mapping from the raw sensor reading to correct values (Feng et al., 2003).

Table 3.3 shows calibrators which are used to calibrate different kinds of sensors.

Table 3.3 Sensors and calibrators

Sensors	Calibrator
RTD temperature sensors	• HART Scientific series 9102S Handheld Dry-wells • MICROCAL 20DPC • Omega series CL3515R
Air temperature sensors	• MICROCAL 20DPC • Omega series CL3515R
Air flow station and pressure transducers	• MICROCAL 20DPC • Hot-wire Thermo-Anemometer (model: Mini air HW PRO-VT50)
Turbine type water flow rate sensors	• Volume bucket and stopwatch (NIST, 2009)
PROTEUS series water flow rate sensors	• Factory calibrated but cross-checked according to NIST guideline
Pyranometer	• Factory calibrated (randomly checked with UoW, UoT and Kortright Conservation Centre weather station data)
Wattnodes	• Factory calibrated but cross-checked by power meter
Air velocity transmitter	• Hot-wire Thermo-Anemometer (model: Mini air HW PRO-VT50)

3.4.1 Temperature sensors

Three types of RTD temperature sensors are used for the measurement of liquid temperature: i) Pt-500 series immersed ΔT RTD sensors, ii) Pt-100 series direct immersed RTD sensors and iii) Pt-100 series surface mounted temperature sensors. Two sources of reference temperature were used for the calibration, i.e. a) ice water and b) handheld dry-wells.

3.4.1.1 Ice water: Pure water at sea level (full atmospheric pressure) freezes at 0°C (32°F) and boils at 100°C (212°F) (Kuphaldt, 2009). Hence, ice water at 0°C (32°F) was used as the reference temperature for the calibration of immersed type Pt-100 and Pt-500 temperature sensors. RTD sensors were connected with the MICROCAL calibrator. Readings were taken when the temperature reaches steady state. Theoretically the reading of sensors in the ice water should be 0°C (32°F), but Figure 3.3 shows that with thermowell the readings varied between 0.63°C (33.13°F) and 0.77°C (33.39°F) for Pt-500 ΔT sensor and -0.32°C (31.42°F) to 0.22°C (32.4°F) for Pt-100 sensors. Without thermowell the lowest reading difference is 0.03°C (0.05°F) for both type of sensors. The main limitation of using pure water as calibrated standard is that it can calibrate at only 0°C (32°F) and 100°C (212°F). It is not possible to calibrate at other temperatures. Hence, a handheld dry-wells calibrator is used.

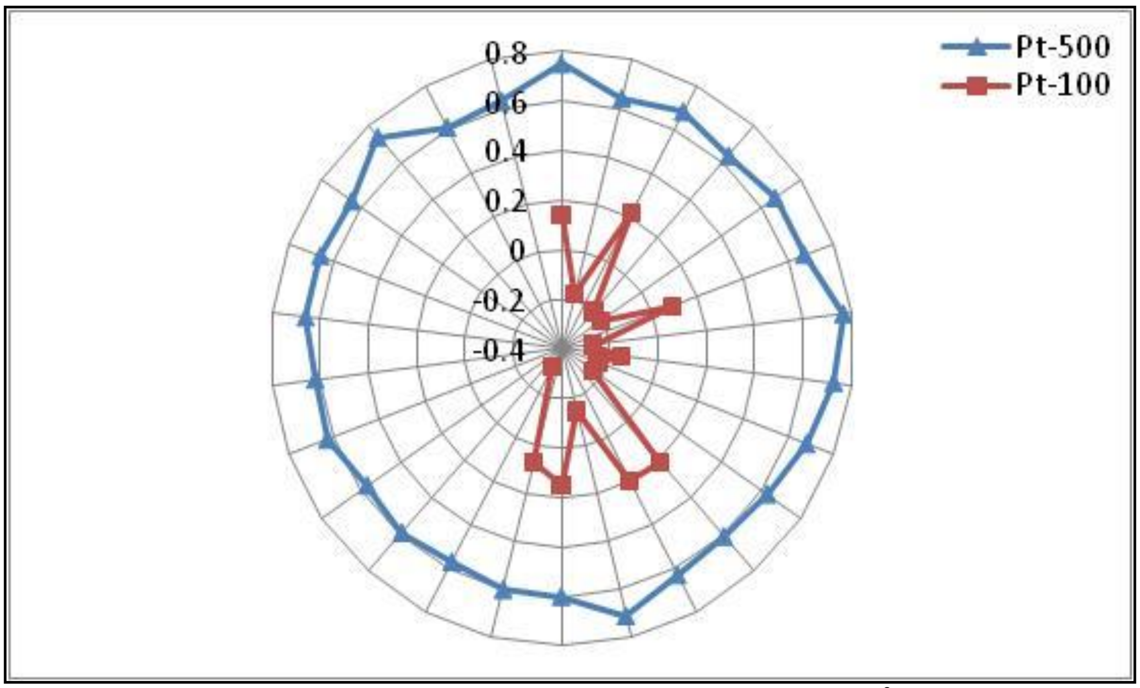

Figure 3.3 Calibrated results of Pt-500 and Pt-100 RTD probe based on 0^{0}C ice water

3.4.1.2 Handheld Dry-wells: This calibrator can create accurate calibration temperatures in the instrument. This device uses metal blocks with blind holes drilled for the insertion of temperature sensors (Kuphaldt, 2009). With the help of this equipment, all ΔT direct immersed temperature sensors (Pt-500) were calibrated from set point 0°C (32°F) to 90°C (194°F) with 10° intervals. Figure 3.4 shows that without thermo-well most of the Pt-500 sensors temperature difference have ranged 0.6°C (1.08°F) to 0.8°C (1.44°F) from the set point temperatures. Similar results have shown in Figure 6, i.e., temperature difference have ranged 0.6°C (1.08°F) to 0.8°C (1.44°F) at 0°C (32°F).

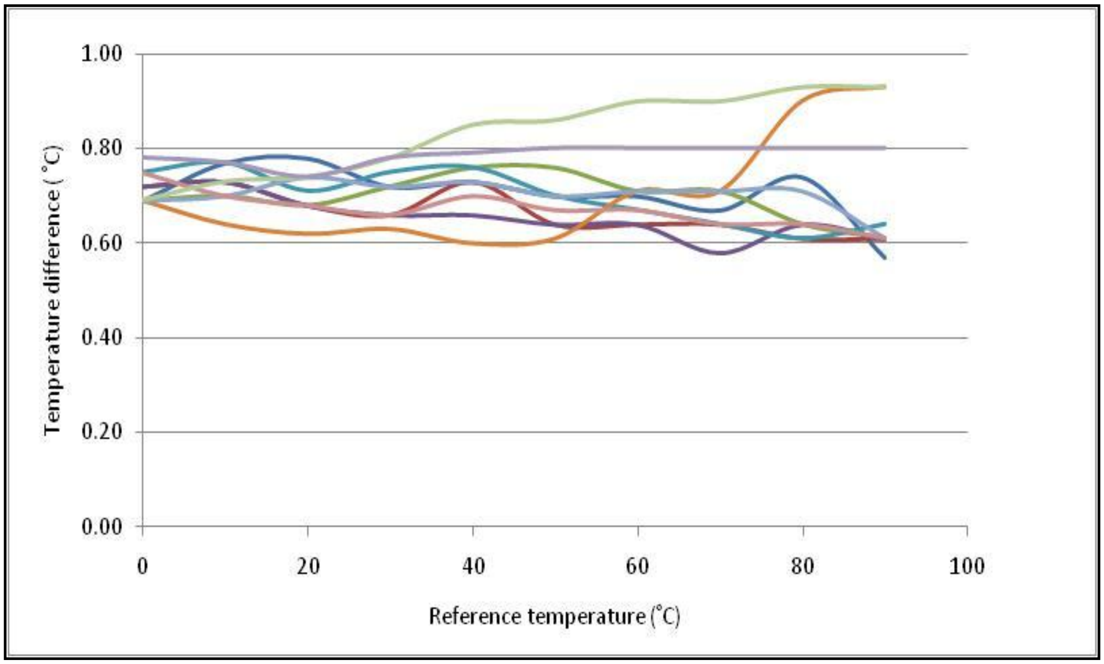

Figure 3.4 Calibrated result of Pt-500 RTD probe based on Handheld Dry-wells temperature settings

Pt-100 series direct immersed temperature sensors were calibrated from set point 0°C (32°F) to 90°C (194°F) with 10° intervals. Figure 3.5 shows that without thermo-well few sensors temperature difference have the ranged from 0.77°C (1.39°F) to 0.93°C (1.67°F) and others have 0.32°C (1.58°F) to 0.39°C (1.70°F).

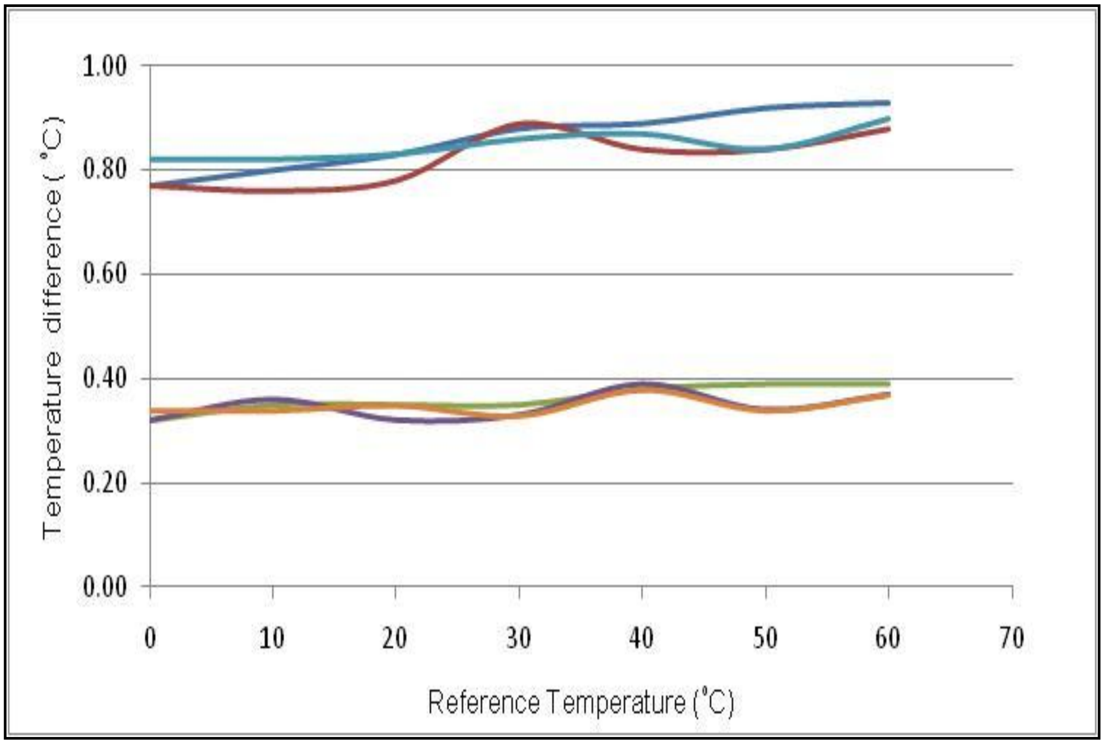

Figure 3.5 Calibrated result of Pt-100 RTD probe based on Handheld Dry-wells temperature settings

Following the same procedure, all 26 Pt-500 and 16 Pt-100 temperature sensors were calibrated. The offset value of each RTD sensor were set to the LabVIEW program.

The calibration data of three kinds of temperature sensors were also analysed according to the off-line calibration system (Feng et al., 2003). Figure 3.6 shows that, as the temperature rises, the sensors temperature increases linearly. From this linear relation an equation is set up for Pt-100 series surface mounted RTD sensors and implemented into the LabVIEW program.

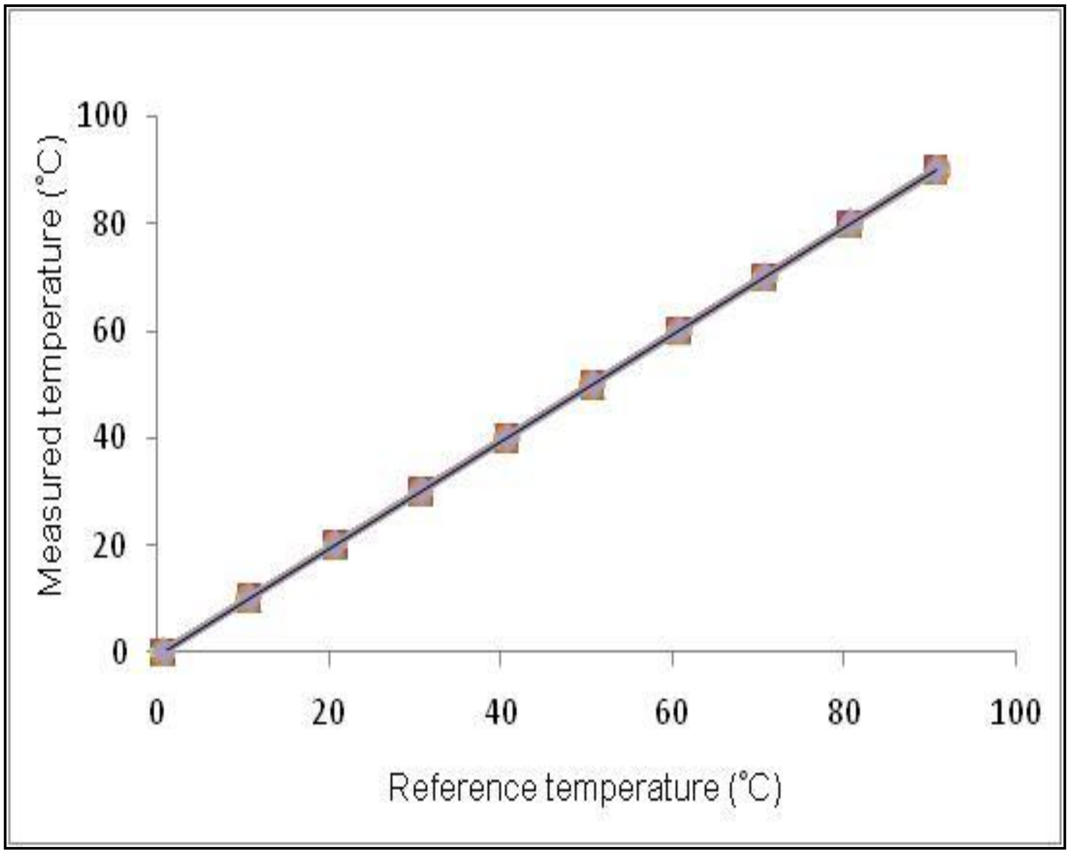

Figure 3.6 Off-line calibrated result based on Handheld Dry-wells temperature settings

3.4.2 Air-Temperature (AT) sensors: These sensors were calibrated with a referenced surface mounted (Pt-100) temperature sensor. This reference sensor was pre-calibrated by the Handheld Dry-wells. During calibration, the tips of both sensors were put adjacent to each other to ensure the accuracy of the temperature readings. AT sensors readings were taken from the LabVIEW program. The referenced sensor reading was taken from the MICROCAL 20DPC calibrator. In this process, more readings were collected for better accuracy.

3.4.3 Pressure transducer: Air flow rate sensor of circular duct consists of two parts. Pitot tube which gives duct pressure difference in inch of water and pressure transducer converts it to mA signal. Monitoring software LabVIEW convert it to air flow rate in CFM. Pressure transducer output in mA is calibrated by the MICROCAL 20DPC calibrator and Ammeter. The pressure transducer output range from 4 to 20 mA corresponding to 0 to 1″ of water column (WC). The reading of the lowest output signal of each sensor was measured. A linear equation was obtained within the calibration range and implemented into the LabVIEW program. The ouput value from the linear equation in CFM is cross-checked by the hot-wire thermo-aneamometer (model: Mini air HW PRO-VT50). The probe of this calibrator was inserted into the duct and measured the velocity at different points across the duct. Figure 3.7 shows the air velocity profile of 15 cm (6 inch) return air duct of ERV. By this method, average air flow rate was evaluated of 48.40 Litre/sec (102 CFM) and at the same time, actual average reading by the monitoring software was 47 Litre/sec (99 CFM), which was 3% less than aneamometer reading.

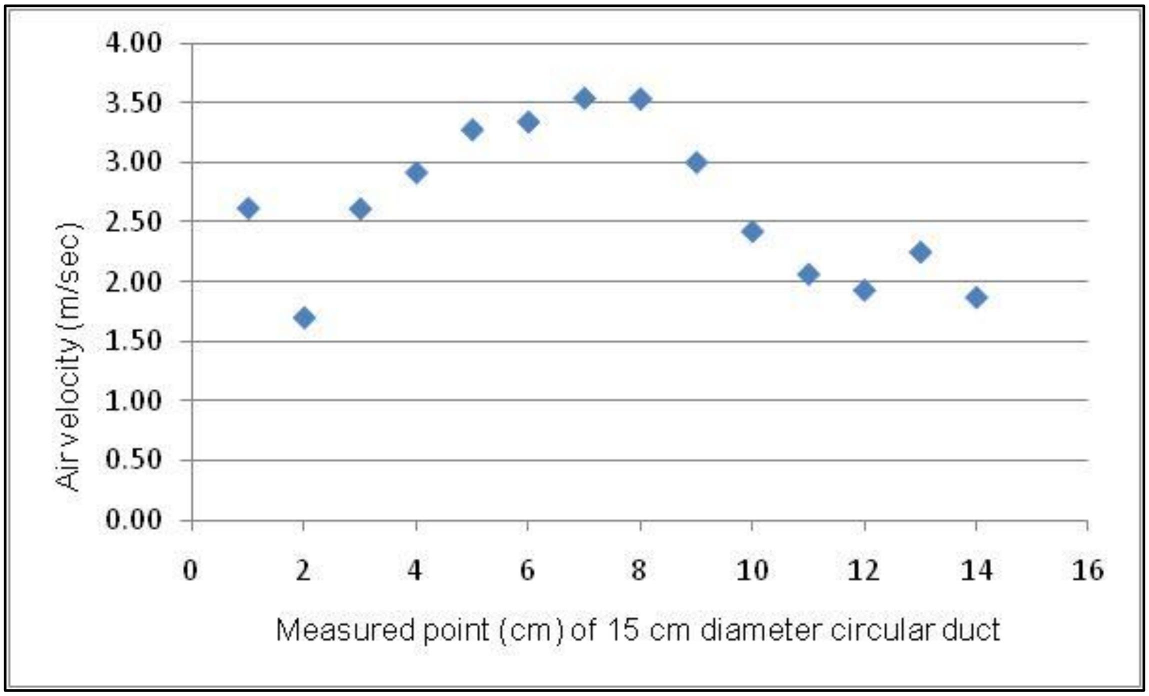

Figure 3.7 Air velocity of 15 cm (6 inch) return air duct of ERV

Although the velocity of air changed continuously, a high flow rate was observed at the centre of the duct. The avergae velocity of the duct was then converted into the air flow rate in CFM by multiplying with the area of the duct cross-section. Practically, it is very hard to get an exact flow rate between these two kinds of calibration systems. In average, there is around ±5% variation between these systems.

3.4.4 Water flow meter: The calibration of this sensor is done according to the NIST (National Institute of Standards and Technology) guideline (NIST, 2009). The water that flowed through the sensor was collected in a volume bucket with the certain time step and then compared with the saved data from the SQL database. This system was repeated three times for more accurate calibration results.

Apart from the calibration of each sensor, error/uncertainty analysis is performed based on the manufacturer supplied sensors and calibrators accuracy value in Appendix B.

Finally, it should be mentioned here that the calibration of sensors is an ongoing routine process to ensure data quality. This monitoring system will continue up to two years.

3.5 DAQ System -- Software

3.5.1 LabVIEW: Figure 3.8 is a snapshot of the front panel of the LabVIEW program. Both low level (temperature, flowrate, RH, etc.) information and high level information (efficiency, effectiveness, heat generation, etc.) can be displayed on the front panel. Raw signals are converted and post-processed at the background of the front panel. All signals, except for power consumption signals, are acquired at a constant sampling time of 5 seconds, whereas a 0.5 second sampling time applies to the electrical power signal. For the flowrate and power consumption, both the rate and total value are calculated within the sampling period.

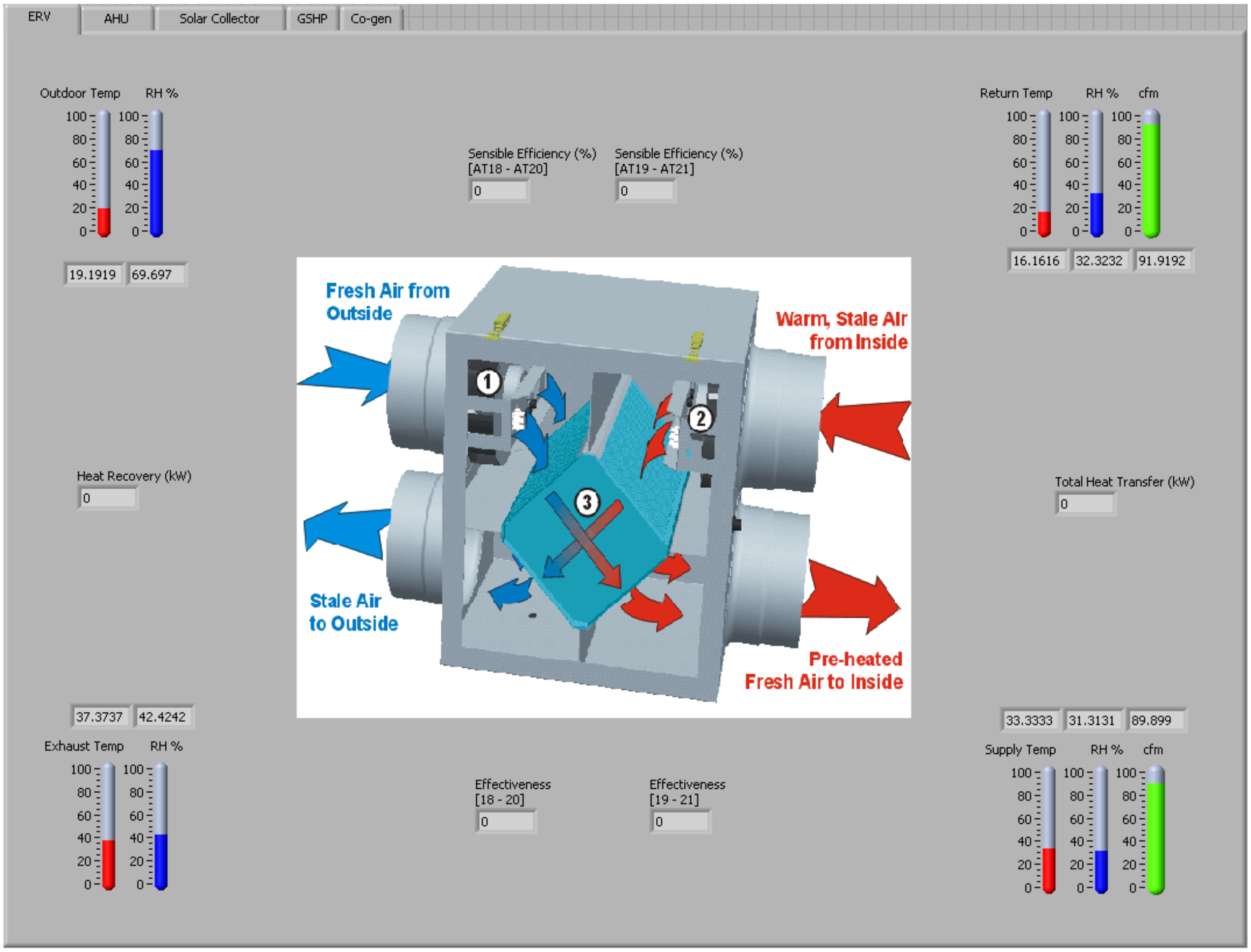

Figure 3.8 Snapshot of LabVIEW front panel

3.5.2 SQL Server Management Studio (SSMS): It is a relational database management system. The user can easily store, retrieve, and manipulate data in this software. Although storage capacity depends on the hard drive, this software has the database capacity of 524272 TB (Terabyte) (SQL Server, 2008)[I]. In this monitoring system, all data from the LabVIEW program are stored into the SQL server database directly. The database structure has three vertical columns which consists of Datestamp, Reading, and Channel. Hence, each row has three horizontal values. At 5 second intervals, each sensor captures 17285 rows/day data, equivalent to 356 KB (Kilobyte). Each day 300 sensors accumulate 107 MB (Megabyte) records. To deal with the large amount of data, this software has been selected.

[I] Retrieved from http://msdn.microsoft.com/en-us/library/ms143432.aspx

Chapter 4

Equations: Energy Consumption, Generation and Efficiency Calculation

For direct calculation in the LabVIEW software, basic equations of power, energy and efficiency of different equipment are illustrated. The sources of these basic equations are the ASHRAE handbooks, TRNSYS manual, different books and articles. In addition, some equations of density and specific heat of liquids, humidity ratio and enthalpy of air are also incorporated.

4.1 Water: Kravchenko (1966) stated that density of water is a function of temperature. He described Equation (1) for pure water density. From 0°C to 100°C, its density varies from 999.82 kg/m^3 to 950.05 kg/m^3. Tanaka et al., (2001) determined the experimental result of water density from 0°C to 40°C. This result is compared with Equation (1), and Figure 4.1 shows that there is a good agreement between the equation and experimental results. Hence, Equation (1) is applied for density of water in thermal energy equations. Specific heat does not change greatly with temperature from 0°C to 100°C and the constant value of water is considered 4.1813 $\frac{kJ}{kg.K}$.

$$\rho_{water} = \left[1 - \frac{(\mathrm{T}-4)^2}{(119000+1365\mathrm{T}-4\mathrm{T}^2)}\right] 1000 \qquad (1)$$

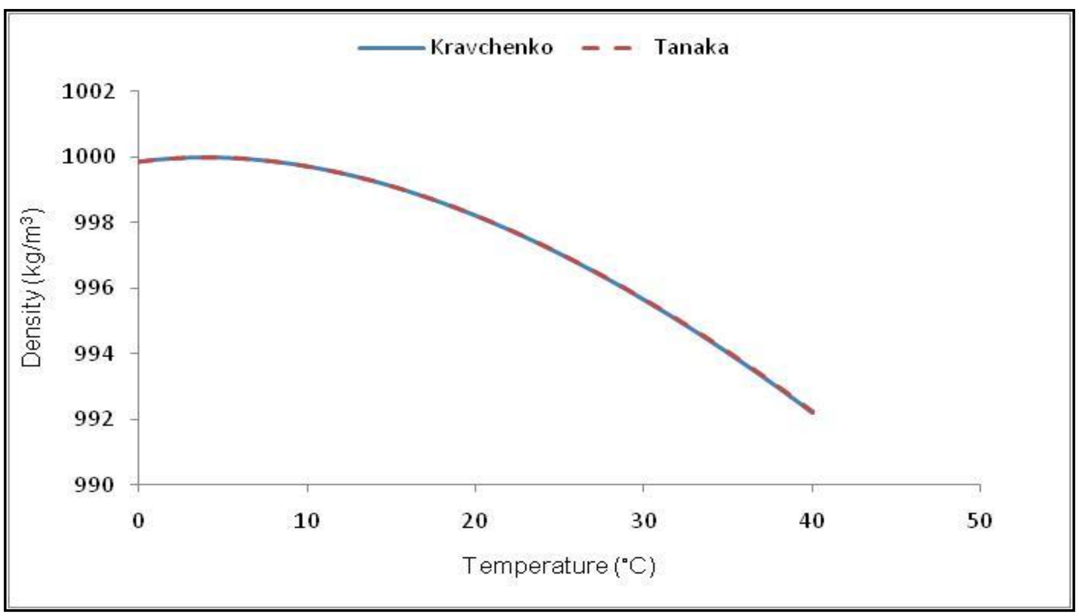

Figure 4.1 Comparison of water density with temperature by Kravchenko Equation (1) and Tanaka et al. data

4.2 Propylene Glycol (PG) solution: PG and water solution (45:55) is used in the solar loop as heat transfer media. From -12°C to 104°C, its density varies from 1060.46 kg/m^3 to 968.20 kg/m^3 and specific heat changes with temperature as well. The CHEM Group Inc[II] has supplied data for density and specific heat of PG. From this data, Equations (2) and (3) have been derived:

$$\rho_{PG} = (-0.0008\mathrm{T}^2 - 0.7184\mathrm{T} + 1051.3) \quad (2)$$

$$c_{PG} = [3.4 + 0.00393(\mathrm{T} + 30)] \quad (3)$$

The value of density is evaluated by Equation (2) and again compared with CHEM Group data. Figure 4.2 shows that there is a good agreement between CHEM group data and Equation (2) results.

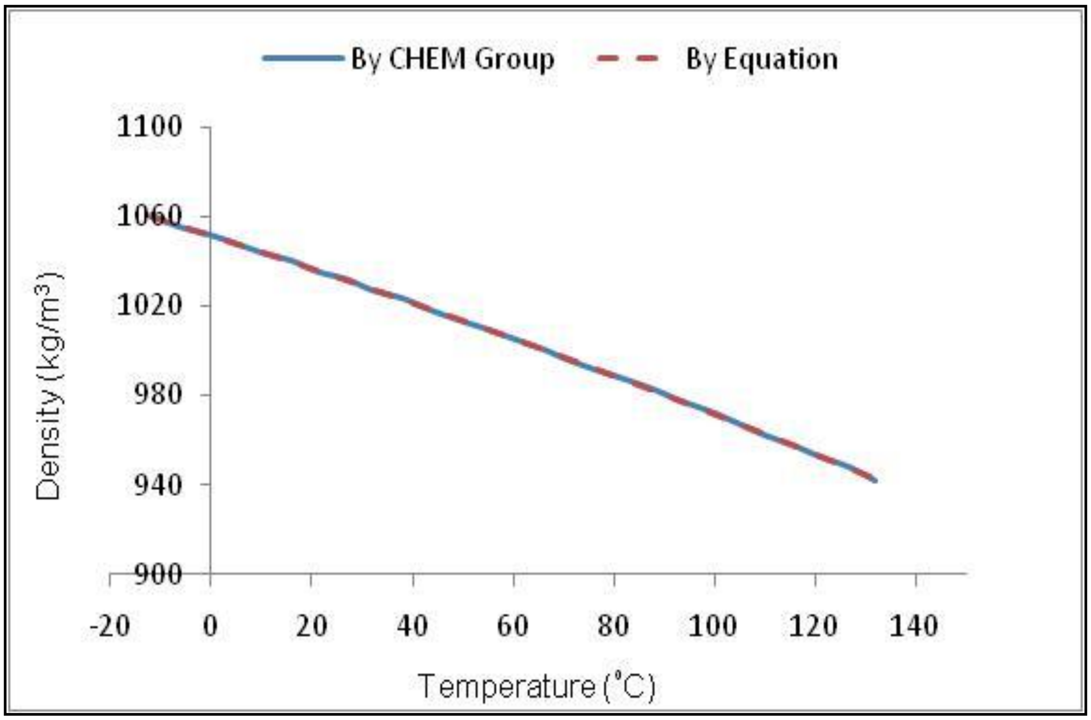

Figure 4.2 Comparison of PG density with temperature by CHEM Group data and equation result

4.3 Water and Propylene Glycol (PG) solution: This solution is used in the ground loop of GSHP. The solution consists of 70% water and 30% PG. The working temperature range

[II] CHEM Group Inc., Indiana, USA is a manufacturer of Propylene Glycol. Their glycol product is ASTM compliant.

of this solution might be from minimum 4°C (Legget and Peckover, 1949) to a maximum of 24°C (measured in the cooling season at site). Hence at low temperature range, the density of this solution (70:30) is considered as constant at 1026 kg/m^3 (based on available information of temperature 15.55°C) and its specific heat is 3.915 $\frac{kJ}{kg.K}$[III] (The Engineering ToolBox, 2005).

4.4 Air: There are available basic equations of enthalpy and humidity ratio in terms of dry bulb temperature and absolute humidity of air**.** Equations (4) and (5) are illustrated with dry bulb temperature and relative humidity of air (Padfield, 1996):

$$\text{Humidity ratio } (\omega) = 3.91 \times 10^{-5}\text{RH}(\%)e^{\frac{17.3016\text{AT}}{(\text{AT}+238.3)}} \quad (4)$$

$$\text{Enthalpy } (h) = (1.007\text{AT} - 0.026) + (2501.3 + 1.86\text{AT})\left[3.91 \times 10^{-5}\text{RH}(\%)e^{\frac{17.3016\text{AT}}{(\text{AT}+238.8)}}\right] \quad (5)$$

The values of humidity ratio and enthalpy are evaluated using Equations (4) and (5) in the monitoring system. These values are compared with the Psychrometric calculator (Psychrometric Calculations, n.d.) ranging from air temperature -30°C to 40°C (increment 5°C) and RH 0%, 20%, 40%, 60%, 80% 100%. There is a good agreement between these equations and the Psychrometric calculator. The comparison is shown in Figures C.1 – C.12 at Appendix-C.

Density of air changes with temperature. From -50°C to 40°C, its density varies from 1.534 to 1.127 kg/m^3 [IV]. Specific heat of air is constant at 1.006 kJ/(kg.K) between these temperatures. From these air densities, Equation (6) has been derived:

$$\rho_{\text{air}} = 7 \times 10^{-8}\text{AT}^3 + 8 \times 10^{-6}\text{AT}^2 - 4.6 \times 10^{-3}\text{AT} + 1.293 \quad (6)$$

It should be noted that all nomenclature of sensors and corresponding units are mentioned in Table 3.2. These units are followed in input values of all equations.

4.5 Energy Consumption, Generation and Efficiency Equations of Equipment in House-A:

4.5.1 Wall Mounted Mini-Boiler: Figure 4.3 shows the sensor locations of the boiler.

[III] Retrieved from http://www.engineeringtoolbox.com/propylene-glycol-d_363.html
[IV] Retrived from http://www.engineeringtoolbox.com/air-properties-d_156.html

1) Thermal power generation, $Q = \rho_{water}\, q\, c_{water}\, (T_{hot} - T_{cold})$. Put the value of ρ_{water} from Equation (1) and c_{water}. Hence, the value of

$$Q_1 = 0.264 FL_5 \left[\left\{ 1 - \frac{(T_9 - 4)^2}{(119000 + 1365 T_9 - 4T_9^2)} \right\} T_9 - \left\{ 1 - \frac{(T_{10} - 4)^2}{(119000 + 1365 T_{10} - 4T_{10}^2)} \right\} T_{10} \right] \qquad (7)^{V}$$

2) Boiler efficiency, $\square_1 = \frac{Q_1}{Gas\ flow\ rate\ (NG_1) \times \mathrm{HHV}} \times 100$ (8)

where Higher Heating Value (HHV) of Natural Gas[VI] = 37.8 $\frac{MJ}{m^3}$

4.5.2 Domestic Hot Water Tank (DHWT): Figure 4.4 shows the sensor locations of the Domestic Hot Water Tank.

1) Thermal power supplied by the boiler, $Q = \rho_{water}\, q\, c_{water}\, (T_{hot} - T_{cold})$. Put the value of ρ_{water} from Equation (1) and c_{water}. Hence, the value of

$$Q_2 = 0.264 FL_4 \left[\left\{ 1 - \frac{(T_7 - 4)^2}{(119000 + 1365 T_7 - 4T_7^2)} \right\} T_7 - \left\{ 1 - \frac{(T_8 - 4)^2}{(119000 + 1365 T_8 - 4T_8^2)} \right\} T_8 \right] \qquad (9)$$

2) Thermal power supplied from the DHWT to the load, $Q = \rho_{water}\, q\, C_{pWater}\, (T_{hot} - T_{cold})$. Put the value of ρ_{water} from Equation (1) and c_{water}. Hence, the value of

$$Q_3 = 0.264 FL_3 \left[\left\{ 1 - \frac{(T_1 - 4)^2}{(119000 + 1365 T_1 - 4T_1^2)} \right\} T_1 - \left\{ 1 - \frac{(T_3 - 4)^2}{(119000 + 1365 T_3 - 4T_3^2)} \right\} T_3 \right] \qquad (10)$$

[V] Constant value, 0.264 = Sp. Heat of water (4.1813 kJ/kg.K)×GPM(0.227 m^3/h)×1000/3600 sec from eq. (1)
[VI] High Heating Value of Natural Gas is taken from Union Gas website (http://www.uniongas.com/aboutus/aboutng/composition.asp)

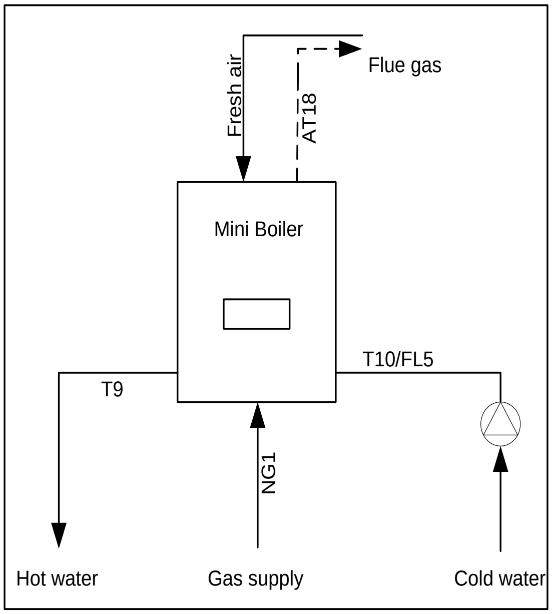

Figure 4.3 Mini-boiler

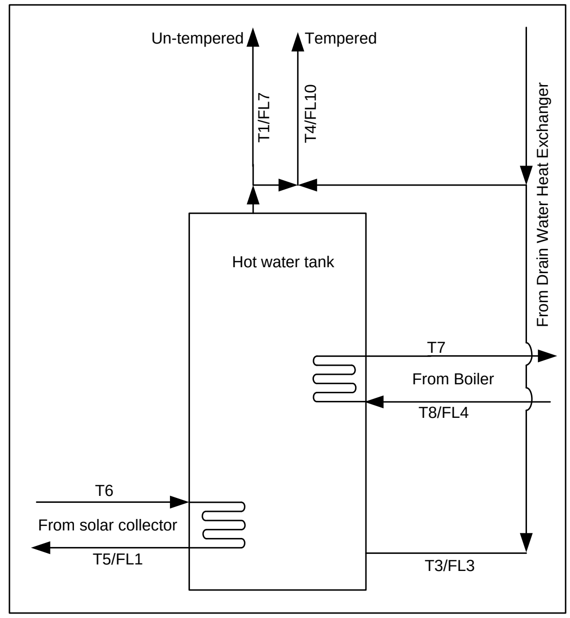

Figure 4.4 DHWT

4.5.3 Heat Recovery Ventilator (HRV): Figure 4.5 shows the sensor locations of the Heat Recovery Ventilator.

1) Amount of heat recovery, $Q = \rho_{air}\, q\, c_{air}\, (AT_{in} - AT_{out})$. Put the value of ρ_{air} and $c_{air,}$ hence the value of

$$Q_4 = 4.75 \times 10^{-4} AF_8(\rho_{11}AT_{11} - \rho_8 AT_8) \qquad (11)^{VII}$$

2) Efficiency, $\square_2 = = \frac{AF_8(\rho_{11}AT_{11} - \rho_8 AT_8)}{AF_{min}(\rho_{10}AT_{10} - \rho_8 AT_8)} \times 100 = \frac{AF_9(\rho_{10}AT_{10} - \rho_9 AT_9)}{AF_{min}(\rho_{10}AT_{10} - \rho_8 AT_8)} \times 100$ (12)

where according to Equation (6)

$$\rho_{11} = 7 \times 10^{-8} AT_{11}^3 + 8 \times 10^{-6} AT_{11}^2 - 4.6 \times 10^{-3} AT_{11} + 1.293$$

$$\rho_8 = 7 \times 10^{-8} AT_8^3 + 8 \times 10^{-6} AT_8^2 - 4.6 \times 10^{-3} AT_8 + 1.293$$

$$\rho_{10} = 7 \times 10^{-8} AT_{10}^3 + 8 \times 10^{-6} AT_{10}^2 - 4.6 \times 10^{-3} AT_{10} + 1.293$$

and $\rho_9 = 7 \times 10^{-8} AT_9^3 + 8 \times 10^{-6} AT_9^2 - 4.6 \times 10^{-3} AT_9 + 1.293$

[VII] Constant value, 4.75×10^{-4} = Sp. heat (1.006 kJ/kg.K) ×CFM (1/2119 m^3/sec)

4.5.4 Flat Plate Solar Collector (FPSC): Figure 4.6 shows the sensor locations of the FPSC.

1) Heat collection, $Q = \rho_{PG}\, q\, c_{pG}\, (T_{hot} - T_{cold})$. Put the value of ρ_{PG} from Equation (2) and $c_{PG,}$ from Equation (3), hence the value of

$$Q_5 = 6.31 \times 10^{-5} FL_1[\{-8 \times 10^{-4} T_6^2 - 7.184 \times 10^{-1} T_6 + 1051.3\}\{3.4 + 3.93 \times 10^{-3}(T_6 + 30)\}T_6 - \{-8 \times 10^{-4} T_5^2 - 7.184 \times 10^{-1} T_5 + 1051.3\}\{3.4 + 3.93 \times 10^{-3}(T_5 + 30)\}T_5] \quad (13)^{VIII}$$

2) Efficiency of collector[IX], $\eta = \frac{Q_5}{AI_T}$

So, $\square_3 = \frac{398.41\, Q_5}{I_T} \times 100$ (14)

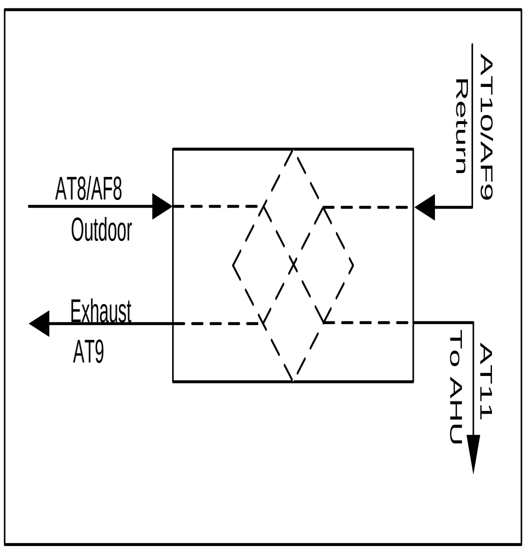

Figure 4.5 HRV

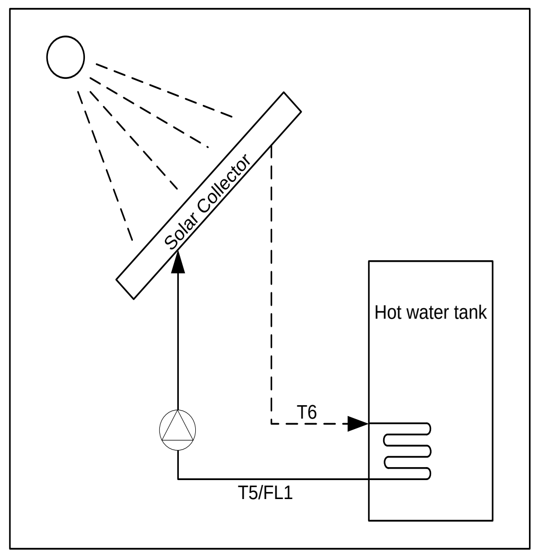

Figure 4.6 FPSC

4.5.5 Drain Water Heat Exchanger: Figure 4.7 shows the sensor locations of the Drain Water Heat Exchanger.

[VIII] Constant value, 6.31×10^{-5} = GPM ($0.227\ m^3/h$)/3600 sec

[IX] A= Gross collector area = 2.51 m^2, PYRANOMETER gives global solar radiation (Direct plus Diffuse) in W/m^2 and constant value, 398.41 = 1000/[Area of collector (2.51 m^2)]

1) Amount of heat recovery, Q = ρ_{water} q c_{water} (T_{hot}-T_{cold}). Put the value of ρ_{water} from Equation (1) and c_{water}. Hence, the value of

$$Q_6 = 0.264FL_3\left[\left\{1-\frac{(T_{16}-4)^2}{(119000+1365T_{16}-4T_{16}^2)}\right\}T_{16}-\left\{1-\frac{(T_{15}-4)^2}{(119000+1365T_{15}-4T_{15}^2)}\right\}T_{15}\right] \quad (15)$$

2) Actual effectiveness, $\varepsilon_1 = \frac{C_3(T_{16}-T_{15})}{C_{min}(T_{13}-T_{15})} = \frac{Q_6}{Q_{max}}$ (16)

$$Q_{max} = 0.264FL_{min}\left[\left\{1-\frac{(T_{13}-4)^2}{(119000+1365T_{13}-4T_{13}^2)}\right\}T_{13}-\left\{1-\frac{(T_{15}-4)^2}{(119000+1365T_{15}-4T_{15}^2)}\right\}T_{15}\right]$$

and FL_{min}= minimum flow rate of FL_3 or FL_{11}

4.5.6 Air Handling Unit (AHU): Figure 4.8 shows the sensor locations of the Air Handling Unit.

1) Heat supplied from the boiler, Q = ρ_{water} q c_{water} (T_{hot}-T_{cold}). Put the value of ρ_{water} from Equation (1) and c_{water}. Hence, the value of

$$Q_7 = 0.264FL_9\left[\left\{1-\frac{(T_{18}-4)^2}{(119000+1365T_{18}-4T_{18}^2)}\right\}T_{18}-\left\{1-\frac{(T_{11}-4)^2}{(119000+1365T_{11}-4T_{11}^2)}\right\}T_{11}\right] \quad (17)$$

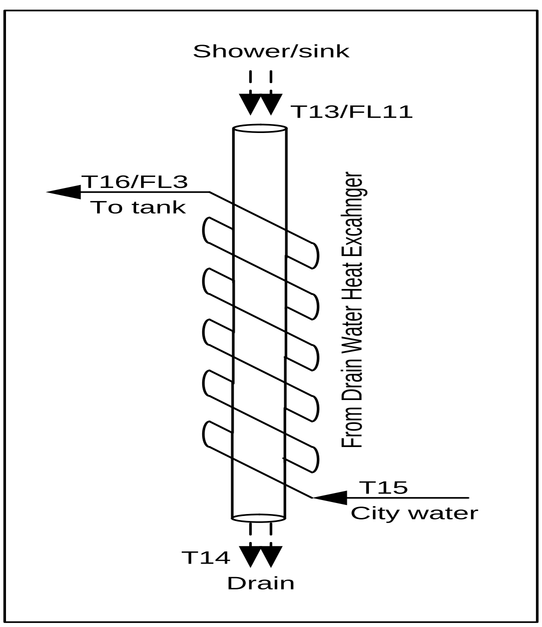

Figure 4.7 DWHE

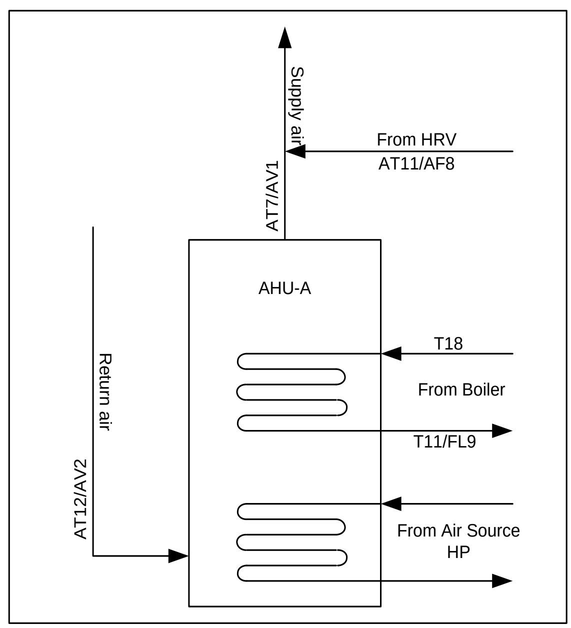

Figure 4.8 AHU

4.5.7 Two Stage Air-Source Heat Pump (TSASHP): Figure 4.8 shows the sensor locations of the TSASHP.

1) $COP_1 = \frac{Q_8}{Q_{Electrical}} = \frac{\rho_{air} AV\, A_{duct}(h_1 - h_2)}{Q_{Electrical}}$ (18)

where $Q_{Electrical}$ = electricity consumption of compressor, indoor and outdoor fan (kW)

Put the value of ρ_{air}, A_{duct}, and h from Equation (5). Hence the value of

$Q_8 =$

$$0.164 AV_1 \left\{ \rho_7 (1.007 AT_7 - 0.026) + (2501.3 + 1.86 AT_7) \left[3.91 \times 10^{-7} RH_7(\%) e^{\frac{17.3016 AT_7}{(AT_7 + 238.8)}} \right] - \rho_{12}(1.007 AT_{12} - 0.026) - (2501.3 + 1.86 AT_{12}) \left[3.91 \times 10^{-7} RH_{12}(\%) e^{\frac{17.3016 AT_{12}}{(AT_{12} + 238.8)}} \right] \right\} \quad (19)^{X}$$

where according to Equation (6)

$$\rho_7 = 7 \times 10^{-8} AT_7^3 + 8 \times 10^{-6} AT_7^2 - 4.6 \times 10^{-3} AT_7 + 1.293$$

and $\rho_{12} = 7 \times 10^{-8} AT_{12}^3 + 8 \times 10^{-6} AT_{12}^2 - 4.6 \times 10^{-3} AT_{12} + 1.293$

and $Q_{Electical} = (W_{Compressor} + W_{Indoor\ \&\ Outdoor\ Fan})$ (20)

4.6 Energy Consumption, Generation and Efficiency Equations of Equipment in House-B:

4.6.1 Domestic Hot Water Tank (DHWT): Figure 4.9 shows the sensor locations of the DHWT.

1) Thermal power supplied by the tank to the TOU tank, Q = ρ_{water} q c_{water} (T_{hot}-T_{cold}). Put the value of ρ_{water} from Equation (1) and c_{water}. Hence, the value of

$$Q_9 = 0.264(FL_2 - FL_5) \left[\left\{ 1 - \frac{(T_{out} - 4)^2}{(119000 + 1365 T_{out} - 4 T_{out}^2)} \right\} T_{out} - \left\{ 1 - \frac{(T_1 - 4)^2}{(119000 + 1365 T_1 - 4 T_1^2)} \right\} T_1 \right] \quad (21)$$

where $T_{Out} = \frac{(FL_2 T_{23} - FL_5 T_{19})}{(FL_2 - FL_5)}$ in (°C)

X Constant value, 0.164 = cross sectional area of supply air duct (0.164 m^2)

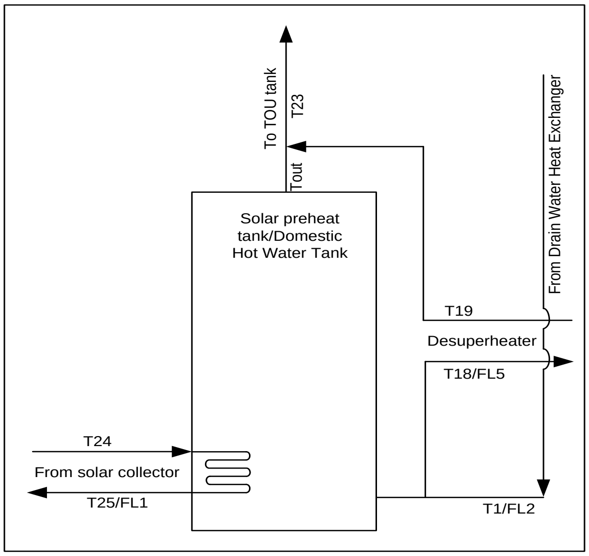

Figure 4.9 DHWT

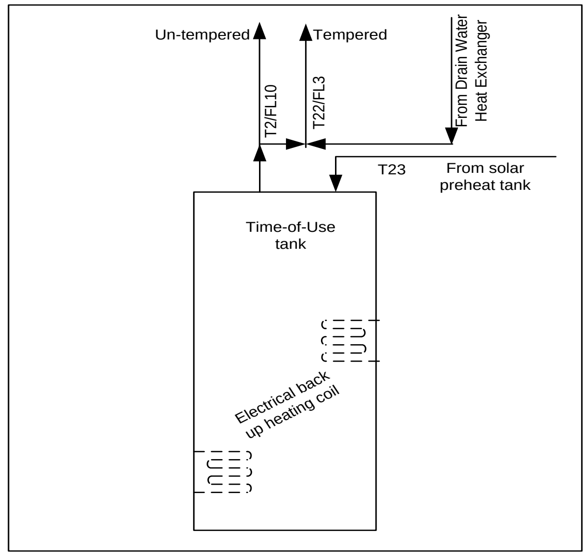

Figure 4.10 TOU

4.6.2 Time-of-Use (TOU) Tank: Figure 4.10 shows the sensor locations of the TOU Tank.

1) Thermal power supplied by the TOU tank to the load, $Q = \rho_{water}\ q\ c_{water}\ (T_{hot}\text{-}T_{cold})$. Put the value of ρ_{water} from Equation (1) and c_{water}. Hence, the value of

$$Q_{10} = 0.264(FL_2 - FL_5)\left[\left\{1 - \frac{(T_2-4)^2}{(119000+1365T_2-4T_2^2)}\right\}T_2 - \left\{1 - \frac{(T_{23}-4)^2}{(119000+1365T_{23}-4T_{23}^2)}\right\}T_{23}\right] \quad (22)$$

2) Efficiency (%) of tank, $\square_4 = \frac{Q_{10}}{\text{Electrical power input in kW}}$ (23)

4.6.3 Ground Source Heat Pump (GSHP): Figure 4.11 shows the sensor locations of the GSHP.

1) Heat supplied by the GSHP to the buffer tank, $Q = \rho_{water}\ q\ c_{water}\ (T_{hot}\text{-}T_{cold})$. Put the value of ρ_{water} from Equation (1) and c_{water}. Hence, the value of

$$Q_{11} = 0.264FL_6\left[\left\{1 - \frac{(T_{16}-4)^2}{(119000+1365T_{16}-4T_{16}^2)}\right\}T_{16} - \left\{1 - \frac{(T_{17}-4)^2}{(119000+1365T_{17}-4T_{17}^2)}\right\}T_{17}\right] \quad (24)$$

2) $COP_2 = \frac{Q_{11}}{Q_{Electrical}}$ (25)

where $Q_{Electical}(kW) = (W_{Compressor} + W_{ground\ loop\ pump})$

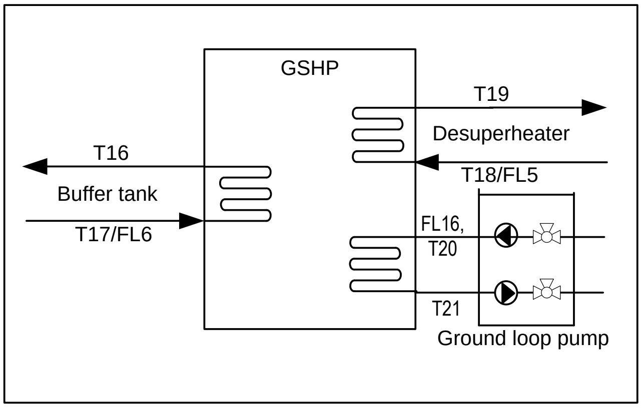

Figure 4.11 GSHP

For horizontal loop to HP:

3) Heat extraction/rejection, $Q_{12} = 0.253FL_{16}(T_{20} - T_{21})$ (26)[XI]

4.6.4 Drain Water Heat Exchanger: Figure 4.12 shows the sensor locations of the DWHE.

1) Amount of heat recovery Q = ρ_{water} q c_{water} (T_{hot}-T_{cold}). Put the value of ρ_{water} from Equation (1) and c_{water}. Hence, the value of

$$Q_{13} = 0.264FL_4\left[\left\{1 - \frac{(T_{26}-4)^2}{(119000+1365T_{26}-4T_{26}^2)}\right\}T_{26} - \left\{1 - \frac{(T_{30}-4)^2}{(119000+1365T_{30}-4T_{30}^2)}\right\}T_{30}\right] \quad (27)$$

2) Actual effectiveness, $\varepsilon_2 = \frac{C_4(T_{26}-T_{30})}{C_{min}(T_{28}-T_{30})} = \frac{Q_{13}}{Q_{max}}$ (28)

where C_4 = Capacity rate for the cold fluid = q ρ c_{water} (kJ/K.sec), C_{min} = smaller capacity rate (kJ/K.sec)

$$Q_{max} = 0.264FL_{min}\left[\left\{1 - \frac{(T_{28}-4)^2}{(119000+1365T_{28}-4T_{28}^2)}\right\}T_{28} - \left\{1 - \frac{(T_{30}-4)^2}{(119000+1365T_{30}-4T_{30}^2)}\right\}T_{30}\right]$$

and FL_{min} = minimum flow rate of FL_4 or FL_{11}

[XI] Constant value, 0.253 = Density of solution (Water:PG = 70:30) 1026 kg/m^3 × Sp. heat 3.915 kJ/(kg.K) × GPM (US) (0.227 m^3/h)/3600 sec

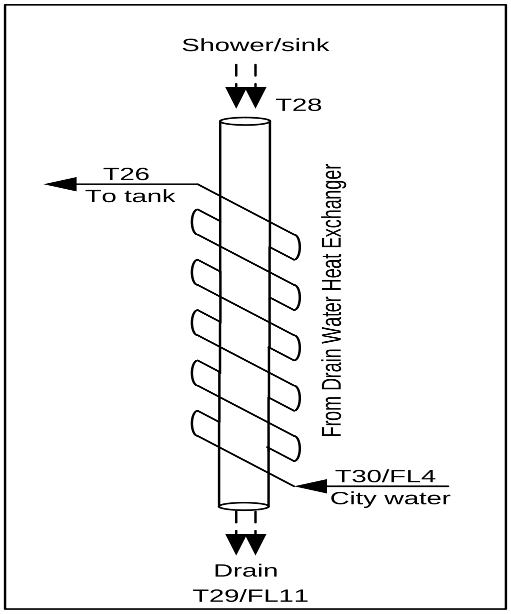

Figure 4.12 DWHE

4.6.5 Evacuated Tube Solar Collector (ETSC): Figure 4.13 shows the sensor locations of the ETSC.

1) Heat collection, Q = ρ_{PG} q c_{PG} (T_{hot} – T_{cold}). Put the value of ρ_{PG} from Equation (2) and $c_{PG,}$ from Equation (3), hence the value of

$$Q_{14} = 6.31 \times 10^{-5} FL_1 [\{-8 \times 10^{-4} T_{24}^2 - 7.184 \times 10^{-1} T_{24} + 1051.3\}\{3.4 + 3.93 \times 10^{-3}(T_{24} + 30)\} T_{24} - \{-8 \times 10^{-4} T_{25}^2 - 7.184 \times 10^{-1} T_{25} + 1051.3\}\{3.4 + 3.93 \times 10^{-3}(T_{25} + 30)\} T_{25}] \quad (29)$$

2) Efficiency of collector, $\eta = \frac{Q_{14}}{AI_T}$

$$\square_5 = \frac{487.80 Q_{14}}{I_T} \times 100 \quad (30)$$ [XII]

[XII] A= Absorber area of collector = 2.05 m^2, PYRANOMETER gives global solar radiation (direct plus diffuse) in W/m^2 and constant value, 487.80 = 1000/[Area of collector (2.88 m^2)]

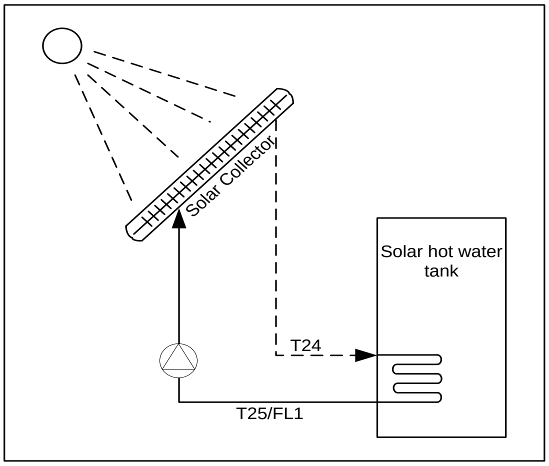

Figure 4.13 ETSC

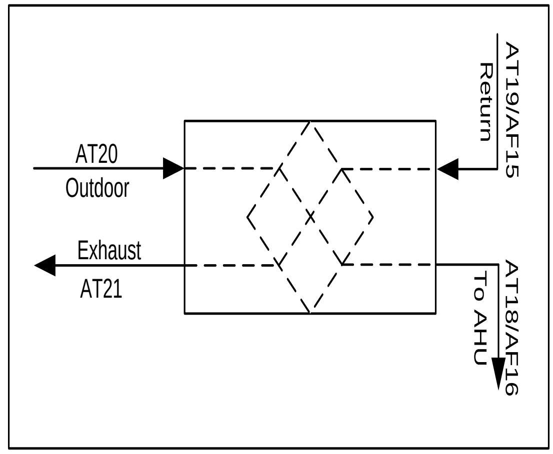

Figure 4.14 ERV

4.6.6 Energy Recovery Ventilator (ERV): Figure 4.14 shows the sensor locations of the ERV.

1) Amount of heat recovery, $Q_{sensible} = \rho_{air}\, q\, c_{air}\, (AT_{in} - AT_{out})$. Put the value of ρ_{air} and $c_{air,}$ hence the value of

$$Q_{15} = 4.75 \times 10^{-4} \mathrm{AF}_{16}(\rho_{18}\mathrm{AT}_{18} - \rho_{20}\mathrm{AT}_{20}) \tag{31}$$

q = airflow rate = $\frac{\mathrm{CFM}}{2119} \quad \frac{m^3}{sec}$

c_{air} = specific heat of air = 1.006 kJ/(kg.K)

2) Sensible efficiency, $\square_6 = \frac{\mathrm{AF}_{16}(\rho_{18}\mathrm{AT}_{18} - \rho_{20}\mathrm{AT}_{20})}{\mathrm{AF}_{\min}(\rho_{19}\mathrm{AT}_{19} - \rho_{20}\mathrm{AT}_{20})} \times 100 = \frac{\mathrm{AF}_{15}(\rho_{19}\mathrm{AT}_{19} - \rho_{21}\mathrm{AT}_{21})}{\mathrm{AF}_{\min}(\rho_{19}\mathrm{AT}_{19} - \rho_{20}\mathrm{AT}_{20})} \times 100$ (32)

where according to Equation (6)

$$\rho_{18} = 7 \times 10^{-8}\mathrm{AT}_{18}^3 + 8 \times 10^{-6}\mathrm{AT}_{18}^2 - 4.6 \times 10^{-3}\mathrm{AT}_{18} + 1.293$$

$$\rho_{20} = 7 \times 10^{-8}\mathrm{AT}_{20}^3 + 8 \times 10^{-6}\mathrm{AT}_{20}^2 - 4.6 \times 10^{-3}\mathrm{AT}_{20} + 1.293$$

$$\rho_{19} = 7 \times 10^{-8}\mathrm{AT}_{19}^3 + 8 \times 10^{-6}\mathrm{AT}_{19}^2 - 4.6 \times 10^{-3}\mathrm{AT}_{19} + 1.293$$

and $\rho_{21} = 7 \times 10^{-8}\mathrm{AT}_{21}^3 + 8 \times 10^{-6}\mathrm{AT}_{21}^2 - 4.6 \times 10^{-3}\mathrm{AT}_{21} + 1.293$

$$\varepsilon = \frac{\text{Actual transfer (of moisture or energy)}}{\text{Maximum possible transfer between airstreams}}$$

Referring to Figure 4.14,

$$\varepsilon_3 = \frac{AF_{16}(\rho_{18}\omega_{18}-\rho_{20}\omega_{20})}{AF_{min}(\rho_{19}\omega_{19}-\rho_{20}\omega_{20})} = \frac{AF_{15}(\rho_{19}\omega_{19}-\rho_{21}\omega_{21})}{AF_{min}(\rho_{19}\omega_{19}-\rho_{20}\omega_{20})} \quad (33)$$

So, latent effectiveness or latent efficiency, $\varepsilon_3 = \frac{AF_{16}(\rho_{18}\omega_{18}-\rho_{20}\omega_{20})}{AF_{min}(\rho_{19}\omega_{19}-\rho_{20}\omega_{20})}$. Put the value of ω from Equation (4), hence the value of

$$\varepsilon_3 = \frac{AF_{16}[\rho_{18}RH18\exp\left(\frac{17.3016AT18}{AT18+238.3}\right)-\rho_{20}RH20\exp\left(\frac{17.3016AT20}{AT20+238.3}\right)]}{AF_{min}[\rho_{19}RH19\exp\left(\frac{17.3016AT19}{AT19+238.3}\right)-\rho_{20}RH20\exp\left(\frac{17.3016AT20}{AT20+238.3}\right)]} \quad (34)$$

$Q_{total} = \rho q\,(h_{in} - h_{out})$

$$Q_{total} = Q_{16} = 4.72\times10^{-4}AF_{16}(\rho_{18}h_{18}-\rho_{20}h_{20}) \quad (35)$$

where, according to Equation (5),

$$h_{20} = (1.007AT_{20} - 0.026) + (2501.3 + 1.86AT_{20})\left[3.91\times10^{-5}RH_{20}e^{\frac{17.3016AT_{20}}{(AT_{20}+238.8)}}\right]\ \frac{kJ}{kg}$$

$$h_{18} = (1.007AT_{18} - 0.026) + (2501.3 + 1.86AT_{18})\left[3.91\times10^{-5}RH_{18}e^{\frac{17.3016AT_{18}}{(AT_{18}+238.8)}}\right]\ \frac{kJ}{kg}$$

and RH = 0.01RH%

5) Sensible Heat Recovery Ratio (SHR) = $\frac{Q_{sensible}}{Q_{total}}$

6) Total efficiency, $\varepsilon_{tot} = \frac{AF\,\rho\,\Delta h}{AF_{tot}\rho_{tot}\Delta h_{tot}} = \frac{AF_{16}(\rho_{18}h_{18}-\rho_{20}h_{20})}{AF_{min}(\rho_{19}h_{19}-\rho_{20}h_{20})}$ (36)

where according to Equation (5),

$$h_{19} = (1.007AT_{19} - 0.026) + (2501.3 + 1.86AT_{19})\left[3.91\times10^{-5}RH_{19}e^{\frac{17.3016AT_{19}}{(AT_{19}+238.8)}}\right]\ \frac{kJ}{kg}$$

4.6.7 Air Handling Unit (AHU): Figure 4.15 shows the sensor locations of the AHU.

1) Heat supplied to AHU, $Q = \rho_{water}\, q\, c_{water}\,(T_{hot} - T_{cold})$. Put the value of ρ_{water} from Equation (1) and c_{water}. Hence, the value of

$$Q_{17} = 0.264FL_8\left[\left\{1-\frac{(T_{14}-4)^2}{(119000+1365T_{14}-4T_{14}^2)}\right\}T_{14} - \left\{1-\frac{(T_{13}-4)^2}{(119000+1365T_{13}-4T_{13}^2)}\right\}T_{13}\right] \quad (37)$$

4.6.8 Solar Wall: Figure 4.16 shows the sensor locations of the Solar Wall.

1) Rate of heat flow by ventilation of the air gap, $Q_V = 2\rho_{air}\, q\, c_{air}\,(T_m - T_{room})$. Put the value of ρ_{air} and c_{air}, hence the value of

$$Q_V = Q_{18} = 9.5 \times 10^{-4} AF_4(\rho_7 AT_7 - \rho_8 AT_8) \quad (38)^{XIII}$$

where according to Equation (6)

$$\rho_7 = 7 \times 10^{-8} AT_7^3 + 8 \times 10^{-6} AT_7^2 - 4.6 \times 10^{-3} AT_7 + 1.293$$

$$\rho_8 = 7 \times 10^{-8} AT_8^3 + 8 \times 10^{-6} AT_8^2 - 4.6 \times 10^{-3} AT_8 + 1.293$$

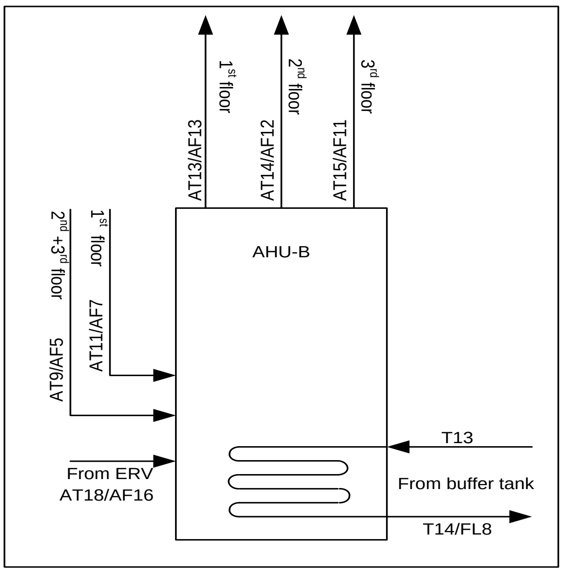

Figure 4.15 AHU

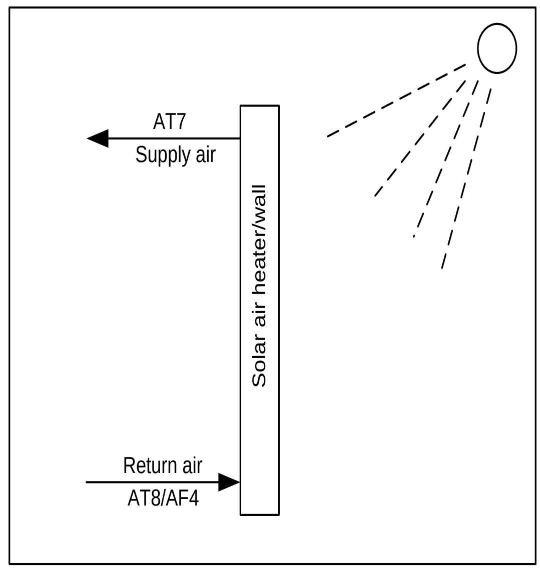

Figure 4.16 Solar wall

4.6.9 PV Cell:

1) Efficiency, $\eta = \frac{P_{out}}{P_{in}} = \frac{\text{Cell output (W)}}{I_T A_{cell}}$ (39)

where P_{out} = Power generation by the PV array in Watt

P_{in} = Product of the radiation of incident light in W/m^2 × surface area of solar cell (m^2).

Total A_{Cell} = 31.0968 m^2 [each cell = (125 × 125 mm^2 – 200 mm^2 = 15425 mm^2), each module = 42 cells, total modules = 48 nos.]

Total module capacity = 4.08 kW (48 modules × 85 W/module)

So, maximum efficiency at STC[XIV], $\square_7 = \frac{4080}{1000x31.0968} \times 100$ = 13.12%

[XIII] Constant 9.5×10^{-4} = 2× sp. heat of air (1.006 kJ/kg.K) ×CFM (1/2119 m^3/sec)

[XIV] STC = Standard Test Condition, i.e., at 25°C, solar irradiance is 1000 W/m^2

4.6.10 Whispergen Micro Combined Heat and Power (CHP) Unit: Figure 4.17 shows the sensor locations of the CHP Unit.

1) Thermal power generation, $Q = \rho_{water}\, q\, c_{water}\,(T_{hot} - T_{cold})$. Put the value of ρ_{water} from Equation (1) and c_{water}. Hence, the value of

$$Q_{19} = 0.264FL_{17}\left[\left\{1-\frac{(T_{32}-4)^2}{(119000+1365T_{32}-4T_{32}^2)}\right\}T_{32}-\left\{1-\frac{(T_{31}-4)^2}{(119000+1365T_{31}-4T_{31}^2)}\right\}T_{31}\right] \quad (40)$$

2) Electrical Efficiency[XV], $\square_8 = \frac{\text{Electrical output (kW)}}{\text{Fuel input (kW)}}\times 100$ (41)

2) Thermal Efficiency, $\square_9 = \frac{Q_{19}}{\text{Fuel input (kW)}}\times 100$ (42)

3) Overall Efficiency, $\square_{10} = \frac{[Electrical\ output\ (kW) + Thermal\ output\ (kW)]}{Fuel\ input\ (kW)}\times 100$ (43)

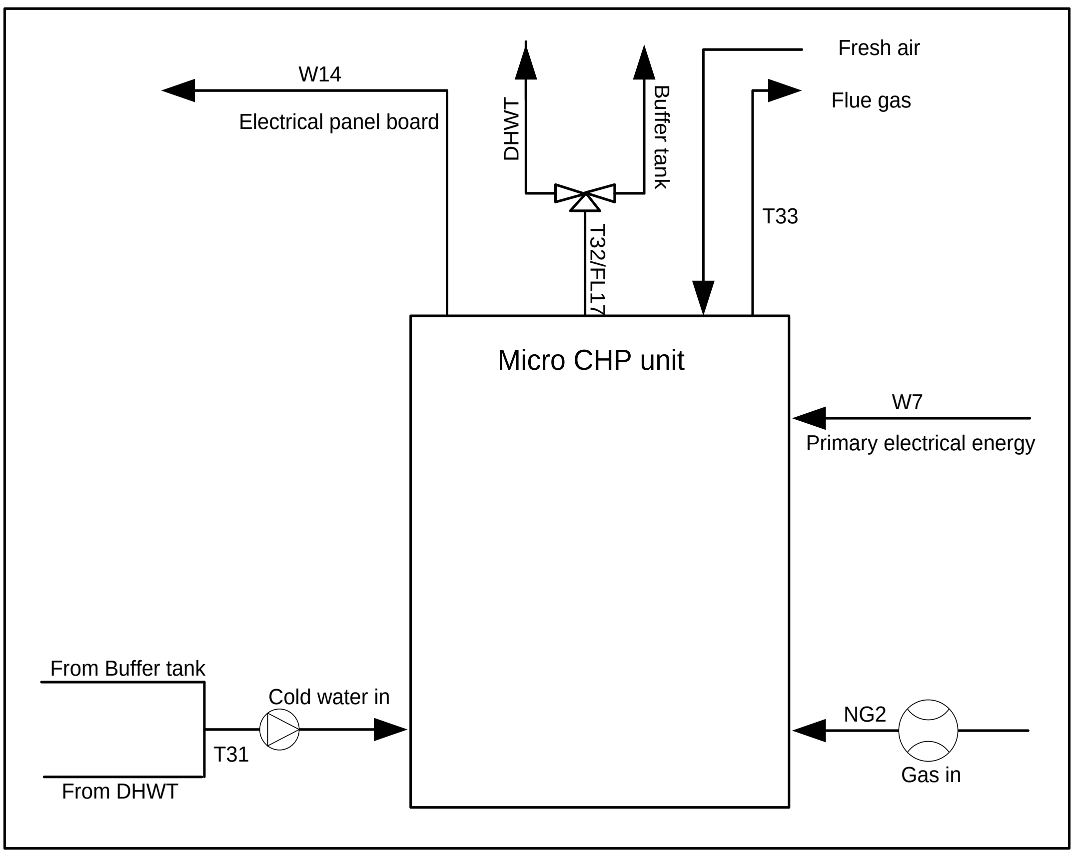

Figure 4.17 CHP unit

[XV] Fuel input = Higher heating value (37,800 kJ/m^3) × Litre/min [1/(60 sec)]×(1/1000) m^3= 0.63 NG_2 kW

Chapter 5

Data analysis

No occupant will live in the twin houses due to the nature of the project. However, the houses are open to the public for visit, and staff can work inside during the day. Therefore, both houses have occupants on the weekdays. The real time data being collected is similar to that in the typical family environment except household activities such as cooking, bathing and laundry. Simulated occupancy system is being implemented with typical residential conditions.

The following main factors are considered for system performance analysis (Efficiency Valuation Organization, 2007):

- outdoor and indoor temperature
- time intervals in seconds, hours or days

5.1 Energy Recovery Ventilator (ERV)

A tight building envelope system is often used in modern houses for energy conservation. Due to the reduction of infiltration in the air tight house, a proper mechanical ventilation system is essential for adequate indoor air quality and human comfort. The ASHRAE standard 62.2 (ASHRAE, 1999) recommends the minimum ventilation rate through the introduction of air-to-air heat recovery system. Typical air heat recovery systems are Heat Recovery Ventilator (HRV) and Energy Recovery Ventilator (ERV), which can filter fresh air, increase or decrease air temperature and/or humidity. An ERV is installed in House-B that can exchange both heat and moisture. Figure 5.1 shows that it consists of a polypropylene heat recovery core, air filters, and a single motor driven inlet and exhaust fan. In the heating season, a heat recovery core captures the heat and humidity from the stale air, and partly transfers them, to the incoming cold fresh air, thus avoiding the dryness problem and providing human comfort as well as saving energy. In the cooling season, the unit reverses the process, preventing the humidity from the outside air from entering the house. This unit totally blocks cross-stream transfer of air, pollutants, biological contaminants, and particulates from the stale air. It also prevents frost formation on the heat exchanger core when the outdoor temperature is below $0^{\circ}C$ ($32^{\circ}F$). To do this, the unit is programmed to defrost the recovery core. During the defrost cycle, the unit operates at maximum speed and the dampers close. According to the manual, the duration of defrost cycling is 6 minutes. The defrost frequency varies according to the outdoor temperature.

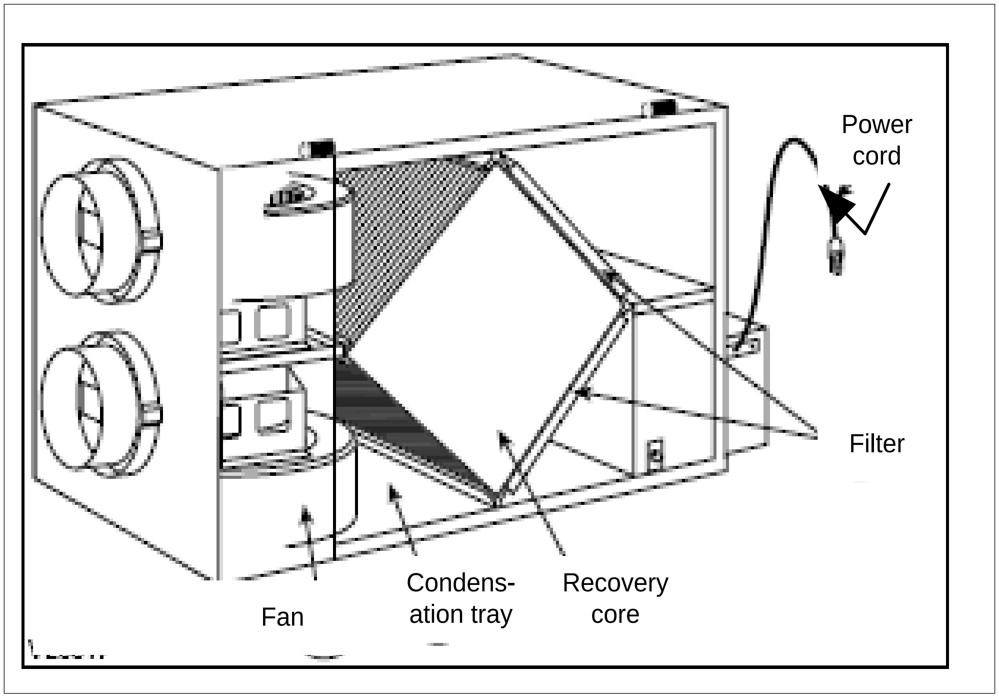

Figure 5.1 Main components of an energy recovery ventilator (ERV) (modified from Vanee ERV manual)

Figure 5.2 shows the daily average indoor/outdoor temperatures and relative humidity from January 6 to 25, 2010. It was found that the average outdoor RH was 71% when the average temperature was -4.05°C (24.71°F). The absolute amount of moisture or water vapour in the cold air was only 2.59 g/m^3 (1.62×10^{-4} lb/ft^3). If the ERV were not installed, the incoming air would be extremely dry with only 13% RH at room temperature. With the ERV, moisture from the exhaust air was transferred to the incoming low moisture fresh air, and the RH value rose to 27%.

According to ASHRAE Standard 62.2-2007, Walker and Sherman (2007) showed that the minimum ventilation rate can be determined from Equation (44).

$$AF(CFM) = 0.01A_{floor}(ft^2) + 7.5(N+1) \quad (44)$$

From Equation (44), the ventilation rate for this 3-bedroom residential house should not be less than 64 CFM (30 L/s) and the optimum humidity range for human comfort should be 30%-60% (ASHRAE, 2000). However, as shown in Figure 5.2, indoor RH remains below 30% for that period. The possible reasons of low RH value can be attributed to: a) high air exchange rate at low outdoor temperature, and b) low internal moisture generation (Walker and Sherman, 2007). It is worth noting that the ventilation rate through the variable speed ERV was kept at 148 CFM (70 L/s) during that period, which is high for a non-occupied house. The light human activity inside the house cannot provide sufficient moisture generation. Figures 5.3 and 5.4 show the sensible/latent heat recovery with respect to the indoor-outdoor conditions. As can be seen, the sensible heat recovery increases linearly as the dry bulb temperature difference increases. The latent heat recovery shows a similar trend with respect to the specific humidity difference, although a small discrepancy was observed.

The supply and return air flow rate of ERV are not balanced. The average supply air flow rate is 1.14 times higher than the return air flow. The reasons for unbalanced air flow are mentioned in Chapter 6 section 8. To calculate efficiency, supply and return air flow rates are considered balanced. Figures 5.5 and 5.6 show the comparison of measured sensible/latent efficiency with manufacturer supplied data. In both figures, measured values are higher than the manufacturer values and differences increase with the decrease of outdoor temperature. The measured and manufacturer values of latent efficiency in Figure 5.6 are very close to each other.

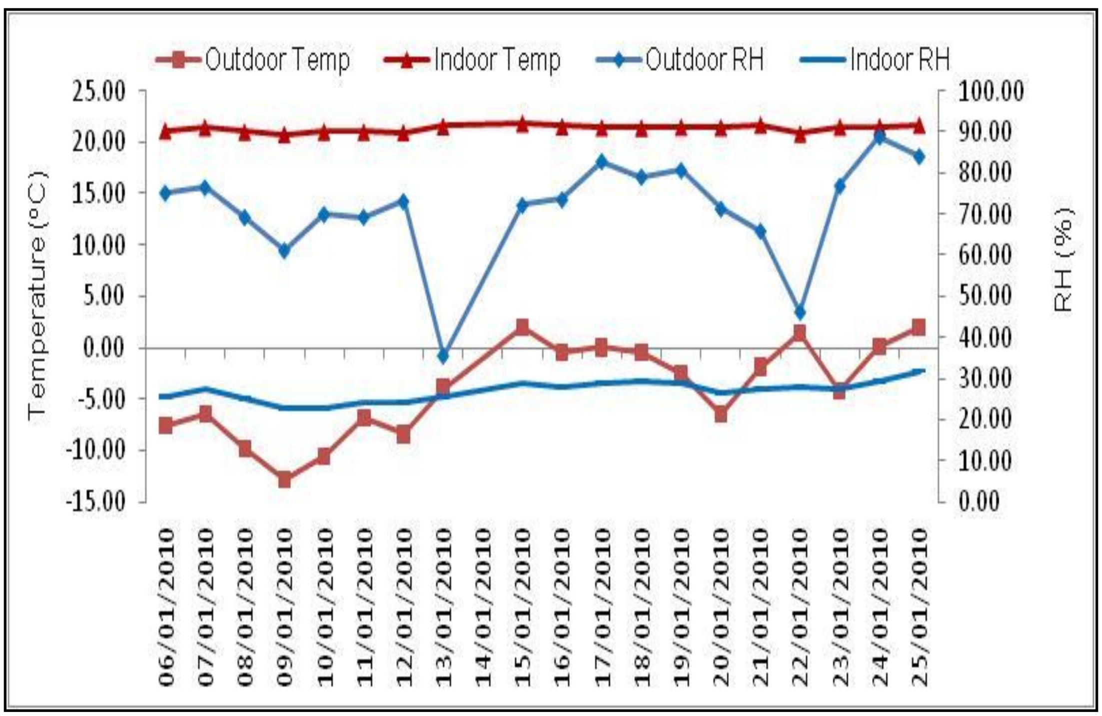

Figure 5.2 Daily average indoor-outdoor temperature and relative humidity during January 6-25, 2010

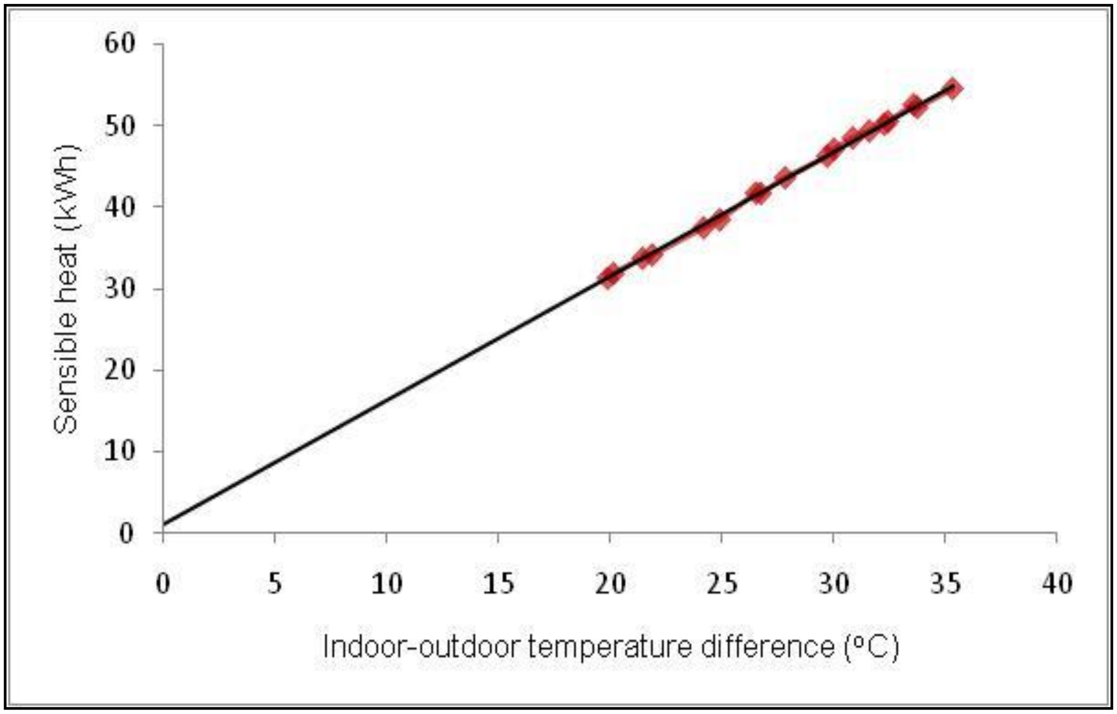

Figure 5.3 Sensible heat recoveries via ERV vs. daily average indoor-outdoor temperature difference from December 23, 2009 to January 11, 2010

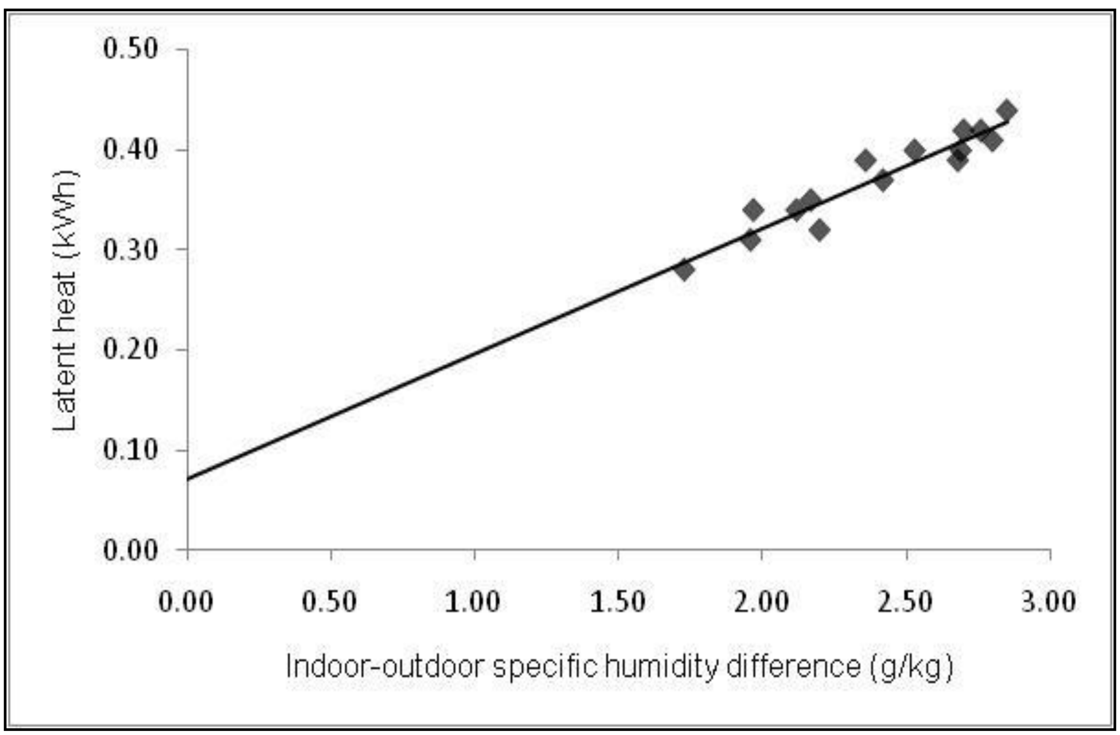

Figure 5.4 Latent heat recoveries via ERV vs. daily average indoor-outdoor specific humidity difference from December 23, 2009 to January 11, 2010

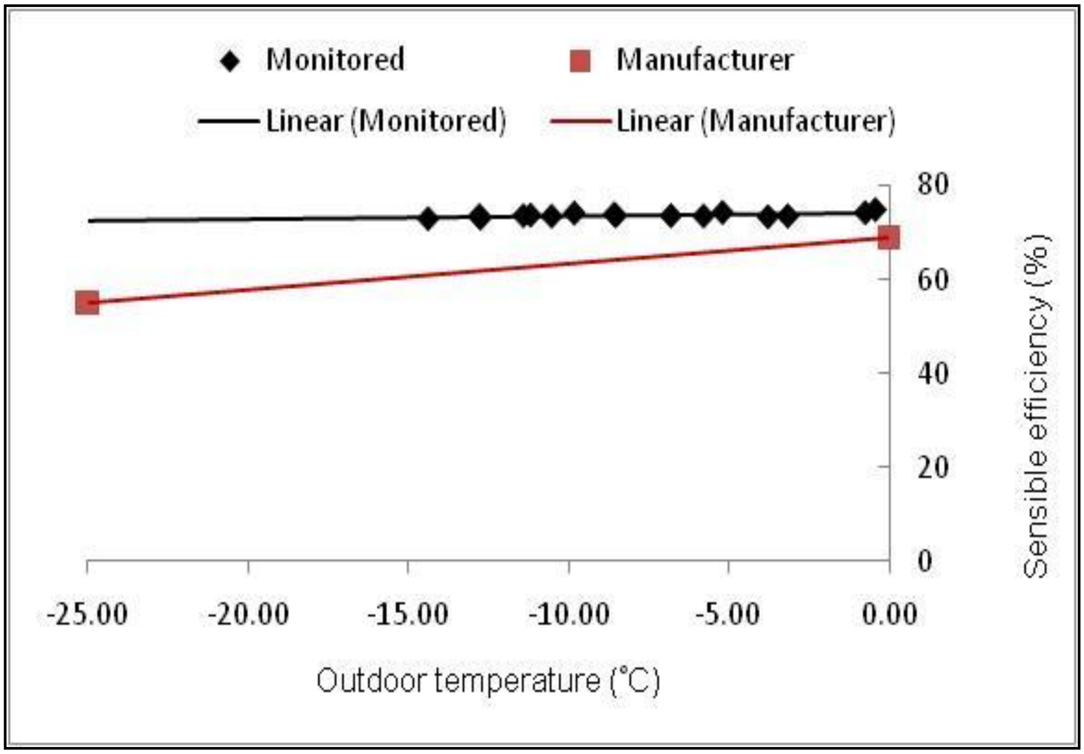

Figure 5.5 Comparison of sensible efficiency of ERV from December 23, 2009 to January 11, 2010 between monitored and manufacturer data

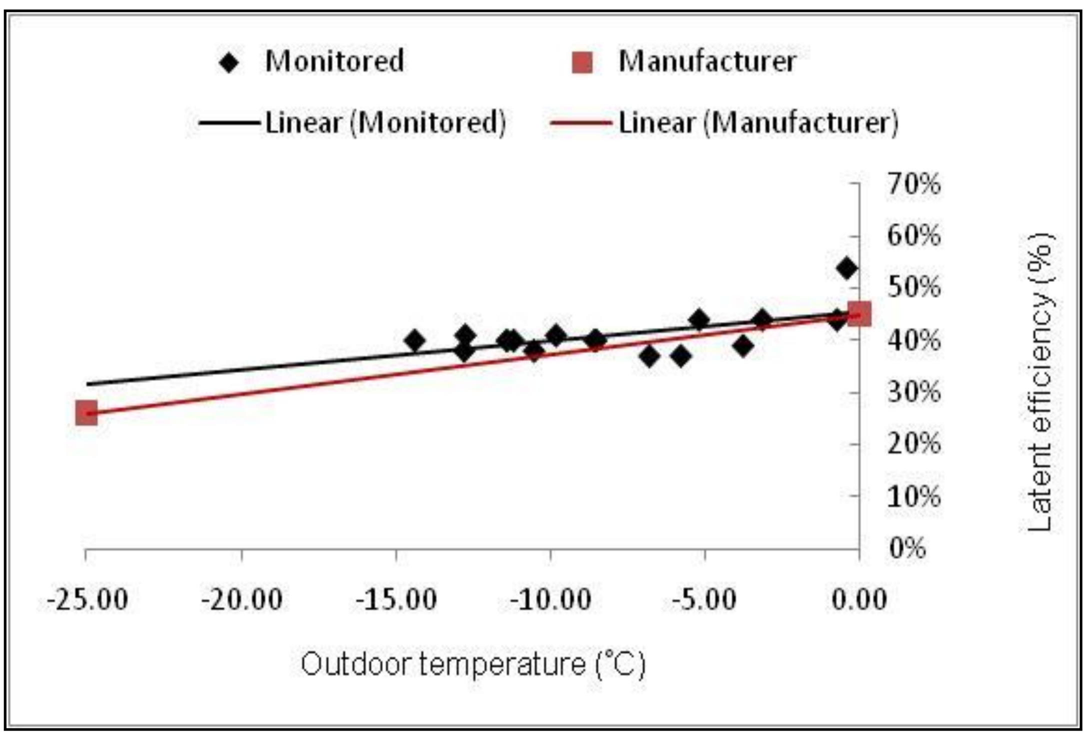

Figure 5.6 Comparison of latent efficiency of ERV from December 23, 2009 to January 11, 2010 between monitored and manufacturer data

5.2 In-floor radiant heating

In-floor radiant heating is a method of heating the space by applying heat underneath or within the floor. Olesen (2002) mentioned that a carpet is not necessary when using this system for space heating, which eliminates a source of pollutants. This is especially helpful for people with allergies. It was also mentioned that in a study, the German Allergy and Asthma Association has shown that this space heating system reduced the favourable living conditions for house dust mites compared to other heating systems. Elovitz (2001) stated that radiant in-floor heat is less prone to stratification but in other space heating systems, the hot air near the ceiling increases as the local indoor-outdoor temperature difference increases. Hence, claims that radiant heat produces appreciable savings by reducing temperature stratification. For space heating in House-B, a radiant in-floor heating system is used in all floors. Figure 5.7 shows the "thin slab over frame floor" system that is used on the 1st, 2nd and 3rd floor of House B. A set of 1.25 cm (0.5 inch) diameter PEX (cross-linked polyethylene) tubing was stapled on the plywood subfloor at 23 cm (9.05 inch) centre to centre distance in the 6.5 cm (2.56 inch) thick cement slab. On top of the cement slab, a 1.5 cm (0.59 inch) thick finished wood floor was installed (Barua et al., 2010). Figure 5.8 shows that the in-floor radiant heating system maintained indoor temperature in winter at around 21°C (69.8°F). This is controlled by an actuator, which has a series of valves that control the hot water flow from the buffer tank to different zones as required. The actuator is operated by the controller, following a demand from the thermostat which makes a decision based on the indoor-outdoor temperature difference. The buffer tank holds warm water at constant temperature around 40°C (105°F) during the heating season.

As shown in Figure 5.9, the space heating increases with the increase of indoor-outdoor temperature difference. Figure 5.10 shows that there is higher heating demand on the 3rd floor. Possible reasons can be attributed to the larger exposed surface area and the higher ceiling, where the highest level is 4.98 m (16 ft) away from the floor. Elovitz (2001) shows that the radiant in-floor heating system is popular in residential and light commercial buildings where the ceiling height is in the range of 2.4 m (8 ft) to 2.7 m (9 ft).

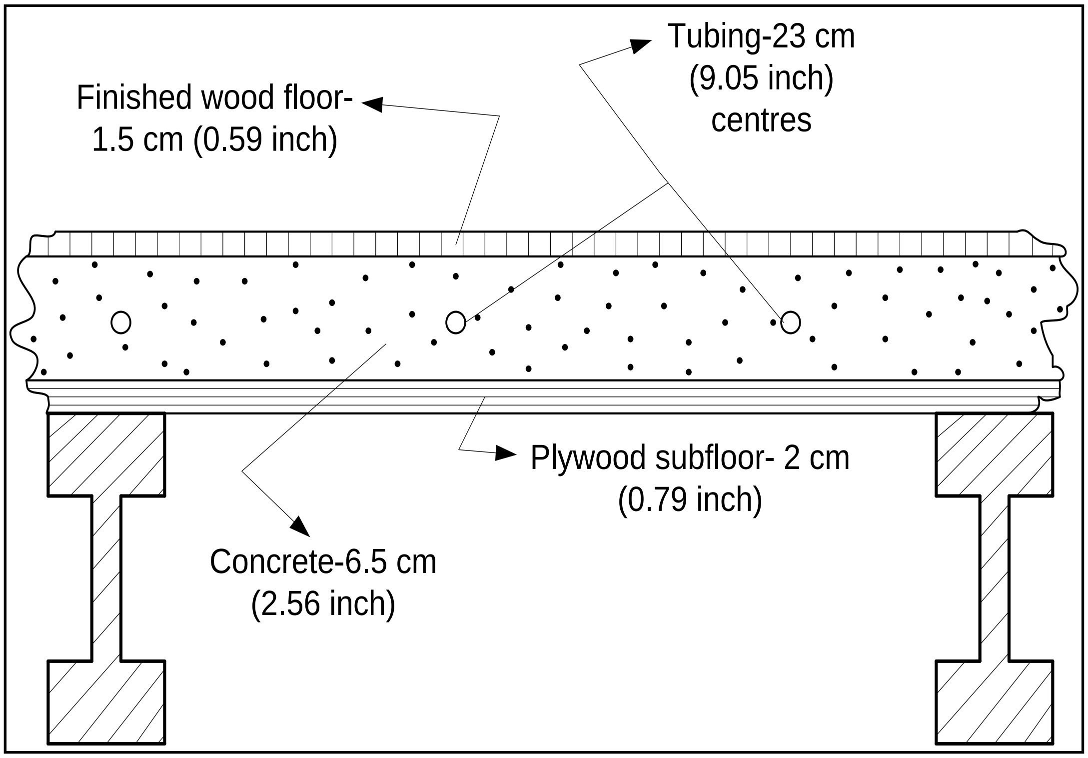

Figure 5.7 Radiant in-floor heating of "thin slab over frame floor" system

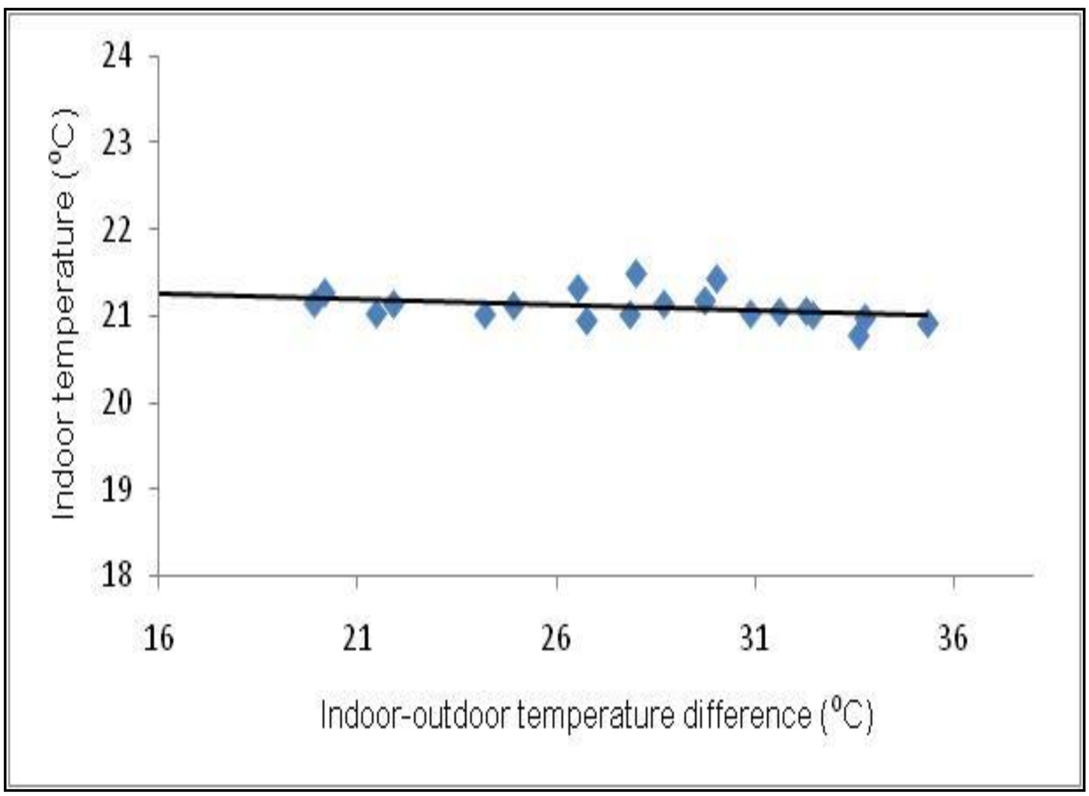

Figure 5.8 Daily average indoor temperature from December 23, 2009 to January 11, 2010

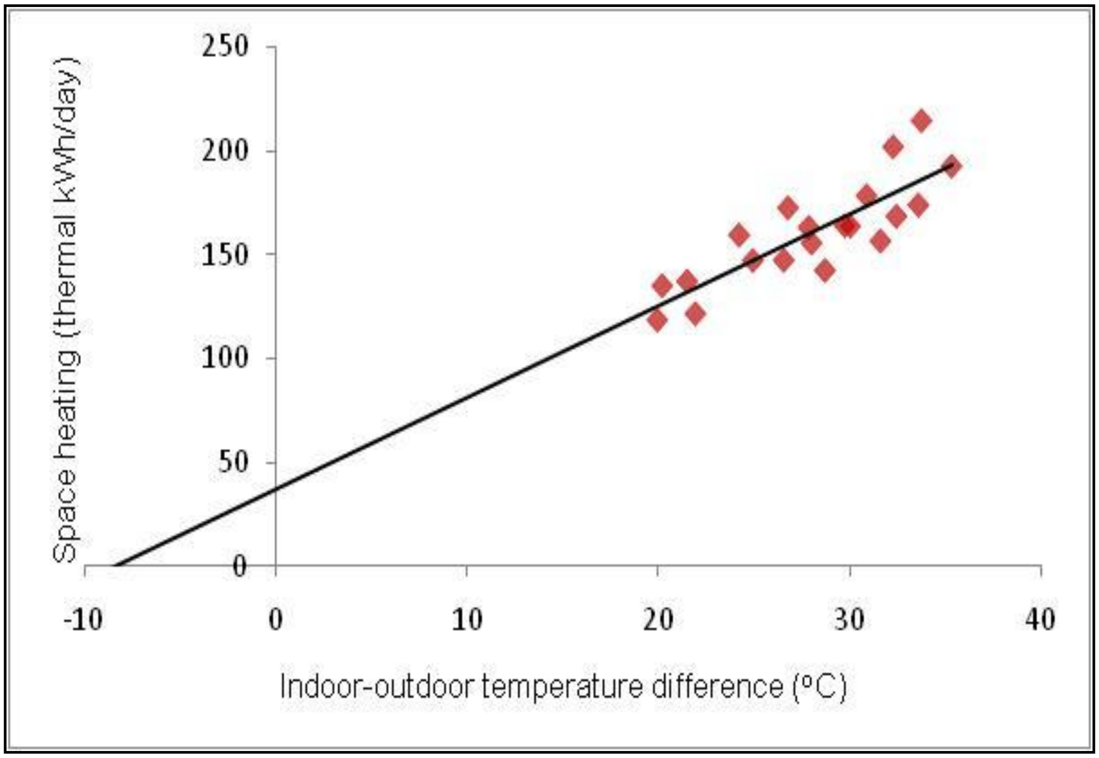

Figure 5.9 Space heating vs. daily average indoor – outdoor temperature difference from December 23, 2009 to January 11, 2010

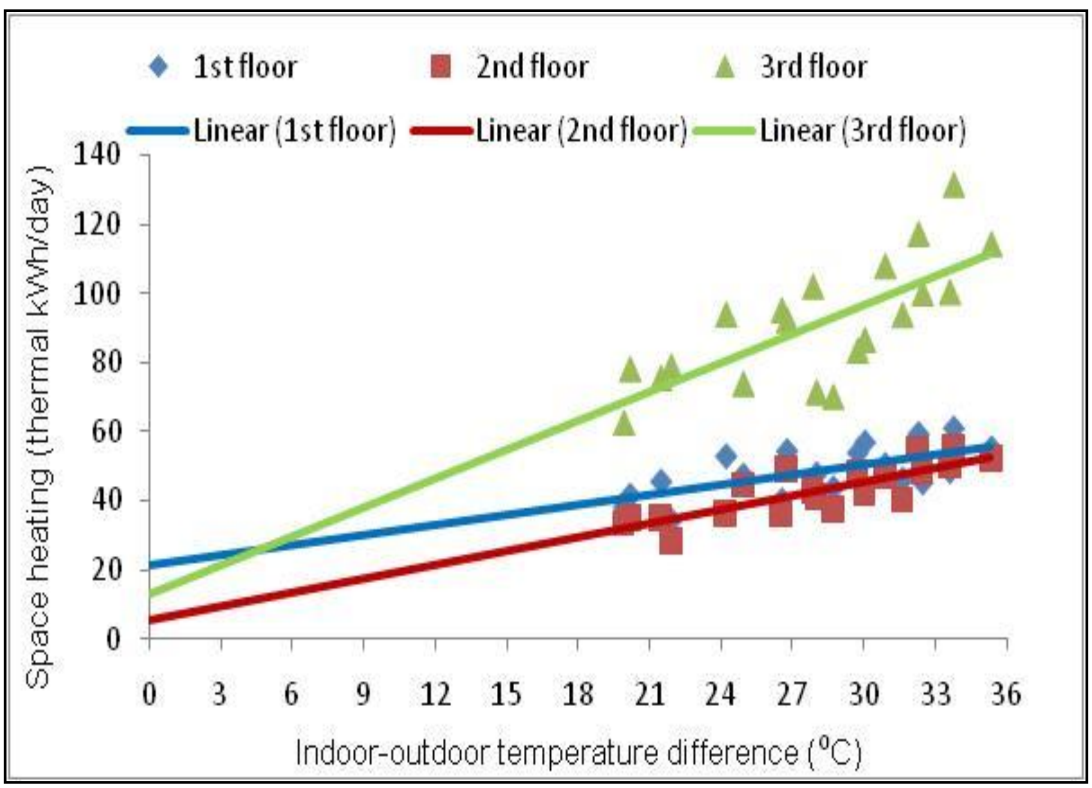

Figure 5.10 Daily space heating at different floors vs. indoor - outdoor temperature difference from December 23, 2009 to January 11, 2010

5.3 Total electricity consumption

Roth and Brodrick (2008) showed that occupant behaviour has a major impact on the building energy consumption. In the archetype houses, most of the appliances are not utilised in full capacity due to the absence of occupants. However, all mechanical and hydronic systems are operated in partial or full load capacity (Barua et al., 2010). Figures 5.11 and 5.12 show the total electricity consumption is mainly influenced by indoor-outdoor temperature difference, indicating that the space heating is the major factor for electricity consumption in the heating season.

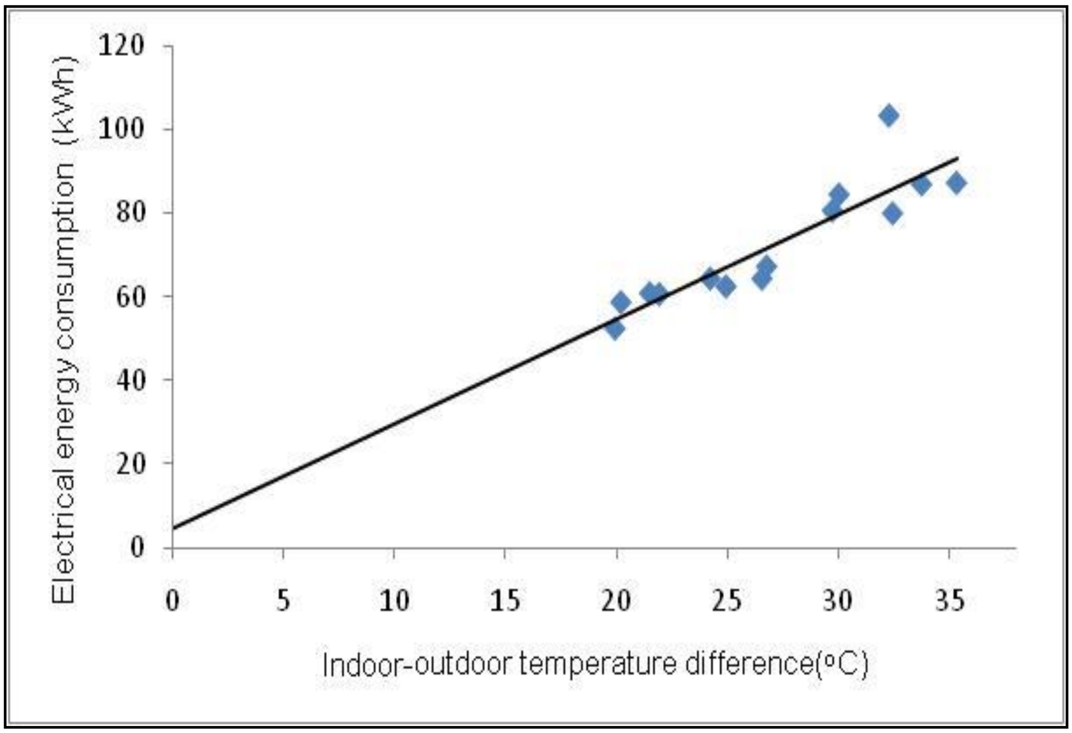

Figure 5.11 Total electricity consumption vs. daily average indoor-outdoor temperature difference from December 23, 2009 to January 5, 2010

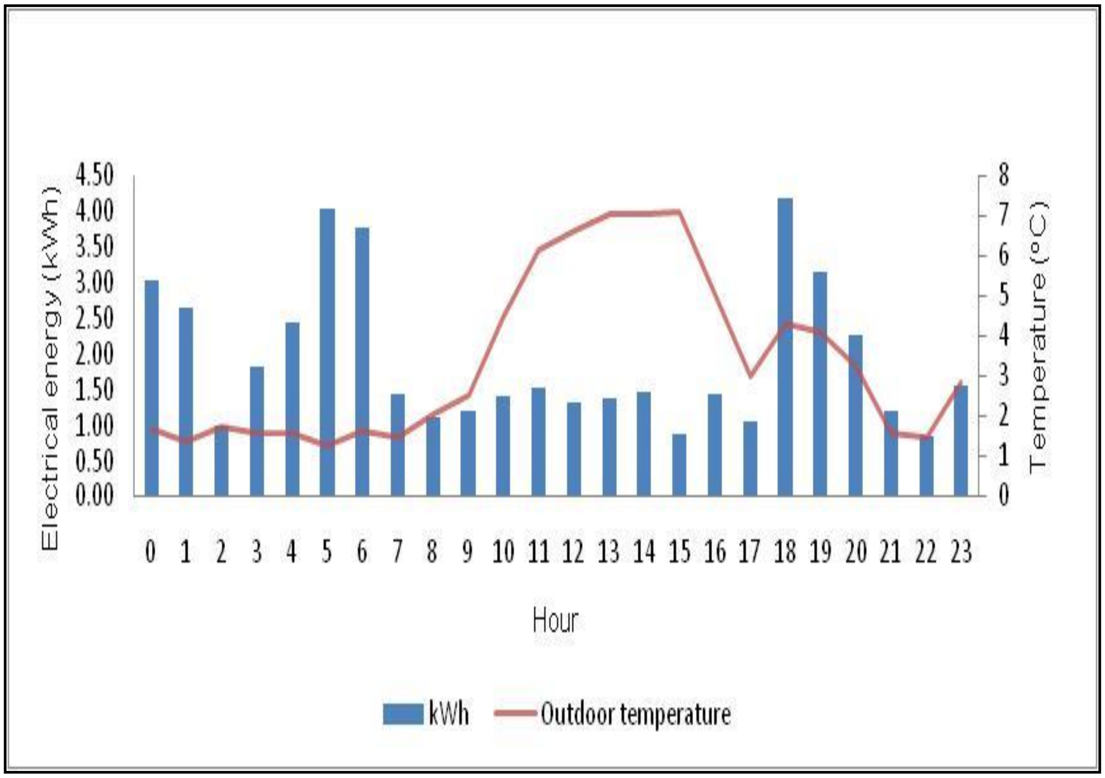

Figure 5.12 Outdoor temperature vs. electricity consumption on Tuesday, Dec 01, 2009

5.3.1 Data validation: Total electrical energy consumption of House-B is measured by both wattnodes and Google powerMeter. Wattnodes measures the pulse of electrical energy by the current transformer (CT), and through the data acquisition system LabVIEW software converts it to kWh. Collected data is saved in the SQL database. Google powerMeter is an energy monitoring tool that enables users to view home energy consumption from anywhere online. It works by taking information from a smart energy meter installed in the home, tracking energy consumption and then sending the data to a user iGoogle homepage. Table 5.1 shows that there is a good agreement between these two different energy monitoring devices.

Table 5.1 Comparison of Wattnodes and Google power meter data of House-B

Date	From Google power meter kWh	From SQL Database kWh
28-May-10	33	32.78
29-May-10	29	28.64
30-May-10	29	28.70
31-May-10	31	31.17
01-Jun-10	32	32.20
02-Jun-10	32	31.85

5.4 Photovoltaic (PV) system

A photovoltaic system is the direct conversion of sun light into electricity at the atomic level of certain materials. Those materials have a property known as the photoelectric effect, which means that they absorb photons of light and release electrons. When these free electrons are captured, electric current flows that can be used as electrical energy (Knier, 2002). A number of solar cells made of photoelectric materials are electrically connected to each other and mounted in a support structure or frame called a module. On the roof of House-B, the monocrystalline photovoltaic system composed of 48 modules was installed. Each module has a capacity of 85 W. The total cell area of all modules is 31.1 m^2 (334.3 ft^2) with combined generation capacity of 4.08 kW. Under standard test conditions (STC), the maximum efficiency of this PV system is 13.12%. Out of 48 modules, 16 modules were installed on the roof surface at a tilt angle (with respect to horizontal base) of 9.46°, 24 modules at an angle of 11.77° and the remaining 8 modules at an angle of 33.69°. All modules were grouped in 3 strings of 16 modules each, which were connected in series to a 5 kW single inverter. This inverter's efficiency is 95.5%. Figure 5.13 shows the typical system components and this PV system is grid connected. To determine the simulation result at different angles by RETScreen, the generation capacity of 4.08 kW is distributed according to the ratio of total cell area: 1.36 kW at angle 9.46°, 2.04 kW at angle 11.77° and 0.68 kW at angle 33.69° (Barua et al., 2010).

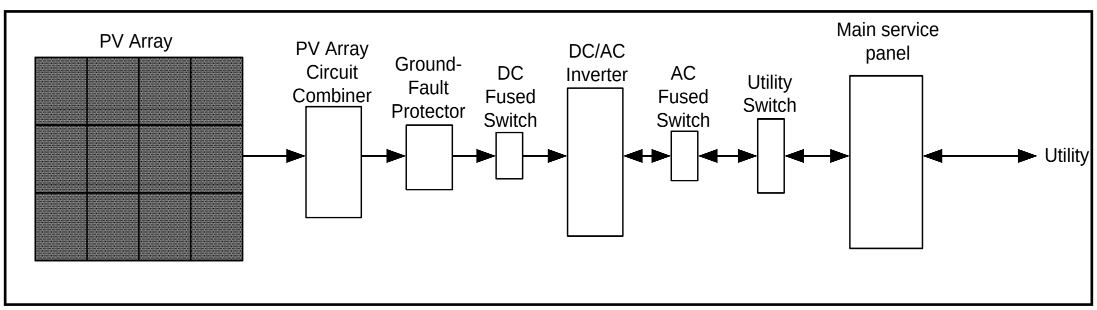

Figure 5.13 Grid-Interactive PV system without battery backup

One year of PV data from September 2009 to August 2010 were collected at Kortright Centre. The evaluation of yearly PV performance has also been conducted using RETScreen. Solar radiation of 20 years' averaged data at Pearson International Airport (PIA) weather station was used in the RETScreen analysis. These solar radiation data were compared with the available data at the University of Waterloo, University of Toronto (Mississauga campus) and Kortright

Conservation Centre weather station, which is the closest station to both PIA and Kortright Centre. It shows that the solar radiation of one year data at the University of Waterloo weather station is 1.74% higher, University of Toronto (Mississauga campus) weather station is 1.56% higher and Kortright weather station is 1.79% higher than the 20-year average data at PIA using RETScreen.

In the RETScreen help menu, maximum array losses due to dirt and snow accumulation are considered 20%. Unlike RETScreen, there are other losses which are mentioned in Table 5.2. There is no available standard PV losses information in Toronto weather conditions. Hence, to evaluate the difference of electrical energy between RETScreen and actual generation, losses of the PV system were set to zero in the analysis.

The results show that yearly electricity generation is 4970 kWh in RETScreen. During one year, PV generated 4160 kWh electricity, which is 16.30 % less than the RETScreen prediction. Possible reasons for underproduction are listed in Table 5.2. Figure 5.14 shows monthly comparison between measured electricity generation and RETScreen from September 2009 to August 2010.

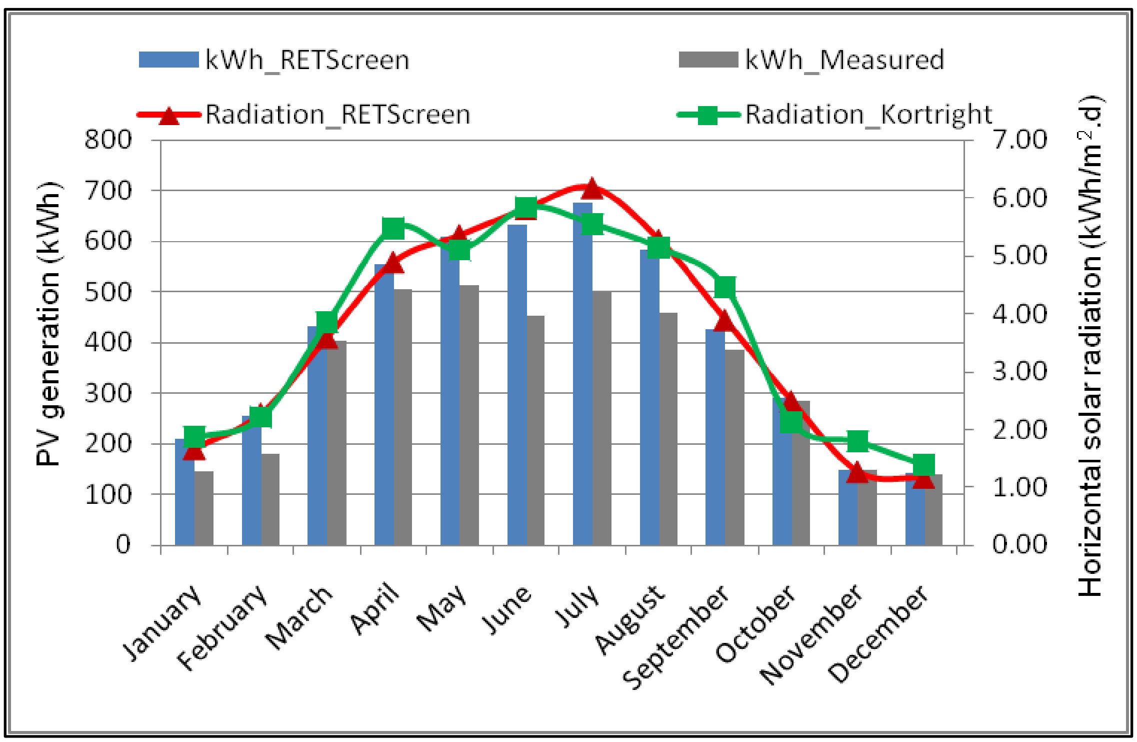

Figure 5.14 Monthly comparison between measured and RETScreen from September 2009 to July 2010 and extrapolated value of August, 2010

One year measured electricity generation by this system can prevent 0.80 MT of CO_2 emission based on hourly average GHG emission factors (Gordon and Fung, 2009). The rule of thumb for Toronto's solar resources shows that each kW PV system can generate 1100 kWh/yr electricity (Exhibition Place, 2009). According to this rule, the existing 4.08 kW PV system can generate approximately 4488 kWh/yr electricity, which is 7.30% higher than the measured data.

Figure 5.15 shows that average daily horizontal solar radiation (measured global radiation on horizontal surface) on 31.1 m^2 PV cell is 15000 W and this array captured only 1662 W (DC) which means that performance only 11% (Figure 5.16) on April 04. But as mentioned earlier, the efficiency of this PV system is 13.12% under STC conditions. Baltus et al., (1997) mentioned underproductions in the PV system were caused by some losses due to interaction between the environment, the inverter and modules. Two different studies of PV losses on roof top grid connections are described in Table 5.2.

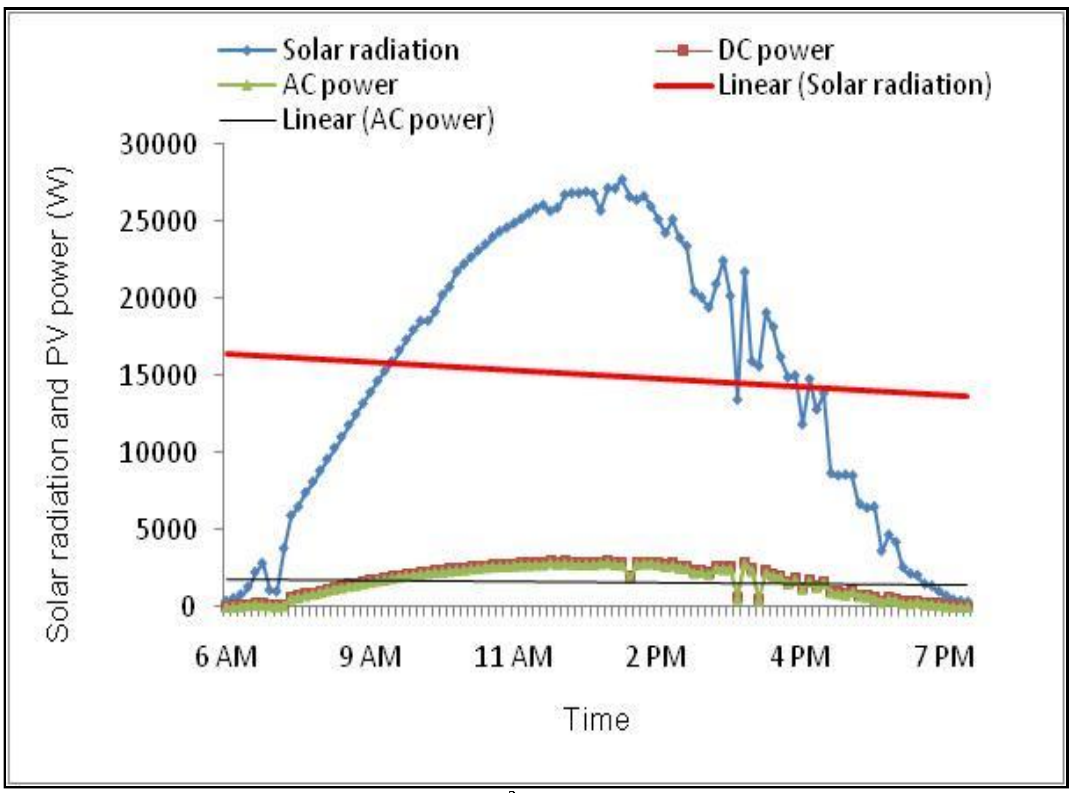

Figure 5.15 Horizontal solar radiation on 31.1 m^2 PV cell and PV DC and AC output on April 04, 2010

In both studies, loss due to snow accumulation is absent but it is a major factor in Canada.

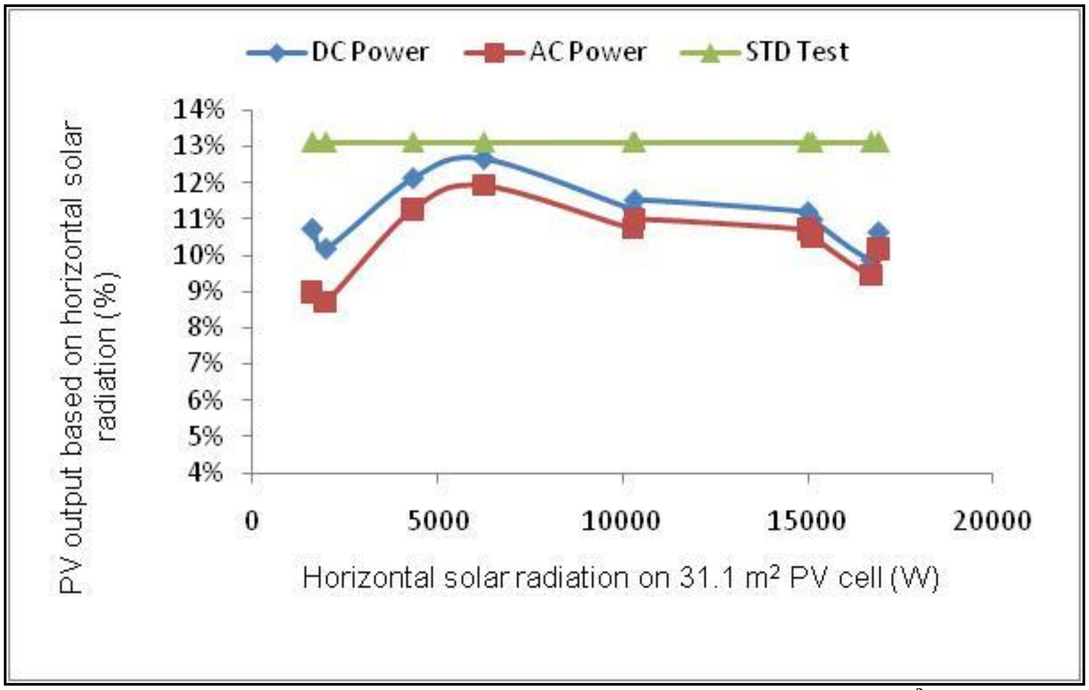

Figure 5.16 PV output based on average daily horizontal solar radiation on 31.1 m^2 cell area

Recently Queen's University Applied Sustainability Research Group of Canada is conducting a study on PV losses due to snow fall on arrays. Data analysis is currently underway to determine the effects of snowfall on the array of panels (Queen's University Applied Sustainability Research Group, 2010).

Table 5.2 Findings of PV losses on roof top grid connected in Zandvoort, Netherland (Baltus et al. 1997) and California Energy Commission (CEC), USA (California Energy Commission, 2001)

Losses	**Zandvoort, Netherland**	**CEC, USA**
Shading losses due to tree	0.7%	
Fundamental module losses	14.3%	
Bad string	2.5%	
Static losses MPP-tracker	1.0%	
Dynamic losses MPP-tracker	1.0%	
Mismatch losses	5.0%	5.0%
Low radiance losses	4.6%	
Temperature losses	4.8%	11.0%
Resistance losses	1.2%	
Inverter losses	9.6%	10.0%
Dirt and dust		7.0%
*Standard test conditions		5.0%
Total losses	44.7%	38.0%

***Standard Test conditions:** Manufacturer rating of the module output often has a production tolerance of ±5%. For a conservative estimate, it is best to use the lowest output.*

5.4.1 Lesson learned from the analysis:

- Sometimes inverter efficiency shows more than 100%. This was observed on February 8 and 20, 2010.
- Although PV array capacity is 4080 W, on August 30, 2009 at 14:03:04 the Xantrex inverter data logger showed that its peak generation (4553 W) exceeded this limit.
- Figure 5.17 shows the relation among PV output, ambient temperature and horizontal solar radiation. When solar radiation increases, ambient temperature and PV output increases and vice-versa when it decreases.
- When ambient temperature increases, PV efficiency (based on horizontal solar radiation) decreases (Figure 5.18).
- King et al., (2002) mentioned that PV performance changes with cell temperature. Both the electrical current generated by the PV cell and its voltage are independently influenced by operating temperature. Figures 5.19 and 5.20 show that as PV temperature increases, voltage typically decreases, current increases, and power generation increases.

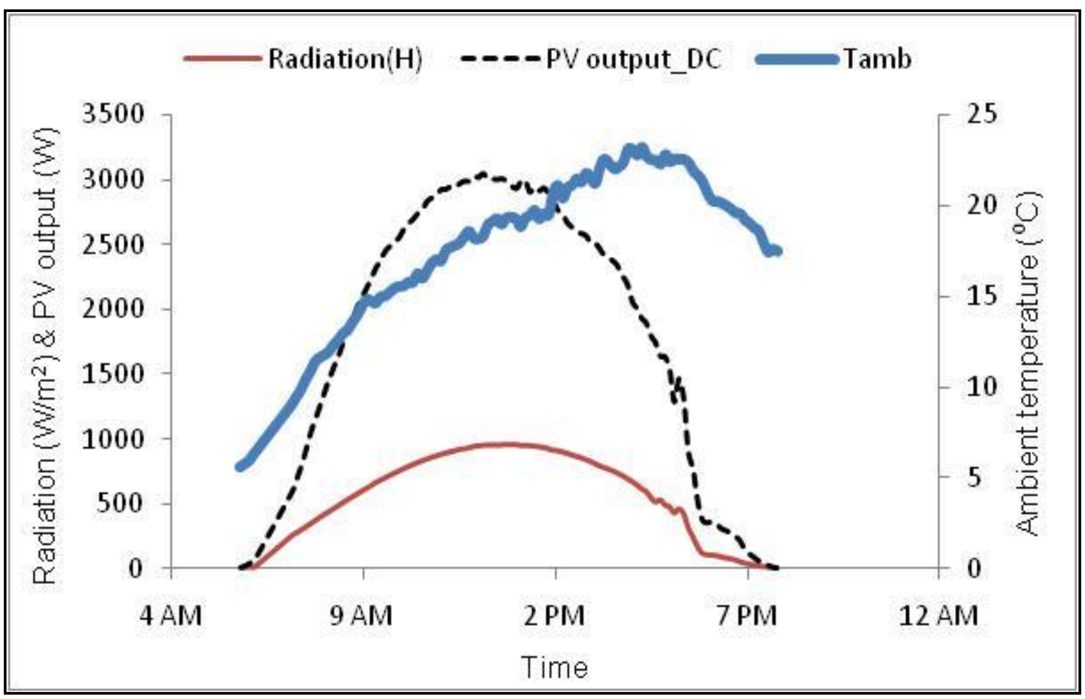

Figure 5.17 Ambient temperature, PV output, and horizontal solar radiation on April 29, 2010

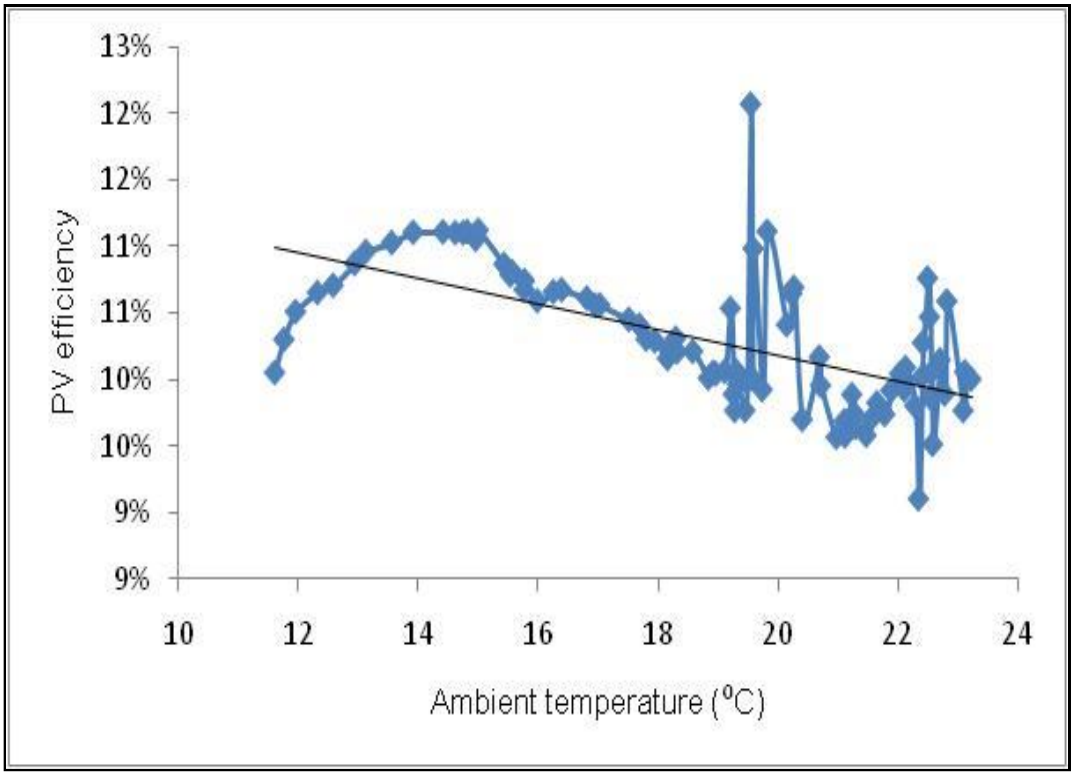

Figure 5.18 PV efficiency based on horizontal solar radiation on April 29, 2010

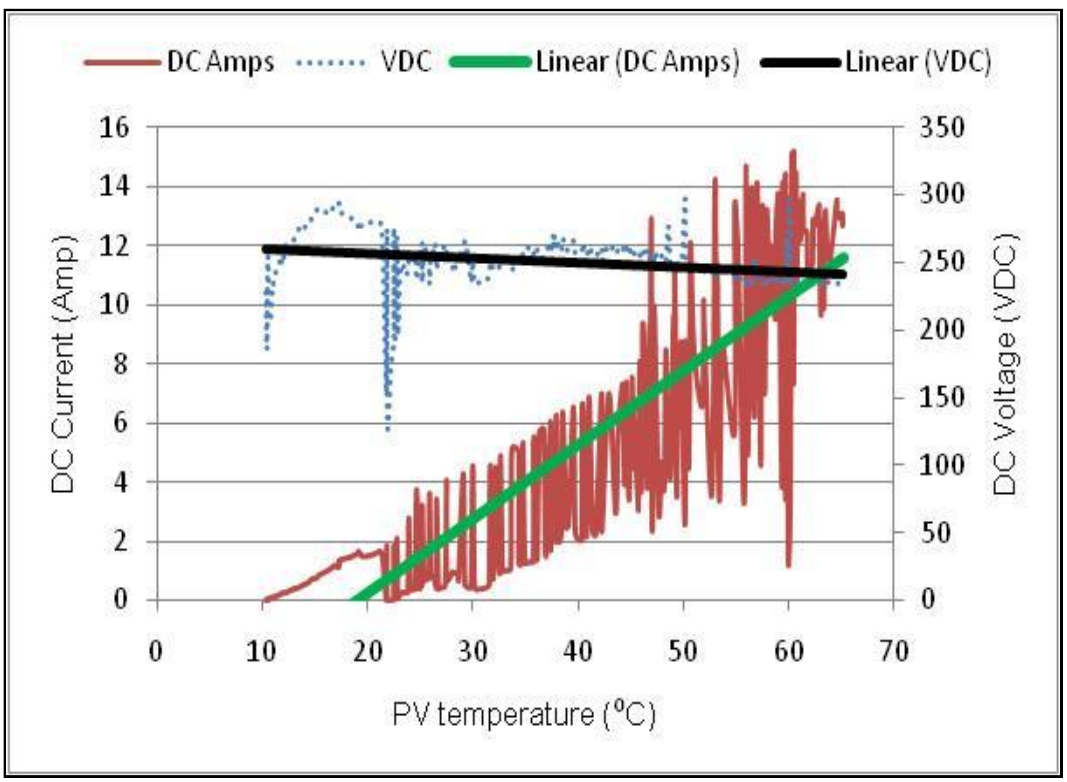

Figure 5.19 PV temperature vs. DC current and DC voltage of PV array on June 04, 2010

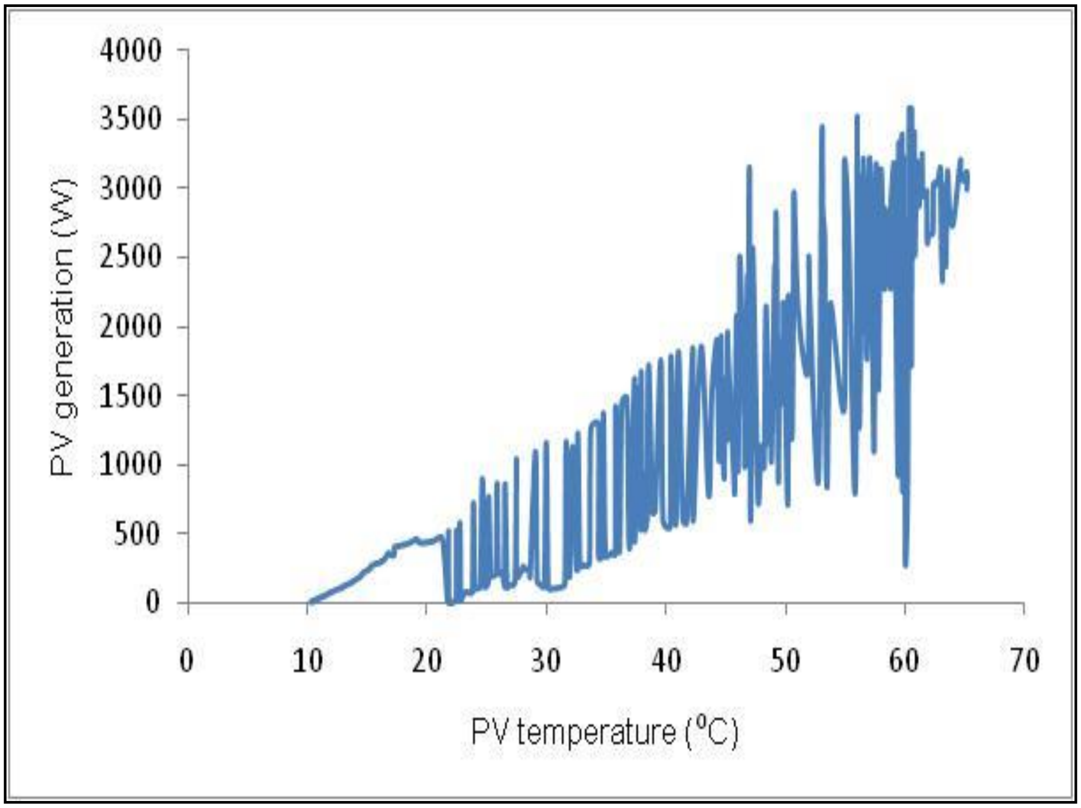

Figure 5.20 PV temperature vs. Power generation of PV array on June 04, 2010

5.4.2 Data validation

Solar radiation: Solar radiation sensor data of House-B pyranometer is validated with the University of Waterloo (UoW), University of Toronto (Mississauga campus) (UoT) and Kortright Conservation Centre weather station. The variation of House-B pyranometer data is 5.09% less than UoW, 11.04% less than UoT and 7.16% less than the Kortright weather station from June 01 to 27, 2010. Figure 5.21 shows average horizontal solar radiation (global radiation measured on horizontal surface) from June 01 to 27, 2010.

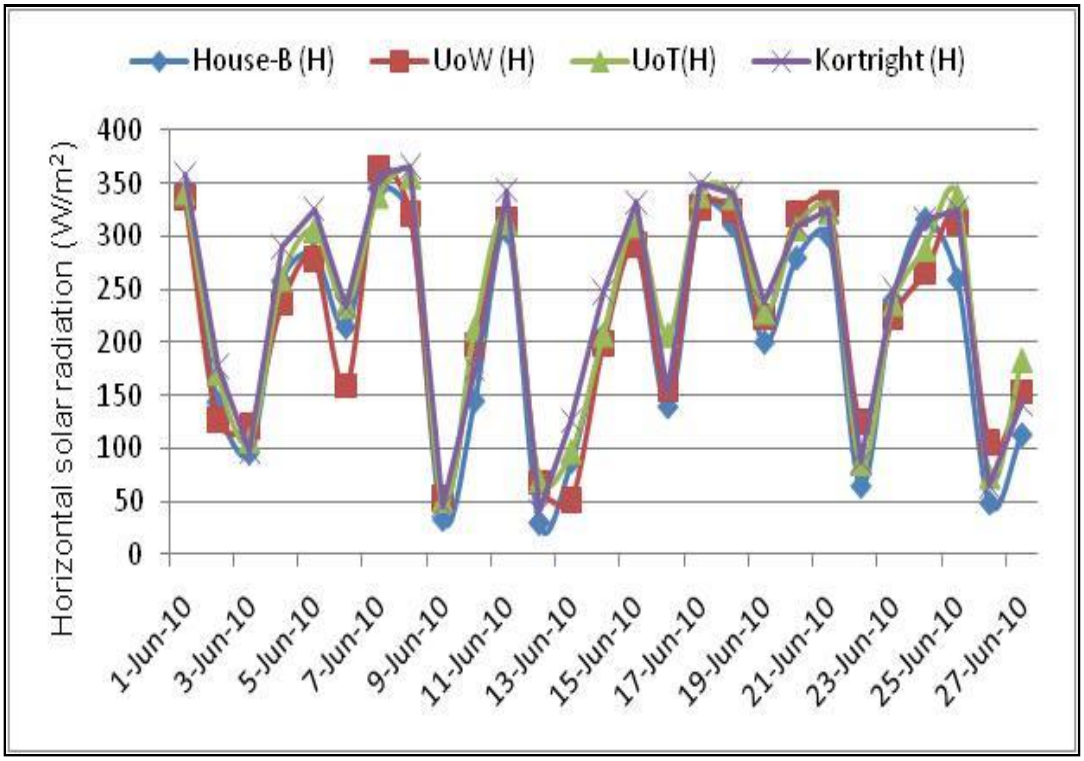

Figure 5.21 Comparison of average horizontal solar radiation among Kortright center (House-B), University of Waterloo (UoW), and University of Toronto (Mississauga Campus) (UoT) and Kortright weather station from June 01-27, 2010

PV output: PV output is measured by wattnode sensors and PV inverter (Xantrex) built-in data logger. PV output during November 20 to 23 from both Xantrex inverter and Wattnodes were analysed. Wattnode reading indicated that there was a small amount of PV output at the night. However this output was not recorded in the Xantrex inverter. The reason is that any signal less than 4 mA will not be recorded in Xantrex. If excluding the readings during the night, data recorded from both sensors show very good agreement (Figure 5.22).

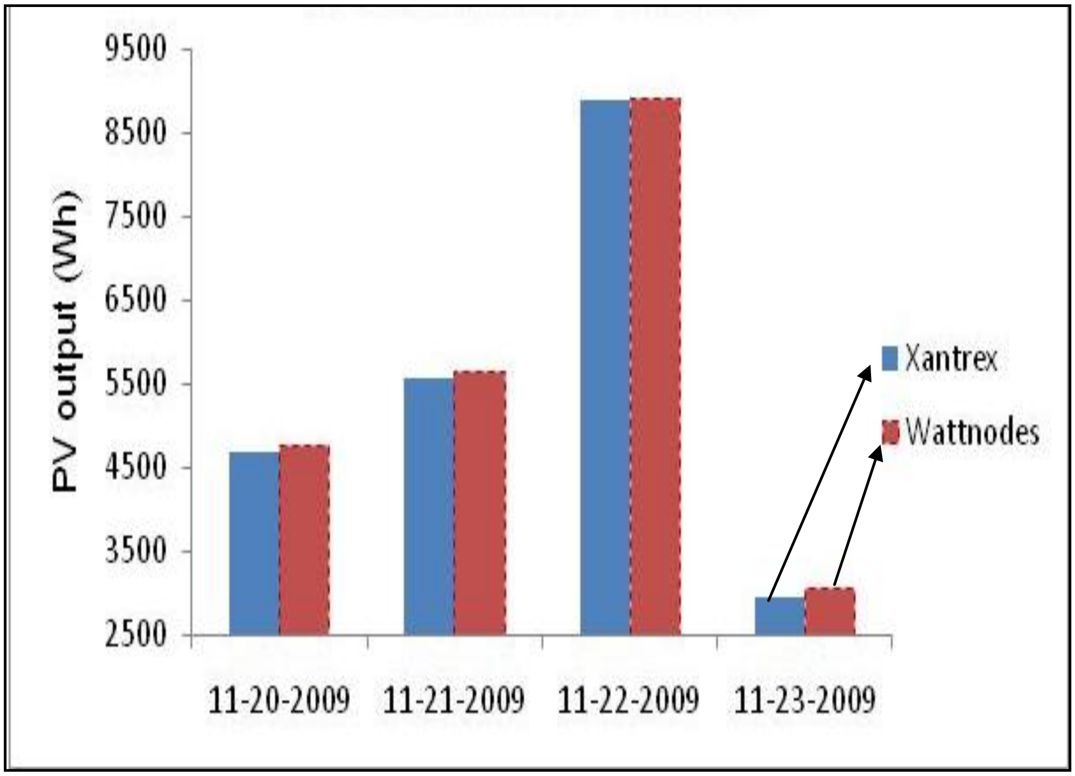

Figure 5.22 PV output measured in Xantrex inverter and Wattnodes

5.5 Micro Combined Heat and Power (CHP) unit

The micro Combined Heat and Power (CHP) unit produces heat and electricity simultaneously. Due to its dual production, high efficiency, low maintenance, light weight, low noise/vibration, and low GHG emission nature, it is becoming popular in the residential sector. Kuhn et al., (2008) mentioned that the micro CHP systems could provide 30-40% of the UK electricity demand by 2050. Hence, the UK government has reduced Value Added Tax (VAT) from 17.5% to 5% for households that install micro CHP systems. The Dutch government has taken similar initiatives. Hongbo and Gao (2009) reported that five countries – Japan, Germany, UK, the Netherlands, and USA – are currently most active in research and introduction of micro CHP systems in the residential sector. They also added that Japan and Germany are competing to lead the market. Onovwiona and Ugursal (2004) reviewed various cogeneration systems for residential use, mainly internal combustion (IC) engines, micro-turbine, fuel cell, and external combustion Stirling engines.

Although the Whispergen micro CHP unit has not been approved yet by the Canadian Standards Association (CSA), the NRCan installed a unit in House-B of this project for long-term study.

This CHP unit is called a personal power station and consists of a Stirling engine. This is a reciprocating engine with 4 cylinders and double-acting. Its cylinders are closed and combustion takes place outside of the cylinder. The working principle of this unit is that burned nitrogen gas repeatedly heats and expands on top of the cylinder, and contracts the gas by water cooled lower part of the same cylinder that raises and lowers the pistons. As a result the rotation of the mechanical system rotates the alternator to generate the electricity. In addition, heat from the flue gas heats the water and cools the engine as well. According to the manual, this unit can produce up to 12 kW of thermal power for hot water generation at maximum temperature of 85°C and 1 kW of electricity at the same time. It has two burners' one is the main burner and the other is the auxiliary burner. Gas consumption for maximum burner firing rate is 1.5m^3/h. It can use any combustible fuel including biomass. The manufacturer claims that the combined heat and power efficiency is more than 90%. Figure 5.23 shows that the hot water is used for both space heating and domestic use. Certain modifications have been made during installation to accommodate the Canadian voltage standard. This unit generates 240V of AC electricity. A step down transformer was set up to downgrade the voltage to 110 V.

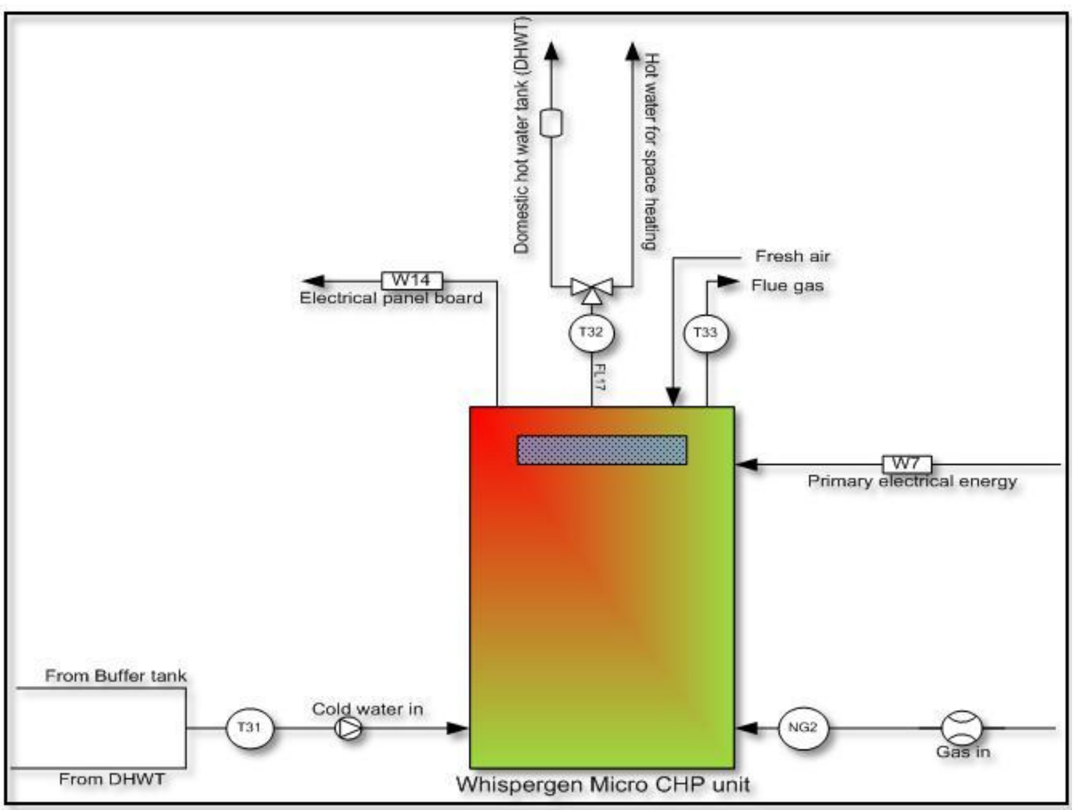

Figure 5.23 Whispergen micro combined heat and power (CHP) unit in House-B

5.5.1Control strategy: To allow the solar collector output on the same DHWT for domestic hot water (DHW) generation, the high set point is 40°C and the low set point is 30°C. For the buffer tank of radiant in-floor heating system, the high set point is 45°C and the low set point is 35°C. This control system is done by LabVIEW program.

5.5.2 Observations from the real time data: This unit was operated from April 6 to May 17, 2010. The analysis has been conducted on the transient nature of this unit.

- At the beginning of each on-cycle, water flow starts about one minute before the gas flow starts.
- At the end of each on-cycle, hot water generation continues after the gas flow stops. As a result, the number of on-cycle increases, thermal efficiency increases, and electrical efficiency decreases (Figure 5.28). The duration of hot water generation without gas flow depends on the set point temperature of the control system.
- Figure 5.24 shows that the average thermal efficiency is 80% and electrical efficiency is 7%. The overall average efficiency is 87% (based on a higher heating value).
- This micro CHP unit can convert one cubic meter gas into about 0.69 kWh of electrical energy and 8.74 kWh of thermal energy, when the low-high set point temperature is 30-40°C for DHW and 35-45°C for space heating.
- Figure 5.25 shows, when the gas flow rate increases from 17 lpm, the overall efficiency decreases.
- There is no standby losses when this unit runs but when it idles, sometimes the losses cross even 400 W.
- An average standby energy loss is 0.69 kWh per day when it is idle.
- Figure 5.26 shows when it is running, the average electricity generation is 732 W.
- Figure 5.27 shows that the total 107 kWh of electricity generated and 11 kWh of standby/parasitic losses are accumulated from April 21 to May 10, 2010. During this period, based on the total electricity production, an average of 10% of parasitic/standby losses is observed. But, parasitic losses greatly depend on the number of on and off cycles. There is power consumption in the pumps, fans, and initial ignition of gas that is the cause of losses during the on and off cycles in every start.
- There is an about 20% power loss after the voltage step down.

- The overall performance of this unit depends greatly on the generated hot water utilization.

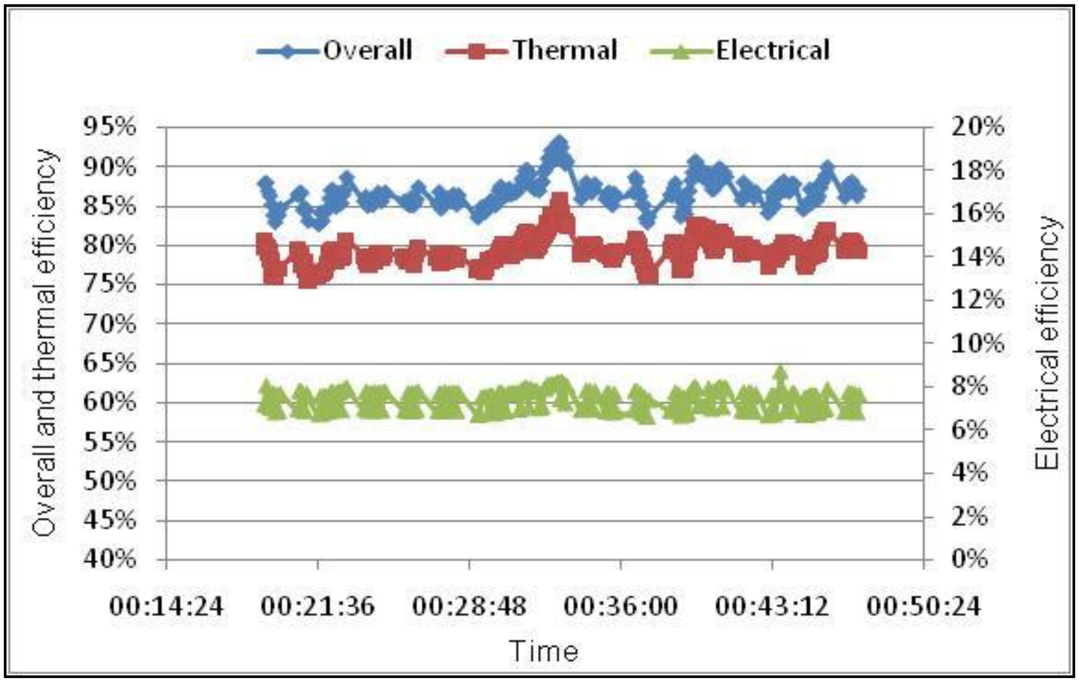

Figure 5.24 Overall, thermal and electrical efficiency on April 08, 2010

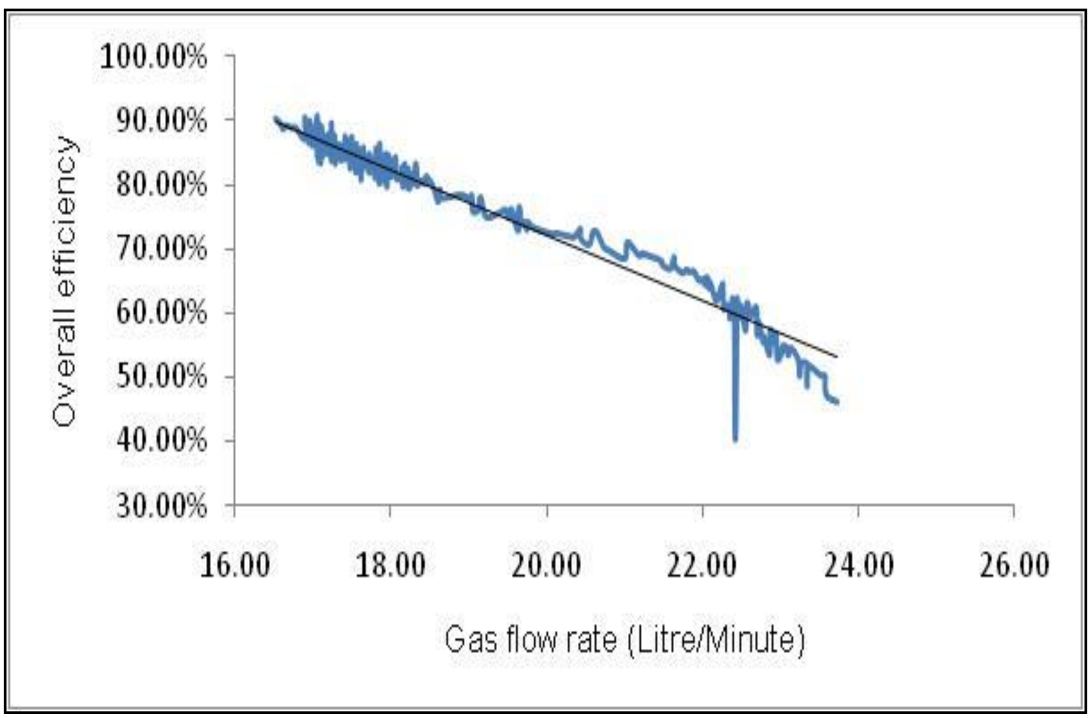

Figure 5.25 Overall efficiency vs. gas flow rate on April 07, 2010

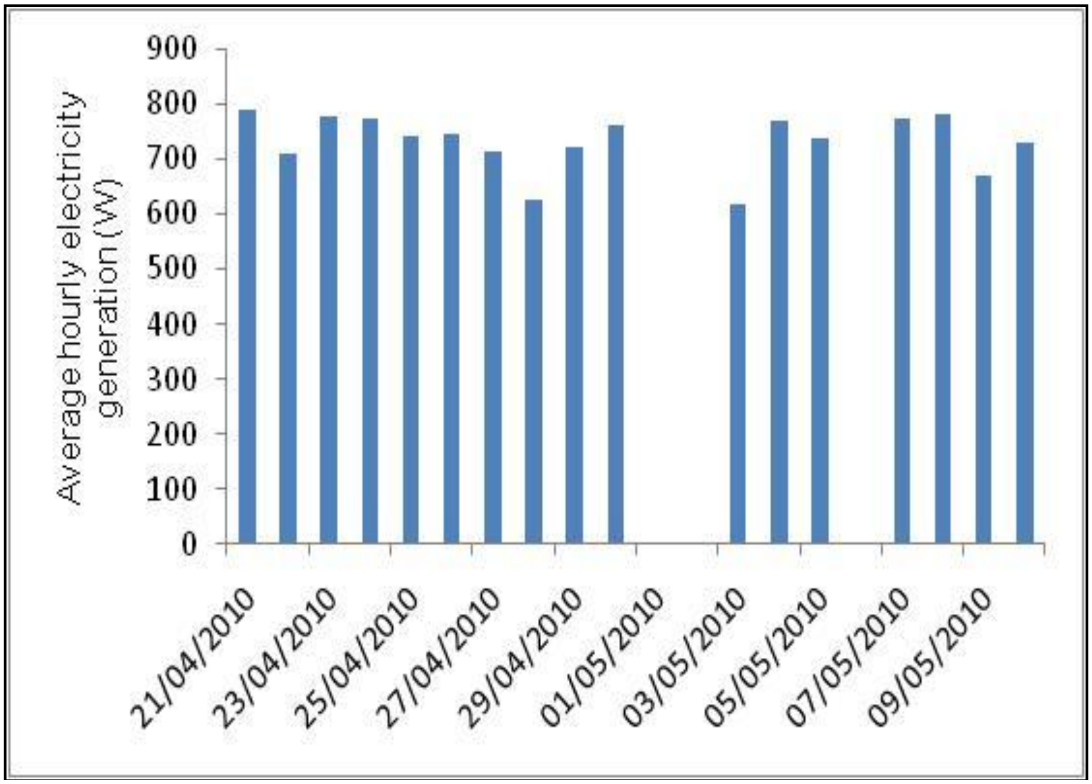

Figure 5.26 Average daily electricity generation from April 21 to May 10, 2010. The unit is idled on May 1, 2 and 6

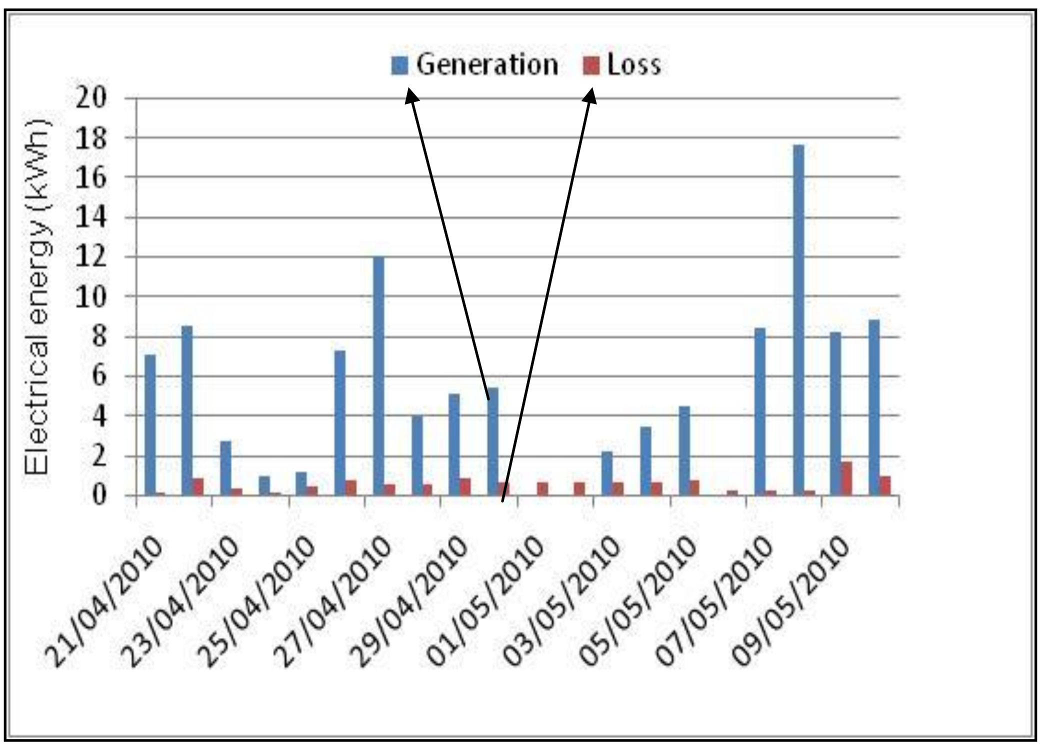

Figure 5.27 Daily electricity generation and standby/parasitic losses from April 21 to May 10, 2010

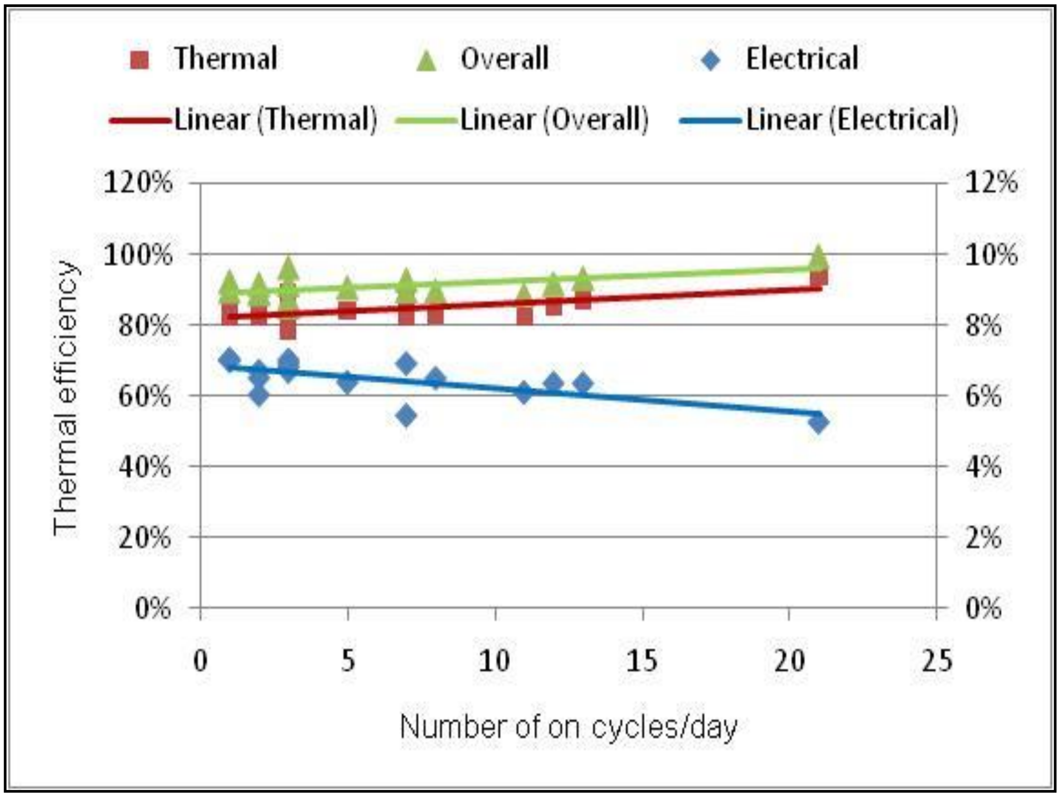

Figure 5.28 Number of on cycles vs. electrical and thermal efficiency from April 21 to May 10, 2010

Similar studies on the Whispergen micro CHP unit have been conducted in Germany, France (Kuhn et al. 2008), and in the CCHT house, Canada (Entchev et al., 2004). Table 5.3 shows the outcome of the Whispergen micro CHP unit.

Table 5.3 Whispergen micro CHP unit test run in Germany, France and CCHT house, Canada (Kuhn et al. 2008 and Entchev et al., 2004)

	Germany	**France**	**CCHT, Canada**
Test run	Single family house (SFH)	Apartment	Test house
Capacity	Thermal 12 kW Electric 1 kW		Thermal 6.5 kW Electric 736 W
Efficiency achieved	Thermal 80% Electric 10%	Thermal 75% Electric 7%	Heating efficiency varied from 74% for hot water to about 79% at the system capacity. Electrical efficiency varied from 5.5 to about 9% at the system capacity.

5.6 Evacuated tube solar collector:

An evacuated tube (heat pipe) solar collector is installed in the south side of House-B at a tilt angle with respect to horizontal base of 25°. The gross, absorber and aperture area of this collector is 2.88 m^2, 2.05 m^2 and 2.11 m^2, respectively. It consists of 20 evacuated tubes of each length of 1870 mm and diameter of 65 mm. Figure 5.29 shows the main components of solar collector of each tube contains a Sol-titanium coated copper absorber that ensures high absorption of solar radiation and low emission of thermal radiation. Pure water is used inside the copper tube as the heat transfer media from the absorber to the condenser, i.e. to Propylene Glycol (Figure 5.30).

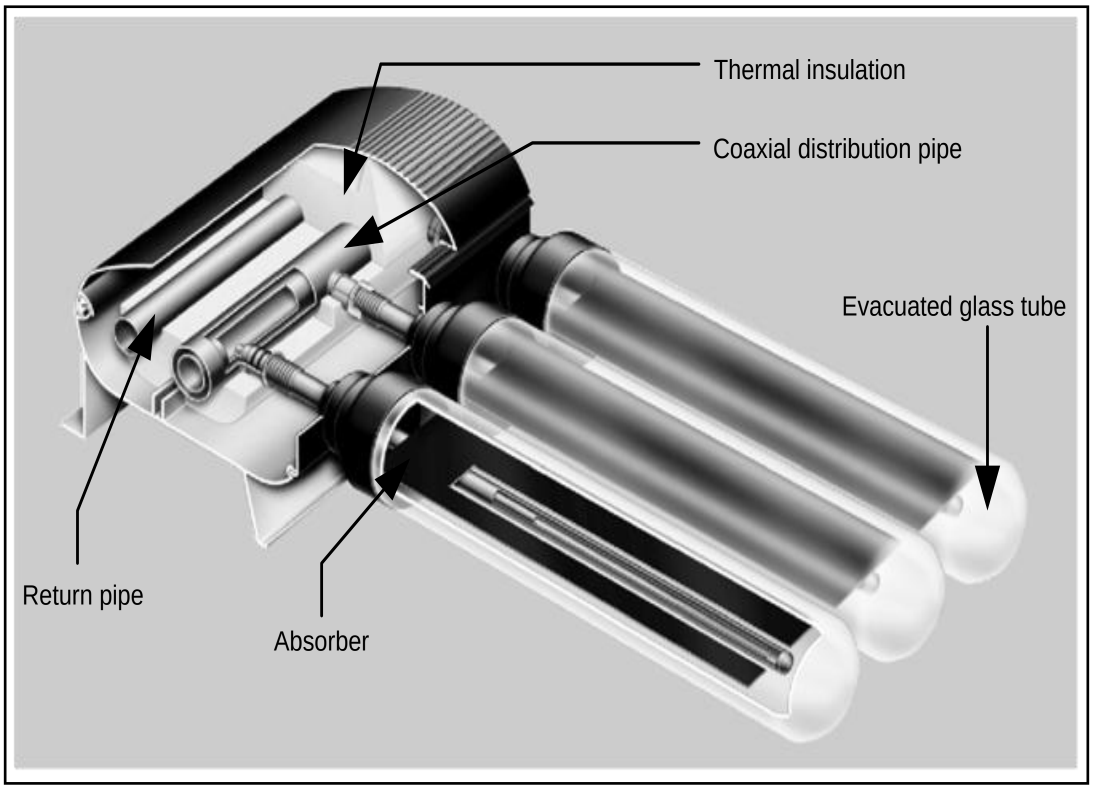

Figure 5.29 Main components of a Evacuated Tube Solar Collector (Vitotech technical guide, 2010)

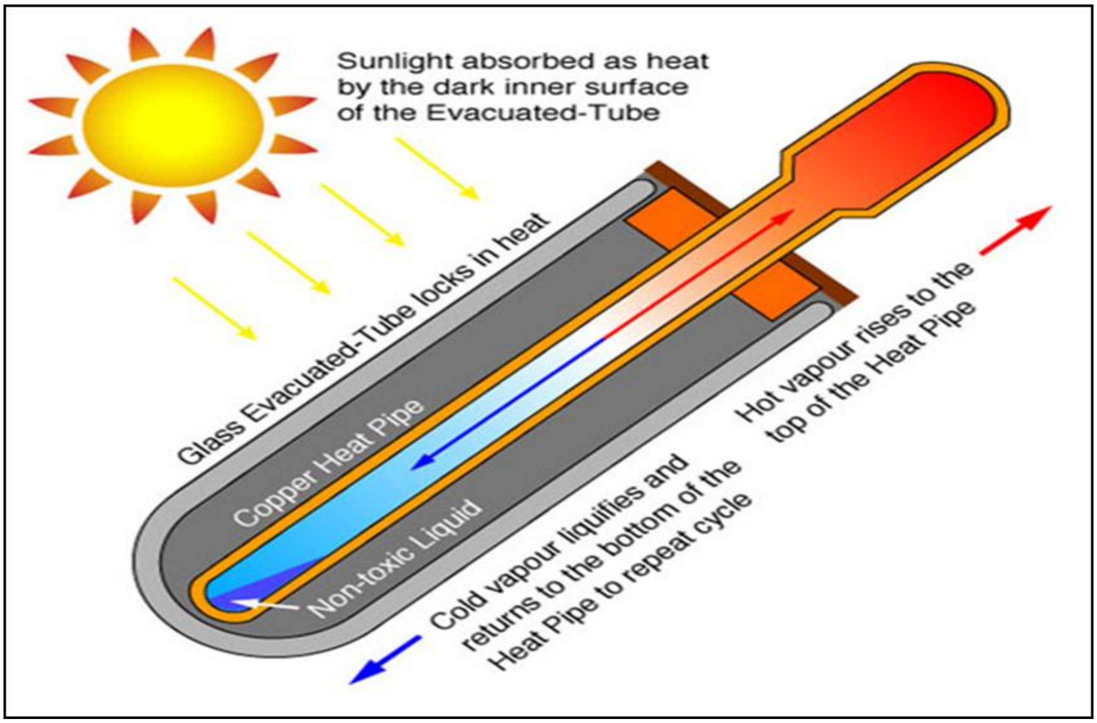

Figure 5.30 Heat absorption mechanism from the solar energy in a Evacuated Tube Solar Collector (http://www.echomaterico.net/blog/?p=497)

It is found in ASHRAE (1999) that the performance of any solar thermal system depends on,

- the heating load,
- the amount of solar radiation, and
- the solar thermal system characteristics.

European Commission Directorate General for Energy and Transport (2004) broadly mentioned that the most important factors affecting the performance of solar domestic hot water system are:

- the collector area and efficiency
- the volume of storage tank
- the system design of heat exchanger and controller
- the solar radiation and air temperature
- the load, i.e., cold water temperature, volume, demand temperature.

ASHRAE (1999) also mentioned that the collector operation is regulated by a controller with the following glycol cycle: 1) overheating protection and 2) auxiliary heating when it is required. A differential controller is used in the current system, which regulates the above operations. The control of the solar hot water system is that the glycol pump starts when the temperature difference between solar collector output and cold water inlet to the pre heat tank exceeds 12°C.

The instantaneous efficiency of this evacuated tube solar collector are analysed with Equation (30) and (45).

According to the European Commission Directorate General for Energy and Transport (2004) recommendations, the efficiency curve for a solar collector should be presented as the second order polynomial Equation (45) of the variable $T^* = (T_m-T_a)/I$

$$\eta = \eta_0 - a_1 T^* - a_2 I (T^*)^2 \qquad (45)$$

where η_0 = optical efficiency, a_1 = thermal loss coefficients in W/(m^2.K), a_2 = thermal loss coefficients in W/(m^2.K^2), I = solar radiation is greater than 800 W/m^2 at a tilt angle of 25° (From RETScreen, ratio of horizontal to tilt angle of 25° solar radiation was determined, and this ratio of a particular month was used to calculate inclined solar radiation), $T^* = (T_m-T_a)/I$, T_m = mean temperature (°C) of PG = $(T_{in}+T_{out})/2$, T_a = ambient temperature in (°C).

The European Commission used the mean temperature of inlet and outlet of PG (T_m) in Equation (45) as $T^* = (T_m-T_a)/I$. The Solar Rating and Certification Corporation (SRCC Document, 1994) and the California Solar Initiative Program (The California Public Utilities Commission (CPUC), 2009) used $T^* = (T_{in}-T_a)/I$, where T_{in} = inlet temperature (°C) of PG.

To determine the efficiency with Equation (45), the following values from the manual are applied (Vitotech technical guide, 2010):

η_0 = optical efficiency = 83.8%,

a_1 = thermal loss coefficients = 1.18 W/(m^2.K),

a_2 = thermal loss coefficients = 0.0066 W/(m^2.K^2),

Equations (30) and (45) are applied on the collected data from June 01-25, 2010 of solar collector. Figure 5.31 shows the instantaneous efficiency curve based on the above equations. The efficiency decreases with the increase of $(T_m-T_a)/I$ value. This trend is showing aforementioned two different efficiency equations. The efficiency of these two equations is very close to each other, but when the $(T_m-T_a)/I$ value increases, the difference of efficiency between the two equations increase.

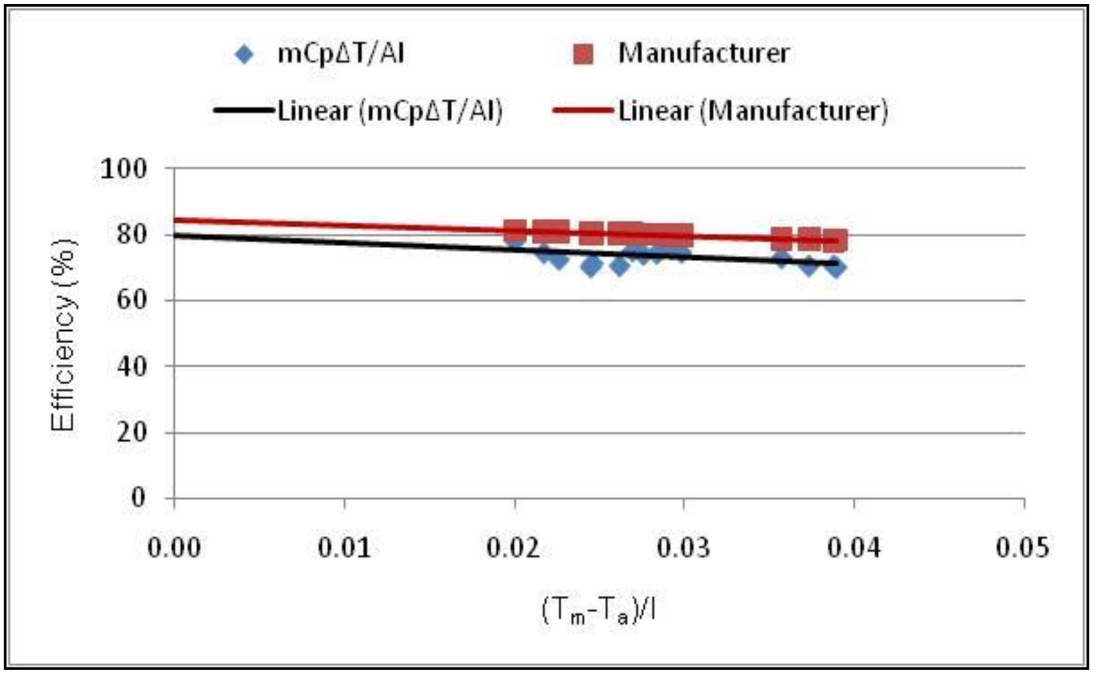

Figure 5.31 Instantaneous efficiency curve from June 01-25, 2010

Figure 5.32 shows that the difference of hot propylene glycol and ambient temperature increases with the increase of solar radiation.

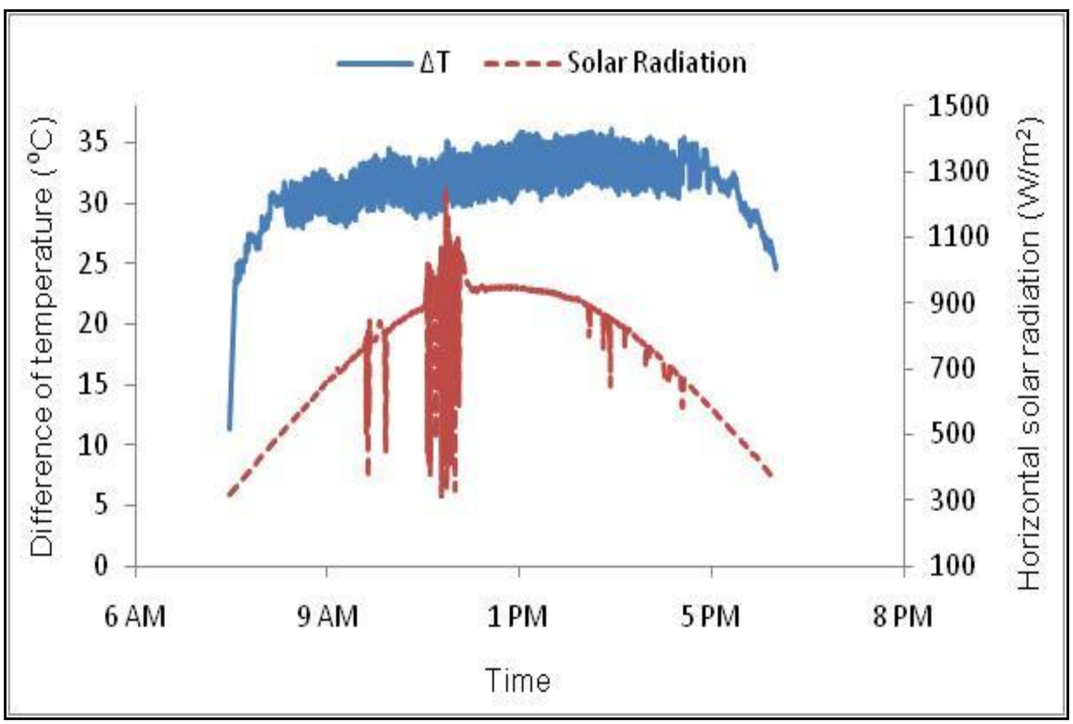

Figure 5.32 Horizontal solar radiation and $\Delta T = (T_{hot\_PG} - T_{amb})$ vs. time on May 19, 2010

5.6.1 System control: A differential controller is used to control the evacuated tube solar collector. The control for the system is simple. The solar system is turned on by a difference between the collector outlet temperature and the domestic cold water temperature. If the collector outlet temperature raises 12°C above the cold-water temperature, the pump is turned on. If the temperature difference falls below 12°C, and the electronic temperature limit reaches maximum 95^{o}C at the control unit, the pump is turned off. The function of a temperature difference of controller relates to the collector and storage temperature.

Chapter 6

Summary of project progress, problems found during implementation, future work, and conclusion

This is a large long term sustainable residential house monitoring project. To implement this monitoring project approximately more than CAD 100,000.00 is required. The author contributed to finish the first phase of the project. His accomplishment is mentioned in Section 6.3. Table 6.1 shows the summary of the project progress.

Table 6.1 Summary of project progress

<table>
<tr><th>Finished work</th><th>Yet-to-be finished task</th><th>Remark</th></tr>
<tr><td>Installation and calibration of proposed sensors in House B, monitoring the following aspects:
• Hydraulic temperature (RTD probe and surface mounted RTD)
• Flow rate (hydraulic)
• Pressure, velocity (duct)
• Air temperature and relative humidity
• Solar radiation
• Power sensors</td><td></td><td>Data collection started from December 2009</td></tr>
<tr><td>Installation and connection of data acquisition system (DAQ) in the basement and in-law suite of House B.</td><td></td><td>Installation of complete DAQ system is finished. Data collection and analysis is going on.</td></tr>
<tr><td>Installation of soil sensors.</td><td></td><td>Data communication issue is solved through wireless connection between DAQ system away from the main system at House B. Data collection and analysis is going on.</td></tr>
<tr><td>Installation and calibration of proposed sensors in House A, monitoring the following aspects:
• Hydraulic temperature (RTD probe and surface mounted RTD)
• Flow rate (hydraulic)
• Pressure, velocity (duct)
• Air temperature and relative humidity</td><td></td><td>Installation of complete DAQ system is finished.</td></tr>
<tr><td>Tested (running successfully) Labview</td><td>Pilot testing</td><td>All finished codes have been</td></tr>
</table>

programming for DAQ system: • Coding for acquiring raw signal from each individual sensor. • Conversion of raw signal into physical parameters. • Programmably overcoming the limitation of 16-bit counter and achieving a 128-bit counting module • Coding for high level calculation, such as efficiency, energy generation/consumption, etc. • Graphical design of display panel for the DAQ system. • Coding to transfer data to third party partner's database. • Structure design to process data acquisition and calculation at various sampling rates. • Recording data to SQL server.	involving multiple sensors have been carried out for programs to run successfully. A benchmark testing will be conducted.	tested and it is running successfully. Data collection and analysis is going on. It is a huge challenge to host these many sensors (300+) with different types of signal on a single machine. An efficient real-time structure was adopted and coded to process all signals at fast rates (0.5s). Data is recording in the SQL server database.

6.2 Problems found during implementation

1) Connection between connector and turbine type water flow sensors should strictly follow the manual instruction. Few sensors were damaged due to the wrong wiring.
2) Teflon tape falling inside the turbine type water flow sensors during installation in the hydronic line may result in the failure of such sensors. Special attention should be paid during the installation.
3) The air temperature and relative humidity sensor was installed upside down in the outdoor fresh air incoming duct. This position results in the moisture condensation on the electronic element, hence the failure of the sensor.
4) Duct air temperature measurement by the air temperature sensor is influenced by the surrounding temperature because of the suction of zone air through the sensors wire port. Therefore, tight sealing is required to minimize the air leakage.
5) The city main water temperature sensor was installed near to the water softening plant in the basement. Hence, the basement air temperature may easily influence the incoming city water temperature. Another RTD sensor should be installed outside the room.
6) Analysis for the solar collector has shown that there is energy back flow from the solar hot water tank to the glycol in the solar collector loop early in the morning.

7) Temperature measurement sensors for all three floors and basement infloor heating loop are installed in the infloor heating tube at the basement. Locations of these sensors are very close to each other except for the basement loop temperature sensors. As a result, when hot water flows from the buffer tank to a particular floor, there is heat exchanged through natural convection to other sensors. Sometimes, return temperature exceeds supply temperature.
8) Fresh air duct from the ERV was connected to the return air duct of the AHU. As a result, the following problems are observed:
    i) Fresh air flow rate from the outdoors is higher than the return air from the zone when the AHU operates. Hence balanced air flow is not observed in the ERV. The AHU fan influenced the ERV fan for sucking more air from outdoors.
    ii) When the AHU runs without ERV operation, fresh air flow rate is observed in the ERV.
    iii) Controlling system of ERV and AHU is not integrated, i.e. the ERV runs without the AHU. As a result, when the ERV runs without the AHU operation, fresh air from the ERV passes through the return air duct of the AHU because the damper of supply air duct is closed.
    iv) To calculate the air flow rate in CFM from the duct air pressure difference for the ERV and AHU duct, a polynomial equation was set up in the LabVIEW software. In the Microsoft Excel spreadsheet application: a six order polynomial trend line equation is prepared from Table 6.2 for circular type 0.1524 m (6″) duct air flow station. This polynomial equation produces error as CFM. For instance, for the six inch duct air flow rate (CFM) = $-40000000X^6 + 30000000X^5 – 9000000X^4 + 1000000X^3 – 104587X^2 + 4991.4X + 4.0067$

        where X = pressure difference in inch of water

        In the same way, a six degree polynomial equation is prepared from Table 6.2 in the Engineering Equation Solver (EES) mathematical software. This polynomial equation gives an accurate result. The accurate air flow rate (CFM) = $-40323500X^6 + 31386100X^5 – 9470840X^4 + 1405890X^3 – 108999X^2 + 5128.98X + 2.63522$

Table 6.2 Manufacturer supplied "pressure difference (inch of water) to air flow rate (CFM)

Pressure difference (X=inch of water)	Air flow rate (CFM) of 6″ circular duct
0.00	0
0.01	50
0.02	71
0.03	87
0.04	100
0.05	112
0.06	122
0.07	132
0.08	141
0.10	158
0.12	173
0.14	187
0.16	200
0.18	212
0.20	224
0.25	250

9) There are two sensible efficiency equations of the ERV for balanced air flow.

a) $\frac{(\text{Leaving air from ERV to AHU} - \text{Outdoor fresh air entering to ERV})}{(\text{Return air from zone entering to ERV} - \text{Outdoor fresh air entering to ERV})} \text{ x } 100$

b) $\frac{(\text{Return air from zone entering to ERV} - \text{Exhaust air leaving from ERV})}{(\text{Return air from zone entering to ERV} - \text{Outdoor fresh air entering to ERV})} \text{ x } 100$

Although all sensors are calibrated properly, there is average 6 to 12% variation of sensible efficiency between these two equations. As mentioned before, air flow rates are not equal between return air from the zone to the ERV and leaving air from the ERV to the AHU.

10) PV output is measured by the two equipment, wattnodes and Xantrex PV inverter built-in data logger. Comparing output data from these two equipments, it is found that for higher PV output, variation is less than 1% and for lower PV output, variation is less than 5%.

11) Ground source heat pump (GSHP) compressor was out of order for the leakage of refrigerant tube from February 13 to June 17, 2010. The compressor was replaced later on and it is operating.

12) There is a leakage in the infloor radiant heating loop on the third floor. An investigation is underway to find the cause of leakage.

6.3Author’s contribution

It is a large monitoring project like Canadian Centre for Housing Technology (CCHT) house in Ottawa. In order to achieve objectives, described in Section 1.2 and to gather good experimental data, it is inevitable to have a powerful monitoring platform. In this regard, author finished following activities for last two years to build a complete monitoring platform:

- For direct calculation in the LabVIEW software, basic equations of power, energy and efficiency of different equipment were illustrated
- Selection of sensors and their locations are based on the energy balance equation of respective equipment
- All sensors were calibrated, especially temperature and flow sensors
- Implementation of sensor and data acquiring system and commissioning
- Validating the collected data by cross-checking
- Thermal performance analysis of equipment/system, and the result is compared with the manufacturer’s manual and different publications
- Determination of the errors of all measured and derived data through uncertainty analysis

6.4 Future work

As an on-going monitoring project, the following work will be carried out:

- Validation of collected data to ensure the accuracy of data.
- Obtaining the base case information without any occupant living in the house.
- Comparing the base case with the occupancy case where occupants of a typical family will live in the house in one summer month and one winter month. The effects of typical resident behaviour on the energy performance of the house can be studied.
- Comprehensive performance analysis of each piece of equipment should be done.
- Using building simulation software to simulate the energy performance of the house and its equipment.
- Creating new components or subprograms to improve the existing building simulation software.
- The data and the improved models can be used for benchmark studies of normalized weather conditions.

6.5 Conclusion

- Project plan was finished to locate various types of sensors on the system.
- Sensors were calibrated, installed and connected to the DAQ system.
- LabVIEW code was developed to collect data, process and store.
- Equations used to calculate high level information were implemented in the code.
- Relational database was adopted in the SQL server to store data.
- Data acquisition and post-analysis are on-going.

Preliminary analysis shows that the indoor-outdoor temperature difference is the primary factor, influencing the ERV performance, in-floor radiant heating and total electricity demand.

The sensible and latent heat recovery of the ERV increases with the increase of indoor-outdoor temperature difference and specific humidity difference, respectively. In the in-floor radiant heating system, a higher heating demand was observed on the 3rd floor. Indoor temperature was maintained constant at 21°C in the winter, regardless of the indoor-outdoor temperature difference. The space heating demand and the total electricity consumption increases linearly with the increase of indoor-outdoor temperature difference. One year of data in the 4.08 kW photovoltaic (PV) systems has been collected. The measured one year output is 16.30% less than the RETScreen analysis, excluding the consideration of other losses. Nevertheless, the yearly measured data is 7.30% less than the prediction based on the rule of thumb of Toronto's solar resources. The average thermal and electrical efficiency of the Whispergen micro combined heat and power (CHP) unit achieved 80% and 7%, respectively. The average overall efficiency achieved 87% (based on a higher heating value of natural gas). The average instantaneous efficiency of the evacuated tube solar collector achieved 74% when solar irradiance is more than 800 W/m^2.

First phase of the project, i.e., the infrastructure of quality data collection is completed. The collected data is analysed, which are consistent with the manufacturer manual and different publications.

6.6 Recommendations

Following recommendations are made to get good quality data from the monitoring system:

- It is important to make a schedule for calibrate the sensors regularly.
- It is essential to check the monitoring program every day by remote log-in to ensure that it is running, and by the same way, checking the "Measurement & Automation" window of LabVIEW software every day to ensure that all sensors are working.
- It should check SQL database regularly to ensure that data is saving properly, and backup the database as well. If there is inconsistent reading found in the database of any sensor, troubleshoot immediately. Hence, regular data analysis is essential to avoid long time insignificant data collection.
- It should be important to make a schedule for preventive maintenance of all mechanical equipment according to manufacturer guideline.
- From time to time, it is important to physically check the duct, hydronic line and equipment for any leakage.

References

ASHRAE. (1999). *Chapter 39: Building Energy Monitoring*. Atlanta: Communications and Publications.

ASHRAE. (2000). *Chapter - 20: Humidifiers.* Atlanta: Communications and Publications.

ASHRAE Guideline 2. (2005). *Engineering Analysis of Experimental Data.* Atlanta, USA, 16-20.

Baltus, C. W. A., Eikelboom, J. A., & Zolingen, V. R. J. C. (1997). *Analytical Monitoring of Losses in PV Systems.* 14th European Photovoltaic Solar Energy Conference. Barcelona.

Barua, R., Zhang, D. & Fung, A. S. (2010). Analysis of Energy Performance of the Sustainable Archetype House at Kortright Centre. *1st International High performance Buildings Conference at Purdue University*. Indiana: Compressor/Refrigeration & Air Conditioning/High Performance Buildings Conferences at Purdue. 3481 (1-8).

Biological Science Institute. (2002). *Research Science.* Retrieved July 12, 2010, from Propagation of Errors in Calculation: www.ferris.edu/htmls/colleges/artsands/biology/researchscience/SIPropagationOfErrors.cfm

California Energy Commission. (2001). *A Guide to Photovoltaic (PV) System Design and Installation.* Sacramento, California: Energy Technology Development Division.

Christian, J. E., Richards, L., Childs, P., Atchley, J., & Moon, H. (2006). Energy Efficiency, SIPS, Geothermal, and Solar PV Used in Near Zero-Energy House. *ASHRAE Transactions.* 112(2), 275-284.

CMHC. (1996). *The EQuilibrium™ Sustainable Housing Demonstration Initiative*. Retrieved April 2010, from Canada Mortgage and Housing Corporation: http://www.cmhc-schl.gc.ca/en/co/maho/yohoyohe/heho/eqho/eqho_002.cfm

Cohen, J. (2010). Mattamy Homes Green Initiative Project: Phase II - Mechanical System Performance Analysis. *Ryerson University, Department of Architectural Sciences*, Toronto.

Dembo, A., NG, K. L. R., Pyrka, A., & Fung, A. S. (2010). *The Archetype Sustainable House: Investigating its potentials to achieving the net-zero energy status based on the results of a detailed energy audit.* International High Performance Buildings Conference. Purdue, Indiana.

Doreen, E. K., Herkel, S., & Wagner, A. (2009). The impact of auxiliary energy on the efficiency of the heating and cooling system: Monitoring of low-energy buildings. *Energy and Building*, 41, 1019-1030.

Dumont, R. (2008). *The Factor 9 Home: A New Prairie Approach Monitoring Final Report.* Saskatoon: Saskatchewan Research Council. 12155-2C08, 1-54.

Efficiency Valuation Organization. (2007). *Concepts and Options for Determine Energy and Water Savings.* San Francisco, California: International Performance Measurement and Verification Protocol. EVO 10000-1.2007, 1, 1-104.

Elovitz, K. M. (2001). Hydronic Heating: Two Systems Compared. *ASHRAE Journal*, July, 36-42.

Entchev, E., Gusdrof, J., Swinton, M., Bell, M., Szadkowski, F., Kalbfleisch, W., Marchand, R. (2004). Micro-generation technology assessment for housing technology. *Energy and Buildings*. Volume: 36, 925-931.

European Commission Directorate General for Energy and Transport. (2004). *Basic European and International Standards on Solar Thermal Glazed Collectors & Solar Domestic Hot Water Systems.* Athens, Greece: Exergia S.A.

Exhibition Place. (2009). *SolarCity: Horse Palace Photovoltaic Pilot Project Findings Report.* Toronto: Exhibition Place.

Feng, J., Megerian, S., & Potkonjak, M. (2003). Model-Based Calibration for Sensor Networks. Retrieved July 16, 2009 from Ryerson University Library. *IEEE Xplore.* 737-742.

Gordon, C. & Fung, A. (2009). Hourly Emission Factors from the Electricity Generation Sector-A Tool for Analyzing the Impact of Renewable Technologies in Ontario. *Canadian Society for Mechanical Engineering*, 33(1), 105-118.

Hongbo, R. & Gao, W. (2009). Economic and enviornmental evaluation of micro CHP systems with different operating modes for residential buildings in Japan. *Energy and Buildings*, *Volume 42*, 853-861.

King, D. L., Boyson, W. E., & Kratochvil, J. A. (2002). Analysis of factors influencing the annual energy production of photovoltaic systems. Conference Record of the 29the IEEE Photovoltaic Specialists Conference,. *IEEE Xplore*. 1356-61.

Knier, G. (2002). How do Photovoltaics Work. *Science@NASA Headline News*.

Kravchenko, V. (1966). Empirical Equation Derived for Temperature Dependence of Density of Heavy Water. *Springer New York*. volume 20, 212

Kuphaldt, T. R. (2009). Lessons in industrial instrumentation. Chapter 13.9: Practical Calibration Standards. California, USA: *Creative Commons.* Version 0.4, 353-355.

Kuhn, V., Klemes, J., & Bulatov, I. (2008). MicroCHP: Overview of selected technologies, products and field test results. *Applied Thermal Engineering*. 2039-2048

Legget, R. F. & Peckover, F. L. (1949). Soil Temperature Studies - A Progress Report. *The 29th Annual Meeting of the Highway Research Board*, USA. 434-445.

Marrone, J. (2007). National view of activities leading to Net Zero Energy Home Construction– a perspective from Natural Resources Canada. Ottawa, Ontario, Canada.

Matrosov, Y. A ., Butovsky, I. N., & Watson, R. K. (1994). Case studies of energy consumption in residential buildings in Russia's middle belt area. *Energy and Buildings*. Volume 20, 231-241.

Miller, G. R., Gilmour, B., Myrans, I. D. C., Lang-Bismillah, A., Cordeiro, I., Jessop, T., Kenny, M., Kostyan, R., Yuen, J. (2008). Sustainable Building Canada on the Move. Chapter: What is Driving Sustainability Today? Toronto, Canada: *Canadian Urban Institute.*13-14.

NIST. (2009). *National Institute of Standards and Technology*. Retrieved July 02, 2009, from www.nist.gov: http://ts.nist.gov/MeasurementServices/Calibrations/flow.cfm#18020C

Olesen, B. W. (2002). Radiant Floor Heating in Theory and Practice. *ASHRAE Journal* , 19-24.

Onovwiona, H. I. & Ugursal, V. I. (2004). Residential cogeneration systems: review of the current technology. *Renewable & Sustainable Energy Reviews*. 1-43.

Padfield, T. (1996). *Equations describing the physical properties of moist air.* Retrieved December 2008, from The physics of the museum environment: http://www.natmus.dk/cons/tp/atmcalc/atmoclc1.htm

Parker, D. S. (1989). Thermal Performance Monitoring Results from the Residential Standards Demonstration Program. *Energy and Buildings*, Volume 13, 231-248.

Parker, D. S. (2009). Very low energy homes in the United States: Perspectives on performance from measured data., *Energy and Buildings*, Volume 41, 512-520.

Psychrometric Calculations. (n.d.). *Material properties*. Retrieved December 2008, from Sugar Engineers: http://www.sugartech.co.za/psychro/index.php

Queen's University Applied Sustainability Research Group. (2010). Effects of snow on photovoltaic performance. Retrieved June 19, 2010, from http://www.appropedia.org/Effects_of_snow_on_photovoltaic_performance

Roth, K. & Brodrick, J. (2008). Home Energy Displays. *ASHRAE Journal*, July, 136-138.

SRCC Document. (1994). Methodology for Determining the Thermal Performance Rating for Solar Collectors. *Florida: Solar Rating & Certification Corporation (SRCC)*.

Solar Buildings Research Network (SBRN). (2010). Retrieved May 9, 2010, from www.solarbuildings.ca: http://www.solarbuildings.ca/en/projects_3

SQL Server. (2008). Retrieved April 03, 2010, from Microsoft Corporation: www.microsoft.com: http://msdn.microsoft.com/en-us/library/ms143432.aspx

Stover, D. (1994). Canada's Advanced Houses. *Popular Science*, Issue: March, 73-78.

Swinton, M. C., Moussa, H., & Marchand, R. G. (2001). *Commissioning Twin Houses for Assessing the Performance of Energy Conserving Technologies.* Proceedings for Performance of Exterior Envelopes of Whole Buildings VIII: Integration of Building Envelopes, Florida. 1-10.

Tanaka, M., Girard, G., Davis, R., Peuto, A., & Bignell, N. (2001). Recommended table for the density of water between 0°C and 40°C based on recent experimental reports. *Metrologia*, Volume 38, 301-309.

The California Public Utilities Commission (CPUC). (2009). *California Solar Initiative Program Handbook.* California: *California Solar Initiative*.

The Engineering ToolBox. (2005). Retrieved December 2008, from Propylene Glycol based Heat-Transfer Fluids: http://www.engineeringtoolbox.com/propylene-glycol-d_363.html

Thomsen, K. E., Wittchen, K. B., & EuroACE. (2008). European national strategies to move towards very low energy buildings. *Danish Building Research Institute.* Hørsholm, Aalborg University, edition 1, 1-35.

TRCA & BILD. (2009). *About: Mission*. Retrieved October 2009, from Toronto and Region Conservation Authority: http://www.sustainablehouse.ca/about/mission.dot

US Department of Energy. (2009). *Recovery Act: Advanced Energy Efficient Building Technologies.* National Energy Technology Laboratory.

Walker, I. S. & Sherman, M. H. (2007). *Humidity Implications for Meeting Residential Ventilation Requirements.* California: Environmental Energy Technologies Division, Ernest Orlando Lawrance Berkley National Laboratory.

Vitotech technical guide. (2010). *Viessmann Limited*. Retrieved April 8, 2010, from www.viessmann.com. http://www.scribd.com/doc/19338747/Viessmann-Vitosol-Thermal-Solar-Collectors-System-Design-Guidelines.

Zhang, D., Barua, R. & Fung, A. S. (2010). Development of Monitoring System for the Sustainable Archetype House at Kortright Centre. *1st International High Performance Buildings Conference at Purdue University*. Indiana: Compressor/Refrigeration & Air Conditioning/High Performance Buildings Conferences at Purdue. 3482 (1-8).

Appendix A: Sensor address, list, type and location

As mentioned earlier, more than 300 sensors are installed in this monitoring system. It is very important to keep proper record of all sensors address, type and location for easy to find and troubleshooting. Figures A.1 and Figure A.2 show the DAQ infrastructure in House-A and House-B. Table A.1 and Table A.2 show sensor address, type and location.

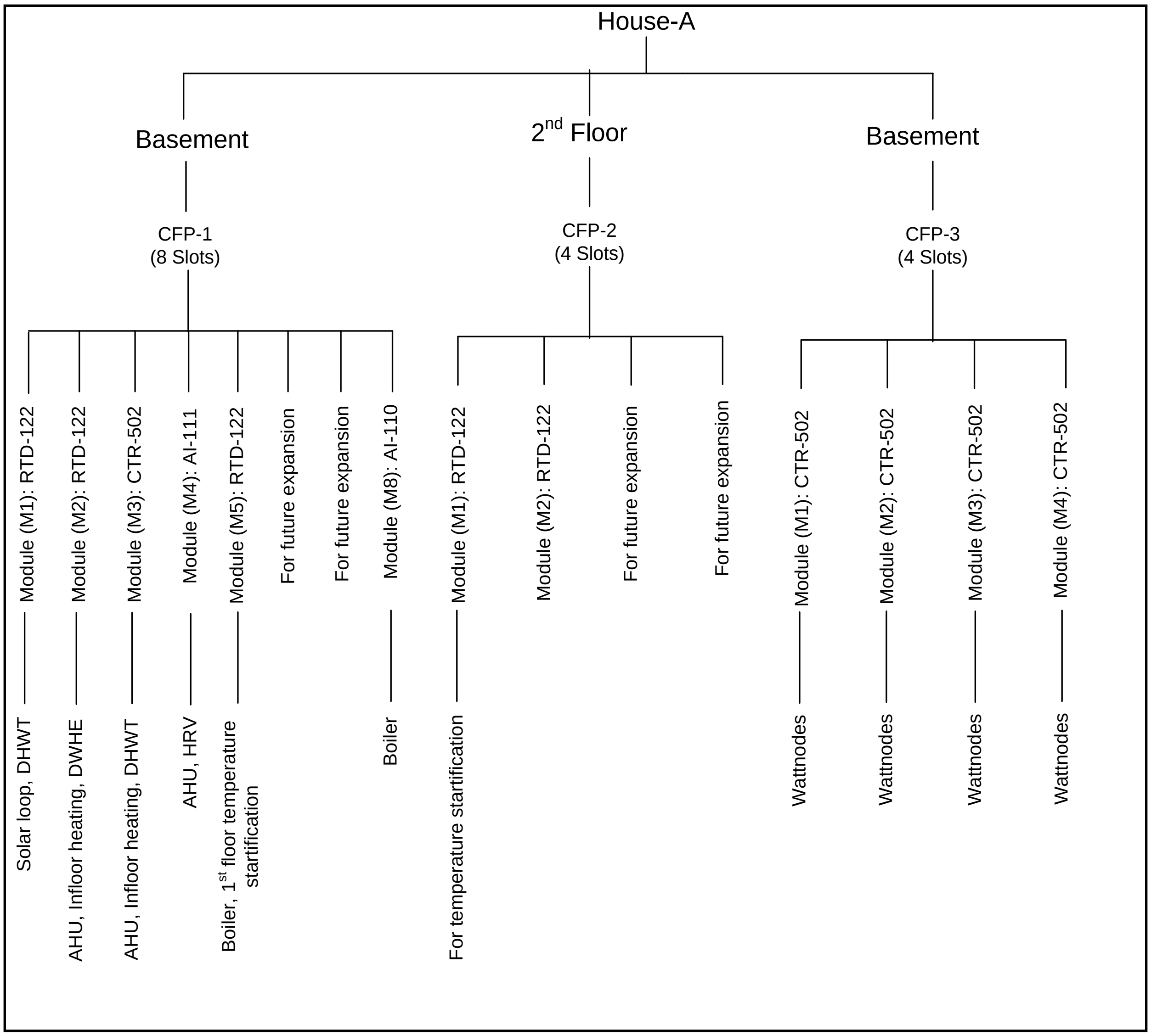

Figure 3 DAQ infrastructure in House-A

Table A.1 Nomenclature of Sensors, Channels, Modules and Compact field point of DAQ systems in House-A

Module: RTD-122 (Output signal: RTD)			
Address	**Sensor**	**Type**	**Location**
A-CFP1-M1-CH1	T1	Pt. 100	Un-tempered water
A-CFP1-M1-CH2	T4	Pt. 100	Tempered water line
A-CFP1-M1-CH3	T5	Pt. 500	Solar collector supply
A-CFP1-M1-CH4	T6	Pt. 500	Solar collector return
A-CFP1-M1-CH5	T19	Pt. 100	Recirculation of DHWT
A-CFP1-M1-CH6	T7	Pt. 500	DHWT return from boiler
A-CFP1-M1-CH7	T8	Pt. 500	DHWT supply to Boiler
A-CFP1-M1-CH8	T3	Pt. 100	City water to DHWT

Module: RTD-122 (Output signal: RTD)			
Address	**Sensor**	**Type**	**Location**
A-CFP1-M2-CH1	T12	Pt. 100	Infloor heating supply
A-CFP1-M2-CH2	T14	Pt. 100	Infloor heating return
A-CFP1-M2-CH3	T11	Pt. 100	Boiler return from A-AHU
A-CFP1-M2-CH4	T18	Pt. 100	Boiler supply to A-AHU
A-CFP1-M2-CH5	T13	Pt. 100 (SM)	Drain water to GWHE
A-CFP1-M2-CH6	T17	Pt. 100 (SM)	Drain water from GWHE
A-CFP1-M2-CH7	T15	Pt. 500	City water to GWHE
A-CFP1-M2-CH8	T16	Pt. 500	Water from DGWHE

Module: CTR-502 (Output signal: Pulse)			
Address	**Sensor**	**Type**	**Location**
A-CFP1-M3-CH1	FL7	Flow rate	Un-tempered water
A-CFP1-M3-CH2	FL10	Flow rate	Tempered water
A-CFP1-M3-CH3	FL6	Flow rate	Recirculation water to DHWT
A-CFP1-M3-CH4	FL1	Flow rate	Solar collector return
A-CFP1-M3-CH5	FL3	Flow rate	From GWHE to DHWT
A-CFP1-M3-CH6	FL8	Flow rate	Boiler to infloor heating
A-CFP1-M3-CH7	FL9	Flow rate	Boiler to A-AHU
A-CFP1-M3-CH8			

Module: AI-111 (Output signal: mA)			
Address	**Sensor**	**Type**	**Location**
A-CFP1-M4-CH1	RH8	Relative Humidity	Fresh air from Outdoor to HRV
A-CFP1-M4-CH2	AT8	Air Temp.	
A-CFP1-M4-CH3	RH9	Relative Humidity	Exhaust air from HRV to outdoor
A-CFP1-M4-CH4	AT9	Air Temp.	
A-CFP1-M4-CH5	RH10	Relative Humidity	Return air from zone to HRV
A-CFP1-M4-CH6	AT10	Air Temp.	
A-CFP1-M4-CH7	RH11	Relative Humidity	Supply air from HRV to zone
A-CFP1-M4-CH8	AT11	Air Temp.	
A-CFP1-M4-CH9	RH12	Relative Humidity	Main return air from zone to AHU

A-CFP1-M4-CH10	AT12	Air Temp.	
A-CFP1-M4-CH11	RH7	Relative Humidity	Main supply air AHU to zone
A-CFP1-M4-CH12	AT7	Air Temp.	
A-CFP1-M4-CH13	AF8	Air Flow station	Fresh air from Outdoor to HRV
A-CFP1-M4-CH14	AF9	Air Flow station	Exhaust air from HRV to outdoor
A-CFP1-M4-CH15	AV1	Air Velocity Meter	Main supply air AHU to zone
A-CFP1-M4-CH16	AV2	Air Velocity Meter	Main return air from zone to AHU

Module: RTD-122 (Output signal: RTD)			
Address	**Sensor**	**Type**	**Location**
A-CFP1-M5-CH1	T9	Pt. 500	Hot water from Boiler
A-CFP1-M5-CH2	T10	Pt. 500	Cold water to Boiler
A-CFP1-M5-CH3	T20	Pt. 100 (SM)	Flue gas duct of Boiler
A-CFP1-M5-CH4	$T_{2'}$	Pt. 100 (SM)	1st floor room temperature at 2′ height
A-CFP1-M5-CH5	$T_{4'}$	Pt. 100 (SM)	1st floor room temperature at 4′ height
A-CFP1-M5-CH6	$T_{6'}$	Pt. 100 (SM)	1st floor room temperature at 6′ height
A-CFP1-M5-CH7	$T_{8'}$	Pt. 100 (SM)	1st floor room temperature at 8′ height
A-CFP1-M5-CH8			

Module: AI-110 (Output signal: mA or mV)			
Address	**Sensor**	**Type**	**Location**
A-CFP1-M8-CH1	NG1	Gas meter	Boiler
A-CFP1-M8-CH2	FL4	Flow rate (Proteus)	DHWT of Boiler loop
A-CFP1-M8-CH3	FL5	Flow rate (Proteus)	Boiler loop
A-CFP1-M8-CH4			
A-CFP1-M8-CH5			
A-CFP1-M8-CH6			
A-CFP1-M8-CH7			
A-CFP1-M8-CH8			

Module: RTD-122 (Output signal: RTD)			
Address	**Sensor**	**Type**	**Location**
A-CFP2-M1-CH1	$T_{2'}$	Pt. 100 (SM)	2nd floor room temperature at 2′ height
A-CFP2-M1-CH2	$T_{4'}$	Pt. 100 (SM)	2nd floor room temperature at 4′ height
A-CFP2-M1-CH3	$T_{6'}$	Pt. 100 (SM)	2nd floor room temperature at 6′ height
A-CFP2-M1-CH4	$T_{8'}$	Pt. 100 (SM)	2nd floor room temperature at 8′ height
A-CFP2-M1-CH5			
A-CFP2-M1-CH6			
A-CFP2-M1-CH7			
A-CFP2-M1-CH8			

Module: CTR-502 (Output signal: Pulse), Sensors type: Watt-node		
Address	**Sensor**	**Location and CT size**
A-CFP3-M1-CH1	4-P3-2	HRV fan: 5 Amps
A-CFP3-M1-CH2	2-P3-2	AHU hot water circulation pump: 5 Amps
A-CFP3-M1-CH3	3-P-1	Two stage ASHP: 30 Amps
A-CFP3-M1-CH4	4-P3-1	Boiler: 5 Amps
A-CFP3-M1-CH5	2-P3-3	Boiler primary loop circulation pump: 5 Amps
A-CFP3-M1-CH6	2-P3-1	DHW storage tank circulation pump: 5 Amps
A-CFP3-M1-CH7	1-PV-3	Panel board receptacles, data logging: 15 Amps Data receptacles 1st floor, broom closet: 15 Amps Data receptacles 2nd floor, east bedroom closet: 15 Amps Data receptacles, attic, east wall: 15 Amps EXIT sign: 15 Amps, and emergency lights: 15 Amps
A-CFP3-M1-CH8	5-P3-1	Basement Floor Drain Pump: 5 Amps

Module: CTR-502 (Output signal: Pulse), Sensors type: Watt-node		
Address	**Sensor**	**Location and CT size**
A-CFP3-M2-CH1	5-P3-2	Solar collector glycol loop: 5 Amps
A-CFP3-M2-CH2	7-P3-3	BRAC Grey water unit: 15 Amps
A-CFP3-M2-CH3	1-PV-1	Grid to house: 100 Amps
A-CFP3-M2-CH4	8-P-1	Lights: 60 Amps, Lighting panel feed, Lighting panel contactor, Foyer, washroom, Kitchen, Dining area, Living room, Living room (future bed room), 2nd floor hall, Master bed room, 2nd floor bed, bath, closet, Attic, and basement.
A-CFP3-M2-CH5	9-P3-2	Receptacles: 60 Amps GP indoor, Adaptable bedroom, 3rd floor, Bedroom 2& 3, Master bedroom, 2nd floor bathroom, 2nd floor hallway, Living room, Foyer, 1st floor bathroom, and smoke detector.
A-CFP3-M2-CH6	5-P3-3	DHW load circulator: 5 Amps
A-CFP3-M2-CH7	10-P3-1	AHU fan and heap filter fan: 15 Amps
A-CFP3-M2-CH8	6-P3-3	Infloor radiant heating pump: ?

Module: CTR-502 (Output signal: Pulse), Sensors type: Watt-node		
Address	**Sensor**	**Location and CT size**
A-CFP3-M3-CH1	6-P3-1	Sewerage pump: 15 Amps
A-CFP3-M3-CH2	7-P3-1	Water softener: 15 Amps
A-CFP3-M3-CH3		
A-CFP3-M3-CH4	11-P-1	Kitchen receptacles: ?
A-CFP3-M3-CH5	12-P1-1	Kitchen fan with light: 30 Amps, Oven: 30 Amps, Cook top: 30 Amps
A-CFP3-M3-CH6	10-P3-3	Fridge: 15 Amps
A-CFP3-M3-CH7	13-P3-1	Dishwasher: 15 Amps
A-CFP3-M3-CH8	13-P3-2	Garage and outdoor receptacles: 15 Amps

Module: CTR-502 (Output signal: Pulse), Sensors type: Watt-node		
Address	**Sensor**	**Location and CT size**
A-CFP3-M4-CH1	13-P3-3	Garage lights: 15 Amps and exterior lights: sahred
A-CFP3-M4-CH2	10-P3-2	Washing machine: 15 Amps
A-CFP3-M4-CH3	7-P3-2	Dryer: 30 Amps
A-CFP3-M4-CH4		
A-CFP3-M4-CH5		
A-CFP3-M4-CH6		
A-CFP3-M4-CH7		
A-CFP3-M4-CH8		

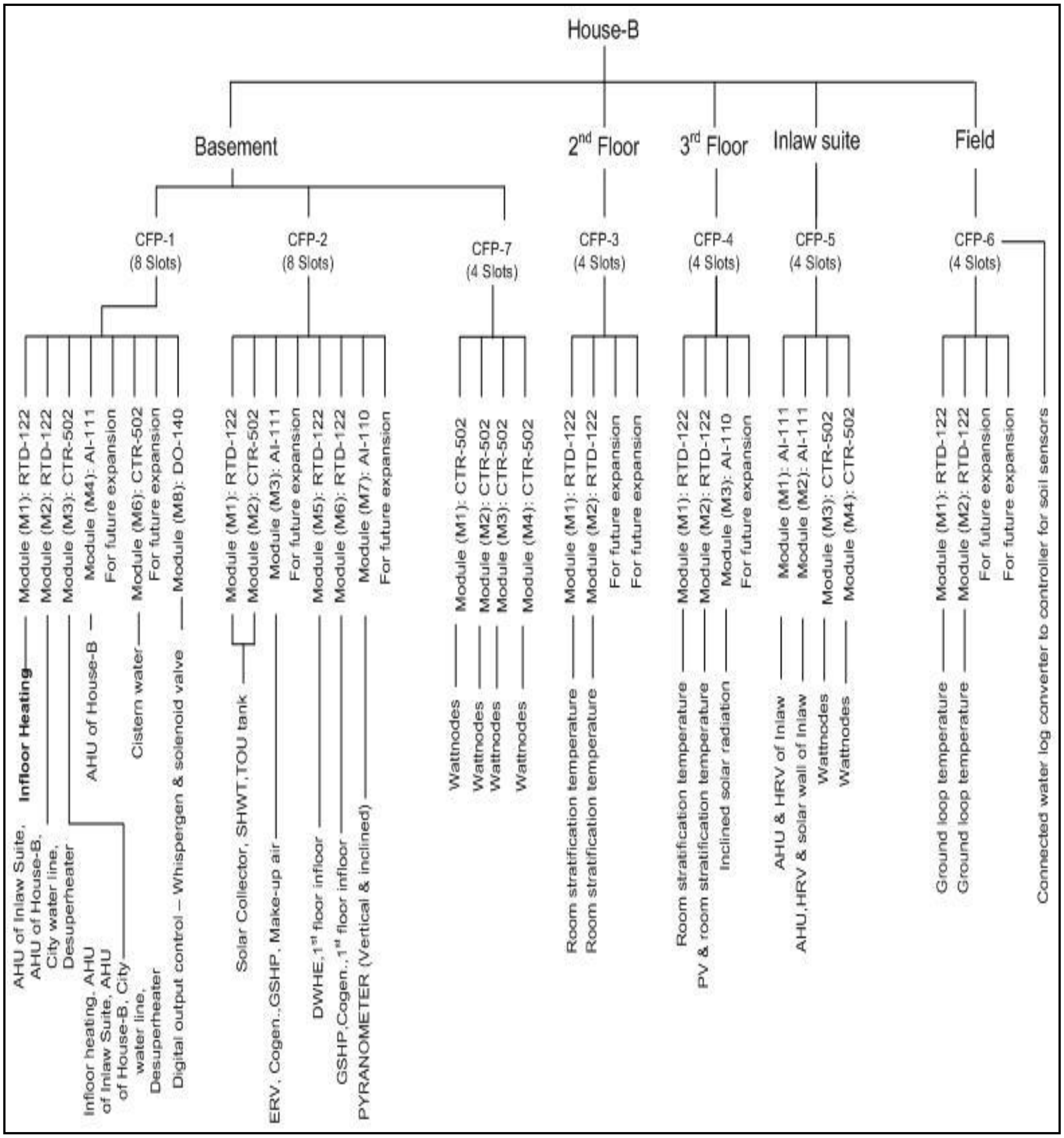

Figure 4 DAQ infrastructure in House-B

Table 3 Nomenclature of Sensors, Channels, Modules and Compact field point in DAQ systems in House-B

Module: RTD-122 (Output signal: RTD)

Address	Sensor	Type	Location
B-CFP1-M1-CH1	T12	Pt. 500	Radiant basement supply
B-CFP1-M1-CH2	T11	Pt. 500	Radiant basement return
B-CFP1-M1-CH3	T10	Pt. 500	Radiant 1st floor supply
B-CFP1-M1-CH4	T9	Pt. 500	Radiant 1st floor return
B-CFP1-M1-CH5	T8	Pt. 500	Radiant 2nd floor supply
B-CFP1-M1-CH6	T7	Pt. 500	Radiant 2nd return
B-CFP1-M1-CH7	T6	Pt. 500	Radiant 3rd supply
B-CFP1-M1-CH8	T5	Pt. 500	Radiant 3rd return

Module: RTD-122 (Output signal: RTD)

Address	Sensor	Type	Location
B-CFP1-M2-CH1	T4	Pt. 500	Buffer tank to Inlaw AHU supply
B-CFP1-M2-CH2	T3	Pt. 500	Buffer tank to Inlaw AHU return
B-CFP1-M2-CH3	T13	Pt. 500	Buffer tank to B-AHU supply
B-CFP1-M2-CH4	T14	Pt. 500	Buffer tank to B-AHU return
B-CFP1-M2-CH5	T18	Pt. 500	Desuperheater return
B-CFP1-M2-CH6	T19	Pt. 500	Desuperheater supply
B-CFP1-M2-CH7	T27	Pt. 100	City water
B-CFP1-M2-CH8			

Module: CTR-502 (Output signal: Pulse)

Address	Sensor	Type	Location
B-CFP1-M3-CH1	FL15	Flow rate	Radiant Basement
B-CFP1-M3-CH2	FL14	Flow rate	Radiant 1st floor
B-CFP1-M3-CH3	FL13	Flow rate	Radiant 2nd floor
B-CFP1-M3-CH4	FL12	Flow rate	Radiant 3rd floor
B-CFP1-M3-CH5	FL9	Flow rate	Buffer tank to Inlaw AHU
B-CFP1-M3-CH6	FL8	Flow rate	Buffer tank to B-AHU
B-CFP1-M3-CH7	FL5	Flow rate	Desuperheater
B-CFP1-M3-CH8	FL4	Flow rate	City water

Module: AI-111 (Output signal: mA)

Address	Sensor	Type	Location
B-CFP1-M4-CH1	RH13	RH	Supply air duct to 1st floor of B-AHU
B-CFP1-M4-CH2	AT13	Air Temp.	
B-CFP1-M4-CH3	RH14	RH	Supply air duct to 2nd floor of B-AHU
B-CFP1-M4-CH4	AT14	Air Temp.	
B-CFP1-M4-CH5	RH15	RH	Supply air duct to 3rd floor of B-AHU
B-CFP1-M4-CH6	AT15	Air Temp.	
B-CFP1-M4-CH7	RH11	RH	Return air duct of 1st floor of B-AHU
B-CFP1-M4-CH8	AT11	Air Temp.	
B-CFP1-M4-CH9	RH9	RH	Return air duct of 2nd & 3rd floor of B-AHU

B-CFP1-M4-CH10	AT9	Air Temp.	
B-CFP1-M4-CH11	AF13	Air Flow	Supply air duct to 1st floor of B-AHU
B-CFP1-M4-CH12	AF12	Air Flow	Supply air duct to 2nd floor of B-AHU
B-CFP1-M4-CH13	AF11	Air Flow	Supply air duct to 3rd floor of B-AHU
B-CFP1-M4-CH14	AF7	Air Flow	Return air duct of 1st floor of B-AHU
B-CFP1-M4-CH15	AF5	Air Flow	Return air duct of 2nd & 3rd floor of B-AHU
B-CFP1-M4-CH16			

Module: CTR-502 (Output signal: Pulse)			
Address	**Sensor**	**Type**	**Location**
B-CFP1-M6-CH1	FL25	Flow rate	Cistern water
B-CFP1-M6-CH2			
B-CFP1-M6-CH3			
B-CFP1-M6-CH4			
B-CFP1-M6-CH5			
B-CFP1-M6-CH6			
B-CFP1-M6-CH7			
B-CFP1-M6-CH8			

Module: DO-410 (Digital control)			
Address	**Control**	**Type**	**Location**
B-CFP1-M8-CH1	CHP	*Pt. 100 (SM)	Buffer tank
B-CFP1-M8-CH2	CHP	Pt. 100 (SM)	Solar hot water tank
B-CFP1-M8-CH3	CHP	Pt. 100 (SM)	Micro Whispergen CHP
B-CFP1-M8-CH4			
B-CFP1-M8-CH5			
B-CFP1-M8-CH6			
B-CFP1-M8-CH7			
B-CFP1-M8-CH8			

*Pt. 100 (SM) Surface mounted temperature sensor

Module: RTD-122 (Output signal: RTD)			
Address	**Sensor**	**Type**	**Location**
B-CFP2-M1-CH1	T24	Pt. 500	Solar collector supply
B-CFP2-M1-CH2	T25	Pt. 500	Solar collector return
B-CFP2-M1-CH3	T23	Pt. 100	Solar pre-heat tank supply to TOU tank
B-CFP2-M1-CH4	T1	Pt. 100	Cold water to solar pre-heat tank
B-CFP2-M1-CH5	T40	Pt. 100	Recirculation water to solar pre-heat tank
B-CFP2-M1-CH6	T22	Pt. 100	Tempered water from TOU tank
B-CFP2-M1-CH7	T2	Pt. 100	Un-tempered water from TOU tank
B-CFP2-M1-CH8	T33	Pt. 100 (SM)	Flue gas from CHP unit

Module: CTR-502 (Output signal: Pulse)			
Address	**Sensor**	**Type**	**Location**
B-CFP2-M2-CH1	FL1	Flow rate	Solar collector supply
B-CFP2-M2-CH2	FL2	Flow rate	Cold water to Solar pre-heat tank
B-CFP2-M2-CH3	FL40	Flow rate	Recirculation water to Solar pre-heat tank
B-CFP2-M2-CH4	FL3	Flow rate	Tempered water from TOU tank
B-CFP2-M2-CH5	FL10	Flow rate	Un-tempered water from TOU tank
B-CFP2-M2-CH6			
B-CFP2-M2-CH7			
B-CFP2-M2-CH8			

Module: AI-111 (Output signal: mA)			
Address	**Sensor**	**Type**	**Location**
B-CFP2-M3-CH1	RH18	RH	Supply air from ERV to AHU
B-CFP2-M3-CH2	AT18	Air Temp.	
B-CFP2-M3-CH3	RH19	RH	Return air from zone to ERV
B-CFP2-M3-CH4	AT19	Air Temp.	
B-CFP2-M3-CH5	RH20	RH	Fresh air from outdoor to ERV
B-CFP2-M3-CH6	AT20	Air Temp.	
B-CFP2-M3-CH7	RH21	RH	Exhaust air from ERV to outdoor
B-CFP2-M3-CH8	AT21	Air Temp.	
B-CFP2-M3-CH9	AF16	Air Flow	Supply air from ERV to B-AHU
B-CFP2-M3-CH10	AF15	Air Flow	Return air from zone to ERV
B-CFP2-M3-CH11	RH25	RH	Outdoor air RH (South side)
B-CFP2-M3-CH12	AT25	Air Temp.	Outdoor air temperature (South side)
B-CFP2-M3-CH13	FL18	Flow rate (SPARLING)	CHP unit (NRCan)
B-CFP2-M3-CH14			
B-CFP2-M3-CH15	RH24	RH	Outdoor air RH (North side)
B-CFP2-M3-CH16	AT24	Air Temp.	Outdoor air temperature (North side)

Module: RTD-122 (Output signal: RTD)			
Address	**Sensor**	**Type**	**Location**
B-CFP2-M5-CH1	T30	Pt. 500	Pre-heat water to GWHE
B-CFP2-M5-CH2	T26	Pt. 500	Warm water from GWHE
B-CFP2-M5-CH3	T28	Pt. 100 (SM)	Drain water to GWHE
B-CFP2-M5-CH4	T29	Pt. 100 (SM)	Drain water from GWHE
B-CFP2-M5-CH5	$T_{B1\_3b\_TOP}$	Pt. 100 (SM)	1st floor infloor top (North end)
B-CFP2-M5-CH6	$T_{B1\_3b\_BOT}$	Pt. 100 (SM)	1st floor infloor bottom (North end)
B-CFP2-M5-CH7	$T_{B1\_2b\_TOP}$	Pt. 100 (SM)	1st floor infloor top (Middle)
B-CFP2-M5-CH8	$T_{B1\_2b\_BOT}$	Pt. 100 (SM)	1st floor infloor bottom (Middle)

Module: RTD-122 (Output signal: RTD)			
Address	**Sensor**	**Type**	**Location**
B-CFP2-M6-CH1	T20	Pt. 500	Supply to ground loop
B-CFP2-M6-CH2	T21	Pt. 500	Return from ground loop
B-CFP2-M6-CH3	T16	Pt. 500	Supply from GSHP to Buffer tank
B-CFP2-M6-CH4	T17	Pt. 500	Return to GSHP from Buffer tank
B-CFP2-M6-CH5	T32	Pt. 500	Supply from CHP to Buffer tank
B-CFP2-M6-CH6	T31	Pt. 500	Return to CHP from Buffer tank
B-CFP2-M6-CH7	$T_{B1\_1b\_TOP}$	Pt. 100 (SM)	1^{st} infloor top (South end)
B-CFP2-M6-CH8	$T_{B1\_1b\_BOT}$	Pt. 100 (SM)	1^{st} floor infloor bottom (South end)

Module: AI-110 (Output signal: mA or mV)			
Address	**Sensor**	**Type**	**Location**
B-CFP2-M7-CH1	PY_V	Pyranometer	Vertical position
B-CFP2-M7-CH2	PY_H	Pyranometer	Horizontal position
B-CFP2-M7-CH3	NG2	Gas meter (SIERRA)	CHP unit
B-CFP2-M7-CH4	FL16	Flow rate (Proteus)	GSHP ground loop
B-CFP2-M7-CH5			
B-CFP2-M7-CH6	FL19	Water flow rate (Omega)	CHP unit (NRCan)
B-CFP2-M7-CH8	FL6	Water flow rate (Proteus)	GSHP to Buffer tank
B-CFP2-M7-CH7	FL17	Water flow rate (Proteus)	CHP unit

Module: RTD-122 (Output signal: RTD)			
Address	**Sensor**	**Type**	**Location**
B-CFP3-M1-CH1	$T_{B2\_1b\_TOP}$	Pt. 100 (SM)	2^{nd} floor infloor top (South end)
B-CFP3-M1-CH2	$T_{B2\_1b\_BOT}$	Pt. 100 (SM)	2^{nd} floor infloor bottom (South end)
B-CFP3-M1-CH3	$T_{B2\_2b\_TOP}$	Pt. 100 (SM)	2^{nd} floor infloor top (Middle)
B-CFP3-M1-CH4	$T_{B2\_2b\_BOT}$	Pt. 100 (SM)	2^{nd} floor infloor bottom (Middle)
B-CFP3-M1-CH5	$T_{B2\_3b\_TOP}$	Pt. 100 (SM)	2^{nd} floor infloor top (North end)
B-CFP3-M1-CH6	$T_{B2\_3b\_BOT}$	Pt. 100 (SM)	2^{nd} floor infloor bottom (North end)
B-CFP3-M1-CH7	$T_{2'}$	Pt. 100 (SM)	2^{nd} floor room temperature at 2′ height
B-CFP3-M1-CH8	$T_{4'}$	Pt. 100 (SM)	2^{nd} floor room temperature at 4′ height

Module: RTD-122 (Output signal: RTD)			
Address	**Sensor**	**Type**	**Location**
B-CFP3-M2-CH1	$T_{6'}$	Pt. 100 (SM)	2^{nd} floor room temperature at 6′ height
B-CFP3-M2-CH2	$T_{8'}$	Pt. 100 (SM)	2^{nd} floor room temperature at 8′ height
B-CFP3-M2-CH3			
B-CFP3-M2-CH4			
B-CFP3-M2-CH5			
B-CFP3-M2-CH6			
B-CFP3-M2-CH7			
B-CFP3-M2-CH8			

Module: RTD-122 (Output signal: RTD)			
Address	**Sensor**	**Type**	**Location**
B-CFP4-M1-CH1	$T_{B3\_1b\_TOP}$	Pt. 100 (SM)	3rd floor infloor top (South end)
B-CFP4-M1-CH2	$T_{B3\_1b\_BOT}$	Pt. 100 (SM)	3rd floor infloor bottom (South end)
B-CFP4-M1-CH3	$T_{B3\_2b\_TOP}$	Pt. 100 (SM)	3rd floor infloor top (Middle)
B-CFP4-M1-CH4	$T_{B3\_2b\_BOT}$	Pt. 100 (SM)	3rd floor infloor bottom (Middle)
B-CFP4-M1-CH5	$T_{B3\_3b\_TOP}$	Pt. 100 (SM)	3rd floor infloor top (North end)
B-CFP4-M1-CH6	$T_{B3\_3b\_BOT}$	Pt. 100 (SM)	3rd floor infloor bottom (North end)
B-CFP4-M1-CH7	$T_{2'}$	Pt. 100 (SM)	3rd floor room temperature at 2′ height
B-CFP4-M1-CH8	$T_{4'}$	Pt. 100 (SM)	3rd floor room temperature at 4′ height

Module: RTD-122 (Output signal: RTD)			
Address	**Sensor**	**Type**	**Location**
B-CFP4-M2-CH1	$T_{6'}$	Pt. 100 (SM)	3rd floor room temperature at 6′ height
B-CFP4-M2-CH2	$T_{8'}$	Pt. 100 (SM)	3rd floor room temperature at 8′ height
B-CFP4-M2-CH3	T40	Pt. 100 (SM)	PV array temperature
B-CFP4-M2-CH4	T41	Pt. 100 (SM)	Outlet air temperature under PV array
B-CFP4-M2-CH5	T42	Pt. 100 (SM)	Inlet air temperature under PV array
B-CFP4-M2-CH6			
B-CFP4-M2-CH7			
B-CFP4-M2-CH8			

Module: AI-110 (Output signal: mA or mV)			
Address	**Sensor**	**Type**	**Location**
B-CFP4-M3-CH1	PY_I	Pyranometer	At 25°
B-CFP4-M3-CH2			
B-CFP4-M3-CH3			
B-CFP4-M3-CH4			
B-CFP4-M3-CH5			
B-CFP4-M3-CH6			
B-CFP4-M3-CH7			
B-CFP4-M3-CH8			

Module: AI-111 (Output signal: mA)			
Address	**Sensor**	**Type**	**Location**
B-CFP5-M1-CH1	RH1	RH	Fresh air from outdoor to Inlaw-HRV
B-CFP5-M1-CH2	AT1	Air Temp.	
B-CFP5-M1-CH3	RH2	RH	Exhaust air from Inlaw-HRV
B-CFP5-M1-CH4	AT2	Air Temp.	
B-CFP5-M1-CH5	RH3	RH	Supply air from Inlaw-HRV to AHU
B-CFP5-M1-CH6	AT3	Air Temp.	
B-CFP5-M1-CH7	RH4	RH	Supply air from Inlaw-AHU to zone
B-CFP5-M1-CH8	AT4	Air Temp.	
B-CFP5-M1-CH9	RH5	RH	Exhaust air from zone to Inlaw-HRV

B-CFP5-M1-CH10	AT5	Air Temp.	
B-CFP5-M1-CH11	RH6	RH	Return air from zone to Inlaw-AHU
B-CFP5-M1-CH12	AT6	Air Temp.	
B-CFP5-M1-CH13	RH7	RH	Supply air from solar wall
B-CFP5-M1-CH14	AT7	Air Temp.	
B-CFP5-M1-CH15	RH8	RH	Return air to solar wall
B-CFP5-M1-CH16	AT8	Air Temp.	

Module: AI-111 (Output signal: mA)			
Address	**Sensor**	**Type**	**Location**
B-CFP5-M2-CH1	AF1	Air Flow station	Return air from zone to Inlaw-AHU
B-CFP5-M2-CH2	AF2	Air Flow station	Exhaust air from HRV to outdoor
B-CFP5-M2-CH3	AF3	Air Flow station	Fresh air from outdoor to Inlaw- HRV
B-CFP5-M2-CH4	AF4	Air Flow station	Return air to solar wall
B-CFP5-M2-CH5	AF18	Air Flow station	Return air from room to HRV
B-CFP5-M2-CH6		DC CT	Solar air heater fan
B-CFP5-M2-CH7		DC CT	PV inverter DC amps
B-CFP5-M2-CH8		Voltage transducer	Solar air heater fan
B-CFP5-M2-CH9		Voltage transducer	PV inverter DC amps
B-CFP5-M2-CH10			
B-CFP5-M2-CH11			
B-CFP5-M2-CH12			
B-CFP5-M2-CH13			
B-CFP5-M1-CH14			
B-CFP5-M1-CH15			
B-CFP5-M1-CH16			

Module: CTR-502 (Output signal: Pulse), Sensors type: Watt-node		
Address	**Sensor**	**Location and CT size**
B-CFP5-M3-CH1	1-PV-1	PV cell forward: 30 Amps
B-CFP5-M3-CH2	1-PV-2	PV cell reverse: 30 Amps
B-CFP5-M3-CH3	2-PV-1	Wind turbine forward: 15 Amps
B-CFP5-M3-CH4	2-PV-2	Wind turbine reverse: 15 Amps
B-CFP5-M3-CH5	4-P3-1 4-P3-2	Emergency EXIT lights and instrumentation: total = 5 Amps
B-CFP5-M3-CH6	4-P3-3	Inlaw-AHU: 15 Amps
B-CFP5-M3-CH7	3-P3-3	Inlaw interior lights: 5 Amps
B-CFP5-M3-CH8	3-P3-2	Inlaw interior receptacles: 15, 15 Amps = 30 Amps

Module: CTR-502 (Output signal: Pulse), Sensors type: Watt-node		
Address	**Sensor**	**Location and CT size**
B-CFP5-M4-CH1	2-PV-3	Garage receptacles and exhaust fan: 15 Amps
B-CFP5-M4-CH2	1-PV-3	Garage interior and exterior lights: total = 15 Amps
B-CFP5-M4-CH3	3-P3-1	Garage exterior GFI receptacles: 15, 15 Amps = 30 Amps
B-CFP5-M4-CH4		
B-CFP5-M4-CH5		
B-CFP5-M4-CH6		
B-CFP5-M4-CH7		
B-CFP5-M4-CH8		

Module: RTD-122 (Output signal: RTD)			
Address	**Sensor**	**Type**	**Location**
B-CFP6-M1-CH1	RTD-2	Pt. 100 (SM)	Supply pipe: beginning of 1st earth loop
B-CFP6-M1-CH2	RTD-1	Pt. 100 (SM)	Return pipe: beginning of 1st earth loop
B-CFP6-M1-CH3	RTD-12	Pt. 100 (SM)	Supply pipe: beginning of 2nd earth loop
B-CFP6-M1-CH4	RTD-11	Pt. 100 (SM)	Return pipe: beginning of 2nd earth loop
B-CFP6-M1-CH5	RTD-9	Pt. 100 (SM)	Return pipe: middle of 2nd earth loop
B-CFP6-M1-CH6	RTD-8	Pt. 100 (SM)	Supply pipe: end of 2nd earth loop
B-CFP6-M1-CH7	RTD-4	Pt. 100 (SM)	Supply pipe: middle of 1st earth loop
B-CFP6-M1-CH8	RTD-3	Pt. 100 (SM)	Return pipe: middle of 1st earth loop

Module: RTD-122 (Output signal: RTD)			
Address	**Sensor**	**Type**	**Location**
B-CFP6-M2-CH1	RTD-7	Pt. 100 (SM)	Return pipe: end of 2nd earth loop
B-CFP6-M2-CH2	RTD-5	Pt. 100 (SM)	Return pipe: end of 1st earth loop
B-CFP6-M2-CH3	RTD-10	Pt. 100 (SM)	Supply pipe: middle of 2nd earth loop
B-CFP6-M2-CH4			
B-CFP6-M2-CH5			
B-CFP6-M2-CH6			
B-CFP6-M2-CH7			
B-CFP6-M2-CH8			

Sensor address	Correspond to Figure 4	Sensor location	Chan-nel	ID	Sensors output
a	S11	12″ from the ground	CH1	SM_a	Soil moisture content
			CH2	EC_a	Soil conductivity
			CH3	Temp_a	Soil temperature
b	S21	42″ from the ground	CH4	SM_b	Soil moisture
			CH5	EC_b	Soil conductivity
			CH6	Temp_b	Soil temperature
c	S31	64″ from the ground	CH7	SM_c	Soil moisture content
			CH8	EC_c	Soil conductivity
			CH9	Temp_c	Soil temperature

d	S12	30″ from the ground	CH10	SM_d	Soil moisture
			CH11	EC_d	Soil conductivity
			CH12	Temp_d	Soil temperature
e	S22	42″ from the ground	CH13	SM_e	Soil moisture content
			CH14	EC_e	Soil conductivity
			CH15	Temp_e	Soil temperature
f	S32	64″ from the ground	CH16	SM_f	Soil moisture content
			CH17	EC_f	Soil conductivity
			CH18	Temp_f	Soil temperature
g	S13	18″ from the ground	CH19	SM_g	Soil moisture content
			CH20	EC_g	Soil conductivity
			CH21	Temp_g	Soil temperature
h	S23	42″ from the ground	CH22	SM_h	Soil moisture content
			CH23	EC_h	Soil conductivity
			CH24	Temp_h	Soil temperature
i	S33	64″ from the ground	CH25	SM_i	Soil moisture content
			CH26	EC_i	Soil conductivity
			CH27	Temp_i	Soil temperature
j	S14	24″ from the ground	CH28	SM_j	Soil moisture content
			CH29	EC_j	Soil conductivity
			CH30	Temp_j	Soil temperature
k	S24	42″ from the ground	CH31	SM_k	Soil moisture content
			CH32	EC_k	Soil conductivity
			CH33	Temp_k	Soil temperature
l	S34	64″ from the ground	CH34	SM_l	Soil moisture content
			CH35	EC_l	Soil conductivity
			CH36	Temp_l	Soil temperature

Module: CTR-502 (Output signal: Pulse), Sensor type: Wattnode		
Address	**Sensor**	**Location and CT size**
B-CFP7-M1-CH1	1-PV-1	Grid to house:100 Amps
B-CFP7-M1-CH2	1-PV-2	House to grid: 100 Amps
B-CFP7-M1-CH3	1-PV-3	Panel board receptacle, data logging, emergency EXIT lights: total = 15 Amps
B-CFP7-M1-CH4	2-P3-3	ERV fan: 5 Amps
B-CFP7-M1-CH5	2-P3-1	B-AHU fan: 15 Amps
B-CFP7-M1-CH6	2-P3-2	Sump and cistern pump: total = 15 Amps
B-CFP7-M1-CH7	3-P-1	GSHP compressor: 50 Amps
B-CFP7-M1-CH8	4-P-1	TOU heating coils: 15 Amps

Module: CTR-502 (Output signal: Pulse), Sensor type: Wattnode		
Address	**Sensors**	**Location and CT size**
B-CFP7-M2-CH1	5-P3-1	GSHP to Buffer tank: 5 Amps
B-CFP7-M2-CH2	5-P3-2	Desuperheater pump: 5 Amps
B-CFP7-M2-CH3	5-P3-3	Earth loop of GSHP: 5 Amps
B-CFP7-M2-CH4	6-P3-1	Buffer tank to B-AHU pump: 5 Amps
B-CFP7-M2-CH5	6-P3-2	Buffer tank to Infloor radiant heating pump: 5 Amps
B-CFP7-M2-CH6	6-P3-3	Buffer tank to Inlaw-AHU pump: 5 Amps
B-CFP7-M2-CH7	10-P-1	Cook top and oven: total= 30 Amps
B-CFP7-M2-CH8	11-P-1	Dryer: 30 Amps

Module: CTR-502 (Output signal: Pulse), Sensor type: Wattnode		
Address	**Sensors**	**Location and CT size**
B-CFP7-M3-CH1	7-PV-1	CHP unit @ Panel: 15 Amps
B-CFP7-M3-CH2	7-PV-2	CHP unit @ Machine: 15 Amps
B-CFP7-M3-CH3	12-P3-1	Basement drain pump: 15 Amps
B-CFP7-M3-CH4	8-P3-1	Basement, kitchen, great room, bathroom, 2nd floor, 2nd floor washroom hallway and 3rd floor receptacles: total= 60Amps
B-CFP7-M3-CH5	8-P3-2	Hot water circulation pump: 5 Amps
B-CFP7-M3-CH6	8-P3-3	Basement lights: 5 Amps
B-CFP7-M3-CH7	9-P3-1	Fridge: 15 Amps
B-CFP7-M3-CH8	9-P3-2	Kitchen fan with lights (Shared)

Module: CTR-502 (Output signal: Pulse), Sensor type: Wattnode		
Address	**Sensors**	**Location and CT size**
B-CFP7-M4-CH1	9-P3-3	Washing machine: 15 Amps
B-CFP7-M4-CH2	7-PV-3	CHP unit circulator pump after X-FMR: 5 Amps
B-CFP7-M4-CH3	12-P3-2	Kitchen, great room, 1st floor bath, dining room lights: total = 5Amps
B-CFP7-M4-CH4	12-P3-3	Solar collector glycol loop: 5 Amps
B-CFP7-M4-CH5	13-P3-1	Upstairs lights and 2nd floor lights: total = 5 Amps
B-CFP7-M4-CH6	13-P3-2	3rd floor lights: 5Amps
B-CFP7-M4-CH7	13-P3-3	Outdoor lighting and receptacles: total= 15 Amps
B-CFP7-M4-CH8		

Appendix B: Experimental Uncertainty Analysis

The uncertainty analysis is performed on the mechanical system/equipment that are analysed in the Chapter 5.

B1 Uncertainty of Sensors and Calibrators: Two error sources are considered in the uncertainty analysis. One is the accuracy value of sensors (Table B.1) and the other is the accuracy value of calibrators (Table B.2). Random error is neglected in this analysis. Square Root Sum of Squares (SRSS) method is followed which means that combine all errors or accuracy by squaring them, adding the squares together and taking the square root of the sum of those squares (ASHRAE Guideline 2, 2005).

$$\text{Overall accuracy of sensors} = \sqrt{A_c^2 + A_s^2} \qquad \text{(B.1)}$$

Where A_c = Calibrator accuracy, and A_s = Sensor accuracy

Overall accuracy of sensors from Equation (B.1) is used in the propagation of errors calculation to determine the accuracy of mechanical system/equipment.

Table B.1 Manufacturer supplied sensors and accuracy

Sensor name	Sensor type	Manufacturer	Model number	Sensor accuracy
Air velocity transmitter	Measure air velocity	Dwyer Instruments Inc.	AVU-1-A	±5.0%
Turbine type flow rate	Measure liquid/water flow rate	Omega/Clark Solution	CFT110	±3.0%
Metering flow switch	Measure liquid/water flow rate	Proteus Industries Inc.	800 Series	±0.5%
Air temperature (AT)/Relative humidity (RH)	Measure AT and RH	Dwyer Instruments Inc.	Series RHT-D	AT=±0.3%, RH = ±3.0%
Differential pressure transducer	Measure air flow rate	Alpha Instruments, Inc.	164	±1.0% FS
Pyranometer	Measure global solar radiation	LI-COR, Inc.	LI-200SZ	±5.0%
Wattnode	Measure electrical energy	Continental Control Systems	WNB-3Y-208-P	±1.0%
RTD sensor (Pt.-100, directly immersed)	Measure Temperature	Omega	PRTF-10-2-100-1/4-6-E	±0.1%
RTD sensor (Pt.-100, surface mount)	Measure Temperature	Omega	RTD-2-F3105-36-T-B	±0.12%

Table B.1 continued

RTD sensor (Pt.-500, directly immersed)	**Measure Temperature**	**Kamstrup**	**65-00-0DO-310**	**N/A**
Gas mass flow meter	Measure gas flow rate	SIERRA Instruments	826-NX-OV1-PV1-V1-T	±1.5%

Table B.2 Manufacturer supplied calibrators and accuracy

Calibrator name	Calibrator type	Manufacturer	Model number	Calibrator accuracy
Hot-wire Thermo Anemometer	Calibrate air velocity transmitter and air flow rate	E Instruments Group LLC	HW PRO-VT50	±3.0%
Hand held dry-well calibrator	Calibrate temperature sensor	Hart Scientific	9102S	±0.25%
Micro calibrator	Calibrate RTD, thermocouple, mA, mV, pulse signal	Eurotron Instruments S.p.A.	Microcal 20DPC (Basic)	±0.02%

B2 Propagation of Errors: It is simple arithmetic calculations with numbers containing uncertainties. Any value cannot measure accurately. A true value can be expressed by its mean and standard deviation, such as X±x, where X is the average and x is the standard deviation of the set of *x*-measurements. When expressed in this way, x is referred to as the *absolute* error in the variable *x*. However, the number and its error can be written as X(1±x/X). The ratio within the parentheses, x/X, is called the *relative error* in the measurement *x*. This ratio is often multiplied by 100 and expressed as a percent. Thus the number 56 ±0.6 cm can be also expressed as 56 cm ± 1.07%. Table B.3 shows the calculation of errors for numerous basic mathematical operations with numbers containing uncertainties (Biological Science Institute, 2002).

Table B.3 Mathematical operation of errors

Calculation	Variables	Uncertainties in Variables	Example Calculation	Error in Result
Addition, Subtraction	X, Y, Z	x, y, z	$W = aX + bY - cZ$	$w = \pm\sqrt{(ax)^2 + (by)^2 + (cz)^2}$
Multiplication, Division	X, Y, Z	x, y, z	$W = \frac{aXY}{Z}$	$\frac{w}{W} = \pm\sqrt{(\frac{x}{X})^2 + (\frac{y}{Y})^2 + (\frac{z}{Z})^2}$

B3 Uncertainty analysis of mechanical system/equipment: Mechanical system/equipment uncertainty result is obtained by using Equation (B.1) and propagation of errors mathematical operation.

B3.1 Energy Recovery Ventilator (ERV): Above uncertainty analysis method is applied to Equations (31), (32), (34) and (35) in Chapter 4 to obtain the following accuracy result:

Overall accuracy of sensible heat recovery = ± 4.51%

Overall accuracy of latent heat recovery = ± 3.27%

Overall accuracy of sensible efficiency = ± 0.82%

Overall accuracy of latent efficiency = ± 6.11%

B3.2 In-floor heating: Above uncertainty analysis method is applied to Equation (37) (for similar equation) in Chapter 4. Overall accuracy of space heating = ± 3.01%

B3.3 Electrical energy: This result is obtained from wattnodes and current transformer (CT) accuracy. Overall accuracy of electrical energy = ± 1.00%

B3.4 PV system: This result is obtained from wattnodes and current transformer (CT) accuracy. Overall accuracy of PV output = ± 1.00%

B3.5 Whispergen micro CHP unit: Above uncertainty analysis method is applied to Equation (43) in Chapter 4. Overall accuracy of efficiency = ± 1.97%

B3.6 Evacuated tube solar collector: Above uncertainty analysis method is applied to Equation (30) in Chapter 4. Overall accuracy of efficiency = ± 6.56%

Appendix C: Validation of Equations (4) and (5) with Psychrometric Calculator

Equation (4) and (5) are compared with the Psychrometric calculator ranging from air temperature -30°C to 40°C (increment 5°C) and RH 0%, 20%, 40%, 60%, 80% 100% (Figure C.1 to C.12). There is a good agreement between these equations and Psychrometric calculator.

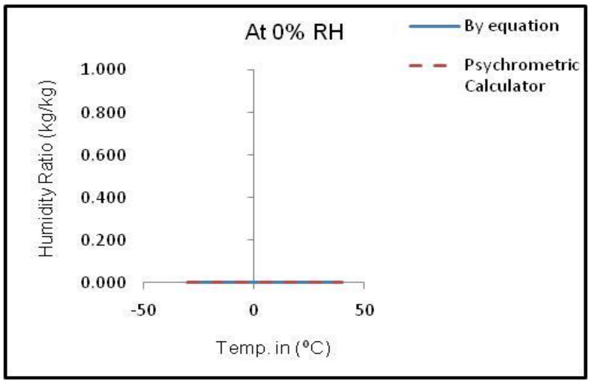

Figure C.1 Temperature and humidity ratio at 0% RH

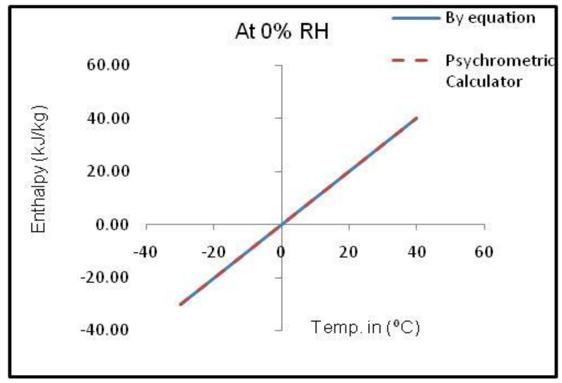

Figure C.2 Temperature and enthalpy at 0% RH

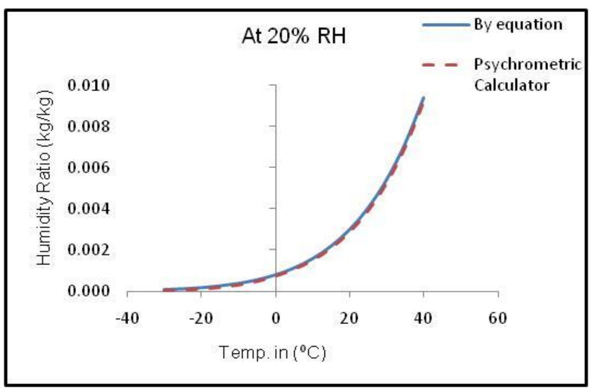

Figure C.3 Temperature and humidity ratio at 20% RH

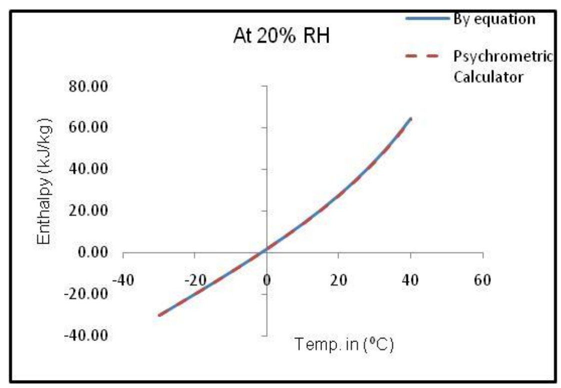

Figure C.4 Temperature and enthalpy at 20% RH

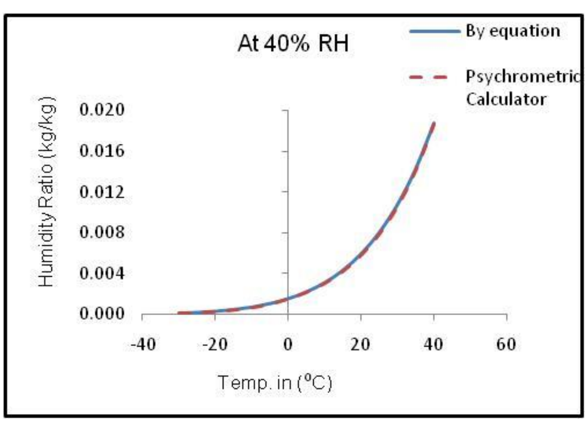

Figure C.5 Temperature and humidity ratio at 40% RH

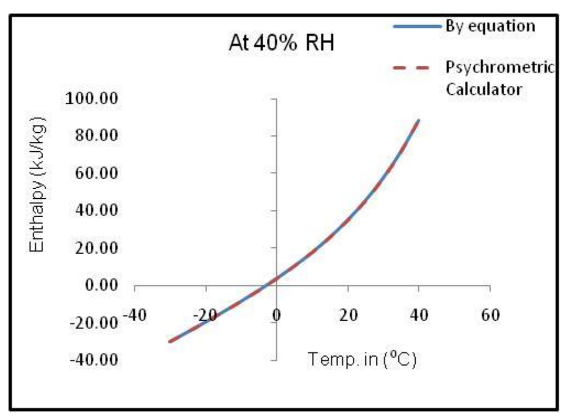

Figure C.6 Temperature and enthalpy at 40% RH

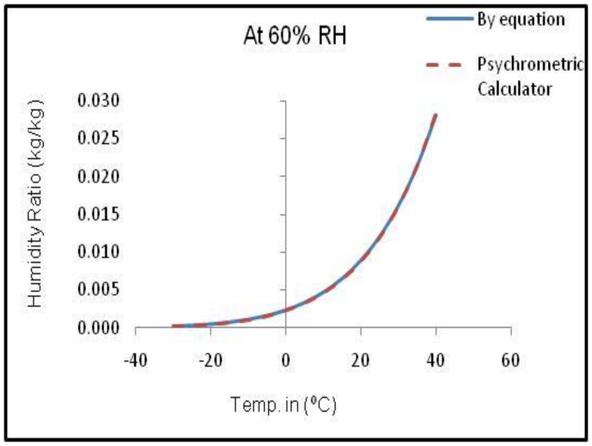

Figure C.7 Temperature and humidity ratio at 60% RH

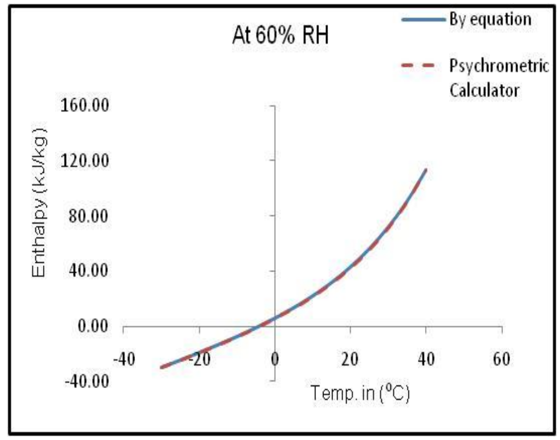

Figure C.8 Temperature and enthalpy at 60% RH

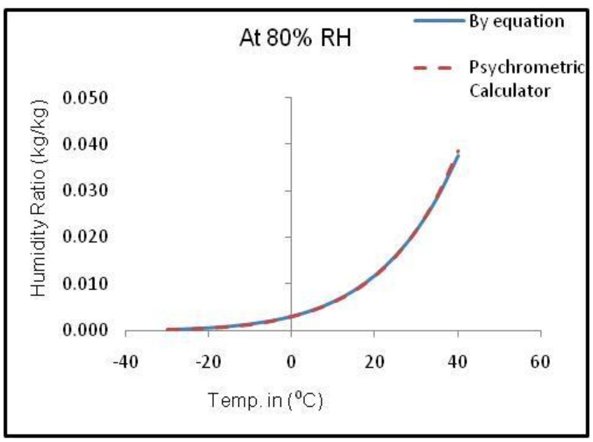

Figure C.9 Temperature and humidity ratio at 80% RH

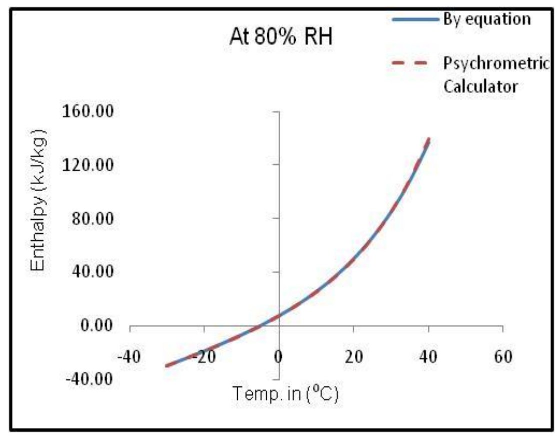

Figure C.10 Temperature and enthalpy at 80% RH

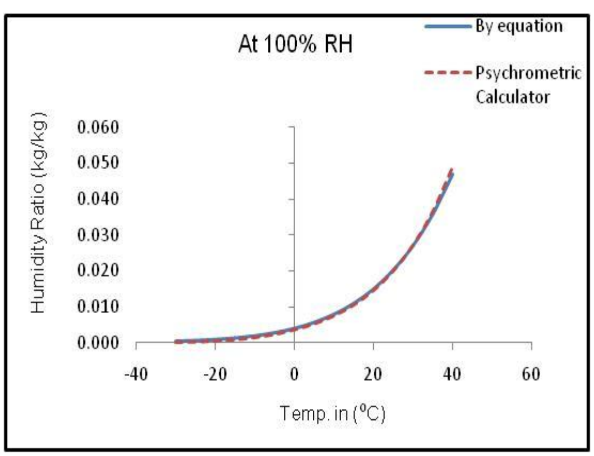

Figure C.11 Temperature and humidity ratio at 100% RH

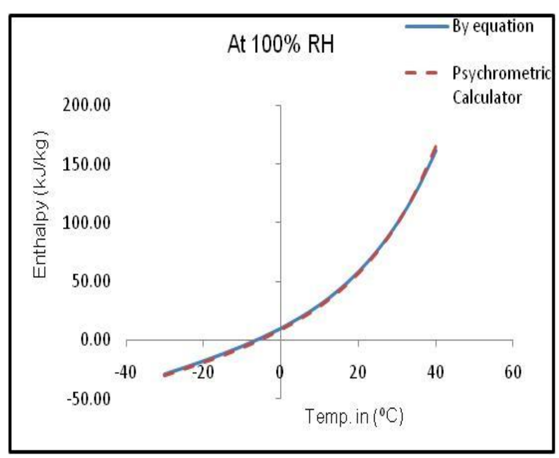

Figure C.12 Temperature and enthalpy at 100% RH

Appendix D: Major equipment photos

From Figures D.1-D.3 show the hydronic and HVAC system of House-A, and from Figures D.4-D.8 show the hydronic, HVAC and renewable energy system in House-B. From Figures D.9-D.11 show the monitoring system.

Figure D.1 Hot water system in House-A

Figure D.2 Heat recovery ventilator (HRV) in House-A

Figure D.3 Heat pump & AHU in House-A

Figure D.4 Hot water system in House-B

Figure D.5 Energy recovery ventilator (ERV) in House-B

Figure D.6 Multi-zone AHU in House-B

Figure D.7 Space heating/cooling unit in House-B

Figure D.8 Solar collectors and roof top PV array

Figure D.9 Compact field point (CFP) at the field for soil sensors

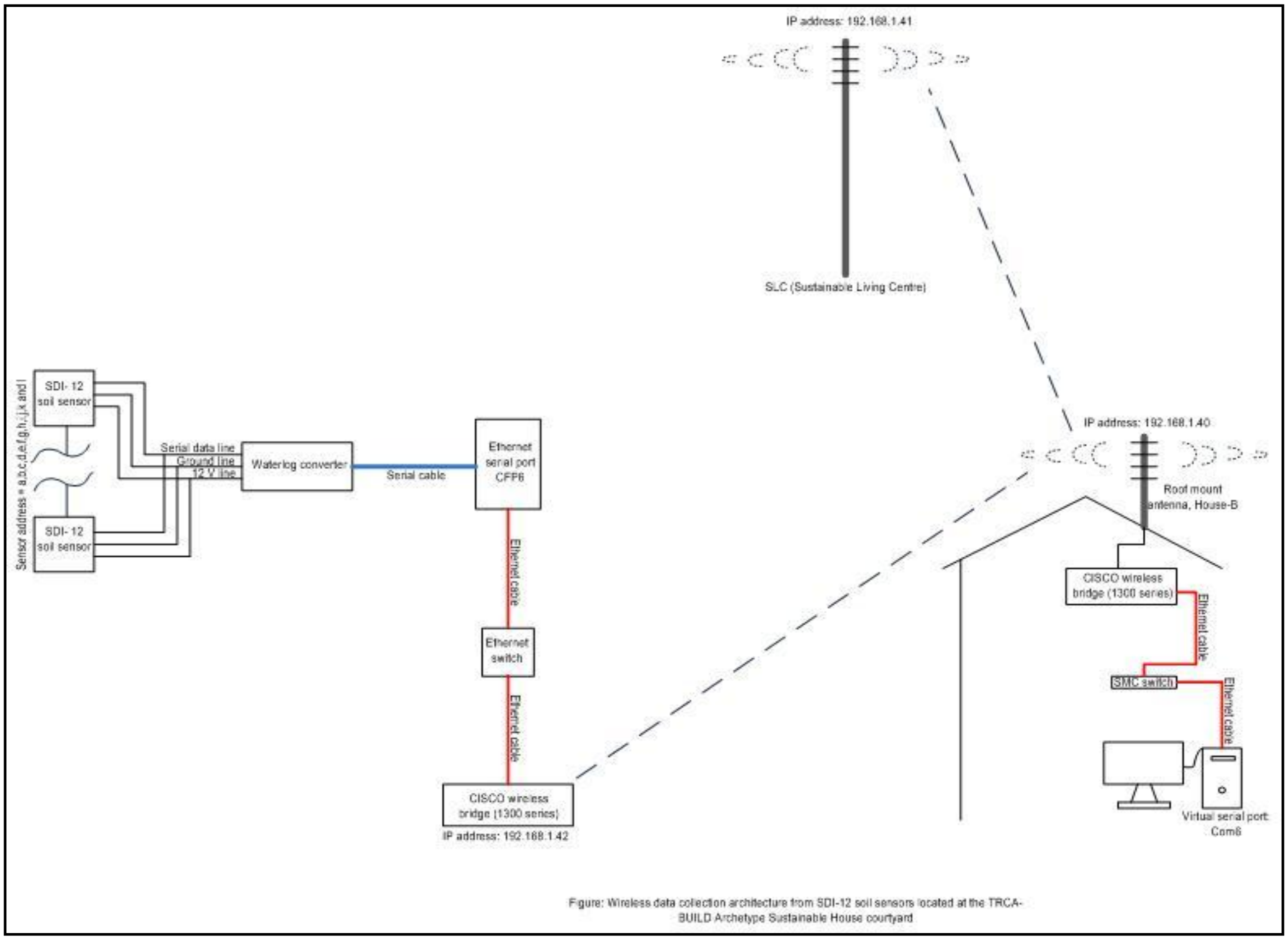

Figure D.10 Remote soil sensors data collection architecture

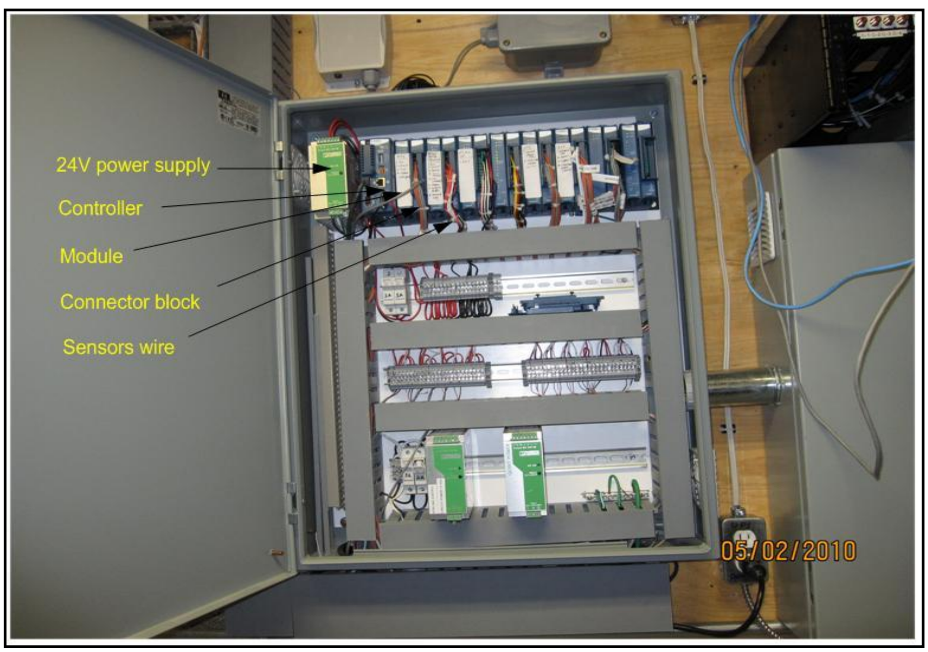

Figure D.11 Compact field point (CFP) in House-B